Chronology of Late Cretaceous Igneous and Hydrothermal Events at the Golden Sunlight Gold-Silver Breccia Pipe, Southwestern Montana

U.S. GEOLOGICAL SURVEY BULLETIN 2155

Chronology of Late Cretaceous Igneous and Hydrothermal Events at the Golden Sunlight Gold-Silver Breccia Pipe, Southwestern Montana

By Ed DeWitt, Eugene E. Foord, Robert E. Zartman,
Robert C. Pearson, *and* Fess Foster

U.S. GEOLOGICAL SURVEY BULLETIN 2155

UNITED STATES GOVERNMENT PRINTING OFFICE, WASHINGTON : 1996

U.S. DEPARTMENT OF THE INTERIOR
BRUCE BABBITT, Secretary

U.S. GEOLOGICAL SURVEY
Gordon P. Eaton, Director

For sale by U.S. Geological Survey, Information Services
Box 25286, Federal Center
Denver, CO 80225

Any use of trade, product, or firm names in this publication is for descriptive purposes only and does not imply endorsement by the U.S. Government

Library of Congress Cataloging-in-Publication Data

Chronolgy of Late Cretaceous igneous and hydrothermal events at the Golden Sunlight gold-silver breccia pipe, southwestern Montana / by Ed DeWitt . . . [et al.].
p. cm.—(U.S. Geological Survey bulletin ; 2155)
Includes bibliographical references.
Supt. of Docs. no. : I 19.3 : 2155
1. Geology, Stratigraphic—Cretaceous. 2. Rocks, Igneous—Montana. 3. Hydrothermal alteration—Montana. 4. Gold ores—Montana. 5. Breccia pipes—Montana. I. DeWitt, Ed. II. Series.
QE75.B9 no. 2155
[QE688]
557.3 s—dc20
[553.4′1′0978667] 96-29319
CIP

CONTENTS

FIGURES

TABLES

CHRONOLOGY OF LATE CRETACEOUS IGNEOUS AND HYDROTHERMAL EVENTS AT THE GOLDEN SUNLIGHT GOLD-SILVER BRECCIA PIPE, SOUTHWESTERN MONTANA

By Ed DeWitt,[1] Eugene E. Foord,[1] Robert E. Zartman,[1]
Robert C. Pearson,[1] *and* Fess Foster[2]

ABSTRACT

Gold mineralization at the Golden Sunlight breccia pipe, southwestern Montana, is related to emplacement of Late Cretaceous alkali-calcic rhyolite and subsequent collapse of the Belt Supergroup wallrock and rhyolite in the pipe. The pipe is inferred to grade downward into an alkalic porphyry molybdenum system. The pipe is cut by alkalic to sub-alkalic lamprophyre dikes and sills, which locally contain high-grade gold where emplaced along late shear zones and vein systems.

Determination of the emplacement age of the rhyolite is hampered by inherited lead or inherited Late Archean zircon from the source region of the rhyolite. An emplacement age of about 80 Ma for the rhyolite can be inferred if a basement age of 2,600 Ma is assumed. This Late Archean age is in agreement with basement ages determined in many parts of southwestern Montana.

A ^{206}Pb-^{238}U whole-rock date of 84±18 Ma from altered and mineralized Belt Supergroup strata and rhyolite in the breccia pipe indicates hydrothermal alteration related to gold mineralization in Late Cretaceous time. Although sericite is a relatively widespread hydrothermal mineral, attempts to date the very fine grained material by the ^{40}Ar-^{39}Ar method did not provide a spectra that could be interpreted unambiguously.

A ^{40}Ar-^{39}Ar plateau date of 76.9±0.5 Ma from biotite phenocrysts in the lamprophyre indciates intrusion of mafic magma and attendant CO_2 metasomatism in the Late Cretaceous. Fission-track data from zircon in the rhyolite are permissive of slow uplift of the Belt Supergroup strata, rhyolite, and lamprophyre between 55 and 50 Ma, but the data are not definitive.

Rhyolitic welded tuff in the informally named units 7, 9, and 11 of the Elkhorn Mountains Volcanics is most similar in chemistry and age to the rhyolite at the Golden Sunlight mine. Trachybasalt in the Adel Mountains Volcanics and andesitic basalt in the informally named unit 8 of the Elkhorn Mountains Volcanics are the most analogous in chemistry and age to lamprophyres at the mine. The rhyolitic rocks appear to be derived from deep crustal sources, but data for the lamprophyres and mafic rocks in the Elkhorn Mountains Volcanics indicate that they were derived from the mantle.

INTRODUCTION

The Golden Sunlight gold-silver deposit is hosted by a breccia pipe that cuts sedimentary rocks of the Middle Proterozoic Belt Supergroup and sills of a Late Cretaceous rhyolite porphyry (Porter and Ripley, 1985; Foster, 1991a, 1991b). At depth, rhyolite porphyry forms the matrix for fragments of the pipe. Creation of the pipe appears to be related to emplacement of an underlying hypabyssal stock related to the sills. Crosscutting the breccia pipe are hydrothermally altered lamprophyre dikes that postdate the gold-silver ore; locally, these dikes may have created areas of high-grade ore in the breccia pipe near their margins. The timing of emplacement of various igneous rocks and the hydrothermal alteration related to mineralization at the deposit is the topic of this paper.

The Golden Sunlight deposit is in the Whitehall mining district, Jefferson County, Montana, on the faulted west limb of a north-plunging syncline of Belt Supergroup sedimentary rocks (fig. 1). The 300- to 700-ft-diameter breccia pipe cuts stratified rocks and rhyolite sills at moderate to high angles (fig. 2). Emplacement of the pipe caused fragments of sedimentary rock and rhyolite porphyry to be downdropped relative to their stratigraphic position outside the pipe (Foster, 1991a, 1991b). Early mining of high-grade

[1]U.S. Geological Survey, Box 25046, Denver Federal Center, Denver, CO 80225.

[2]Golden Sunlight Mines, Inc., 453 MT Highway 2 East, Whitehall, MT 59759.

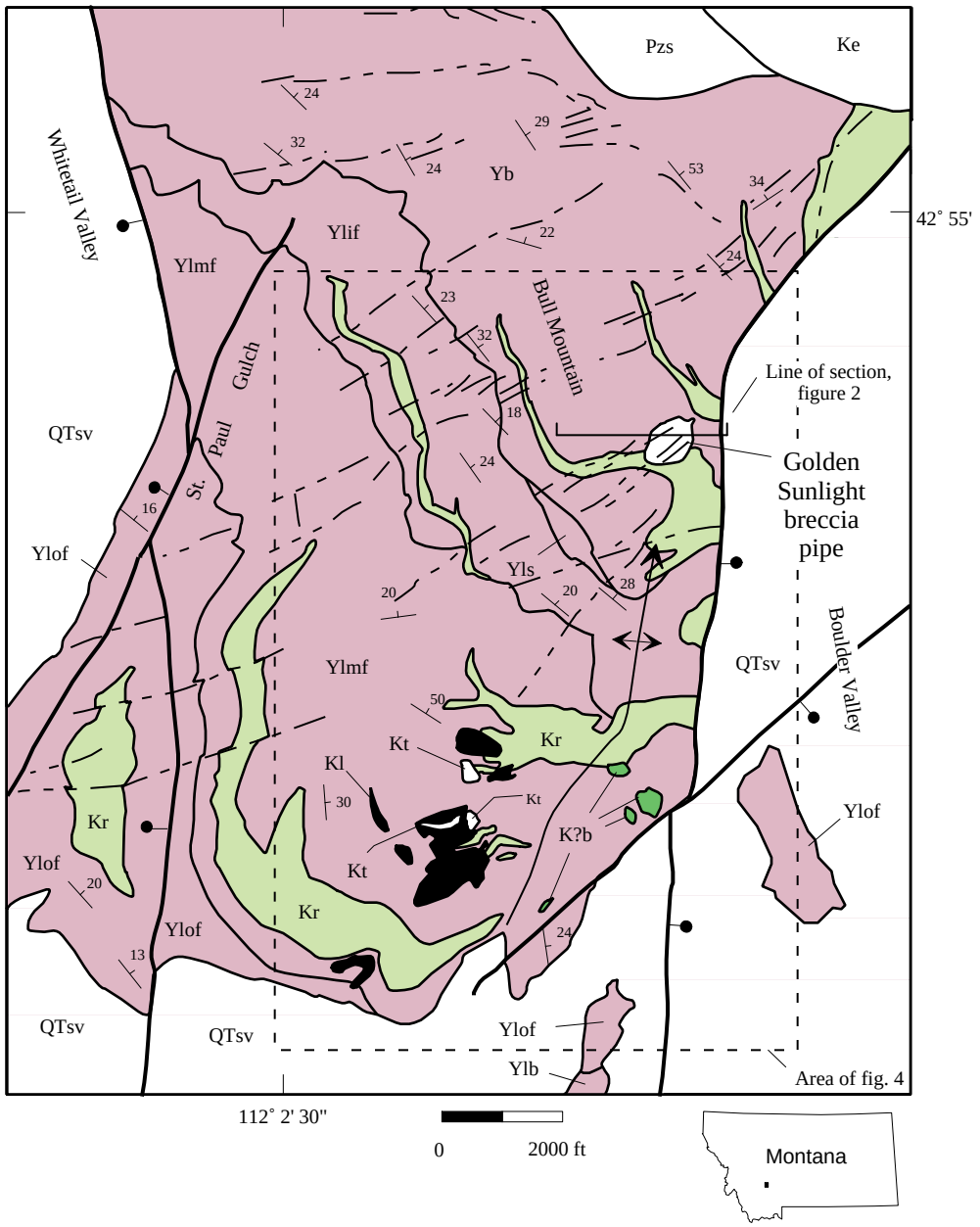

Figure 1 (above and following page). Generalized geologic map of the Golden Sunlight mine area. Modified slightly from Foster (1991a). Line of section for figure 2 and area of figure 4 shown.

gold and silver in the region was concentrated along northeast-striking, high-angle faults and shear zones, some of which cut the breccia pipe and along which lamprophyre dikes have been emplaced (fig. 2) (Porter and Ripley, 1985). These structures are thought to be part of a regional, northeast-striking zone of crustal weakness that has been intermittently active from the Proterozoic to the present (Foster and Chadwick, 1990; Foster 1991a).

Because some hydrothermally altered and mineralized lamprophyre dikes are preferentially emplaced along structures that cross-cut the breccia pipe, their relationship to mineralization of the breccia pipe has been ambiguous. Certainly their emplacement is later than that of the pipe, and the simplest interpretation is that lamprophyre emplacement postdates mineralization. But, because the northeast-striking shear zones, veins, and dikes contain high-grade ore in places, a mineralizing process was obviously continuing during emplacement of the lamprophyre bodies. Was that process the same one that created the breccia pipe, or was it a different one? In this paper, we present petrologic and geochronologic data that bear on the timing and genesis of the breccia pipe and lamprophyre intrusion.

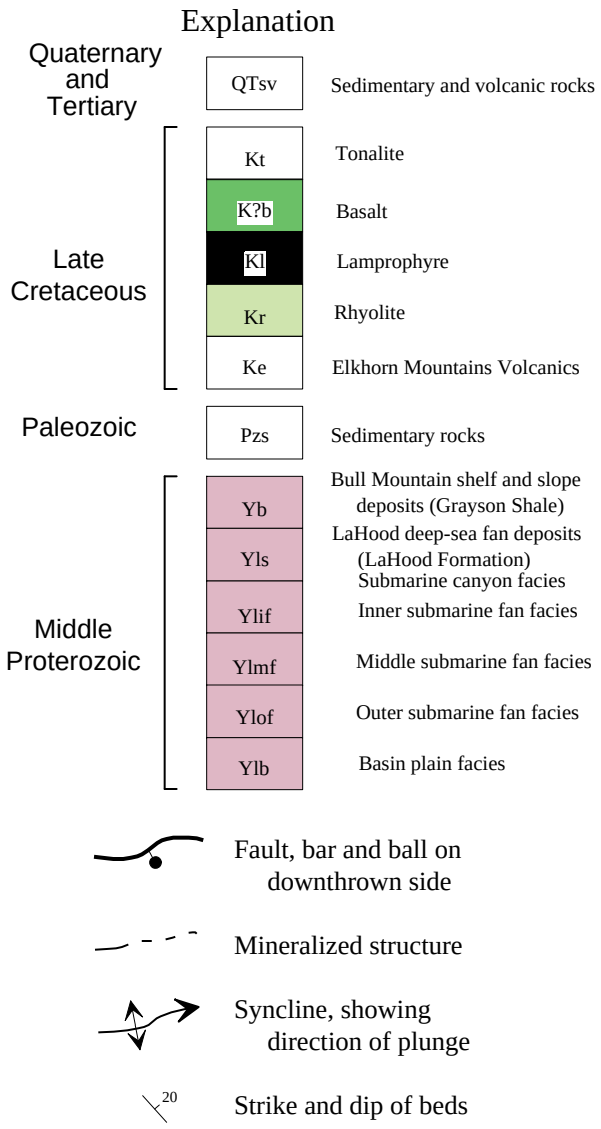

ACKNOWLEDGMENTS

Without the extensive logistical, financial, and technical support of the staff of Golden Sunlight Mines, Inc., this paper would not have been possible. Generous access to the open pit and to core and surface samples was made possible by the mine staff. Many of our samples were collected with the assistance of Walter Coppinger of Trinity University, who also supplied location information for the samples of Swanson (1989). We thank David Allerton for preparing mineral separates used for isotopic age determinations and R.A. Zimmerman for determining the fission-track dates and aiding in the interpretation of the data. We thank Ross Yeoman and L.W. Snee for completing the ^{40}Ar-^{39}Ar analyses of mineral separates from the mine area. Reviews of this manuscript by W.C. Day, G.B. Sidder, G.A. Desborough, and Walter Coppinger are gratefully acknowledged.

IGNEOUS ROCK SUITES

Our study concentrates on the petrologic, chemical, and chronologic history of the igneous rocks in the vicinity of the Golden Sunlight mine because both rhyolite and lamprophyre are spatially associated with ore in the breccia pipe or in late veins, respectively. Three chemically distinct igneous rock units intrude clastic and carbonate-bearing sedimentary rocks of the Belt Supergroup in the area. The oldest unit is composed of hypabyssal sills and dikes of rhyolite (unit Kr, figs. 1 and 2) that cut sedimentary rocks. This rhyolite also forms the matrix of the Golden Sunlight breccia pipe and is assumed to compose a hypabyssal stock beneath the deposit. The rhyolite was investigated in detail to determine the timing of its emplacement. Also studied was the nature of hydrothermal alteration related to emplacement of the rhyolite and breccia pipe.

Younger than the rhyolite are numerous lamprophyre dikes that cut the breccia pipe (unit Kl, figs. 1 and 2). The petrology and alteration of these bodies was studied in detail because the dikes have a distinctive and unusual chemistry and an equally unusual alteration assemblage dominated by magnesite. Possibly related to the lamprophyre bodies are dark-gray, fine-grained olivine basalt and basalt porphyries (unit K?b, fig. 1) exposed on the southern flank of Bull Mountain, south of the mine, where the basalt is in contact with strata of the Belt Supergroup and rhyolite sills. These bodies are typically vesicular, are not altered, and probably postdate mineralization, although direct evidence is lacking. The basalt and basalt porphyries are undated but are presumed to be related to the lamprophyre bodies. Geochemical characteristics of these mafic rocks are summarized here because we do not deal with them in depth in this report. Mineralogically, the basalt contains phenocrysts of olivine altered to chlorite, very pale green clinopyroxene, and minor opaque minerals. The groundmass consists of intermediate-composition plagioclase and clinopyroxene intergrown in a felted texture. Chemically, the one analyzed rock is an alkali-calcic olivine basalt (classification of De LaRoche and others, 1980) that is very Mg rich. The chondrite-normalized rare-earth-element pattern (REE_{CN}) for the sample is light-rare-earth-element enriched (LREE-enriched) and resembles those for many of the lamprophyre bodies.

Felsic plutonic rocks contained in irregular, small, plutonic bodies (unit Kt, fig. 1) probably are the youngest in the area, but age relations to the rhyolite are unclear. Because rocks of this unit are not believed to be related to mineralization, they were investigated only in a cursory fashion. Plutonic rocks of the Boulder batholith are exposed to the west of the mine. The two plutonic bodies south of the mine (fig. 1) may be related to the Boulder batholith.

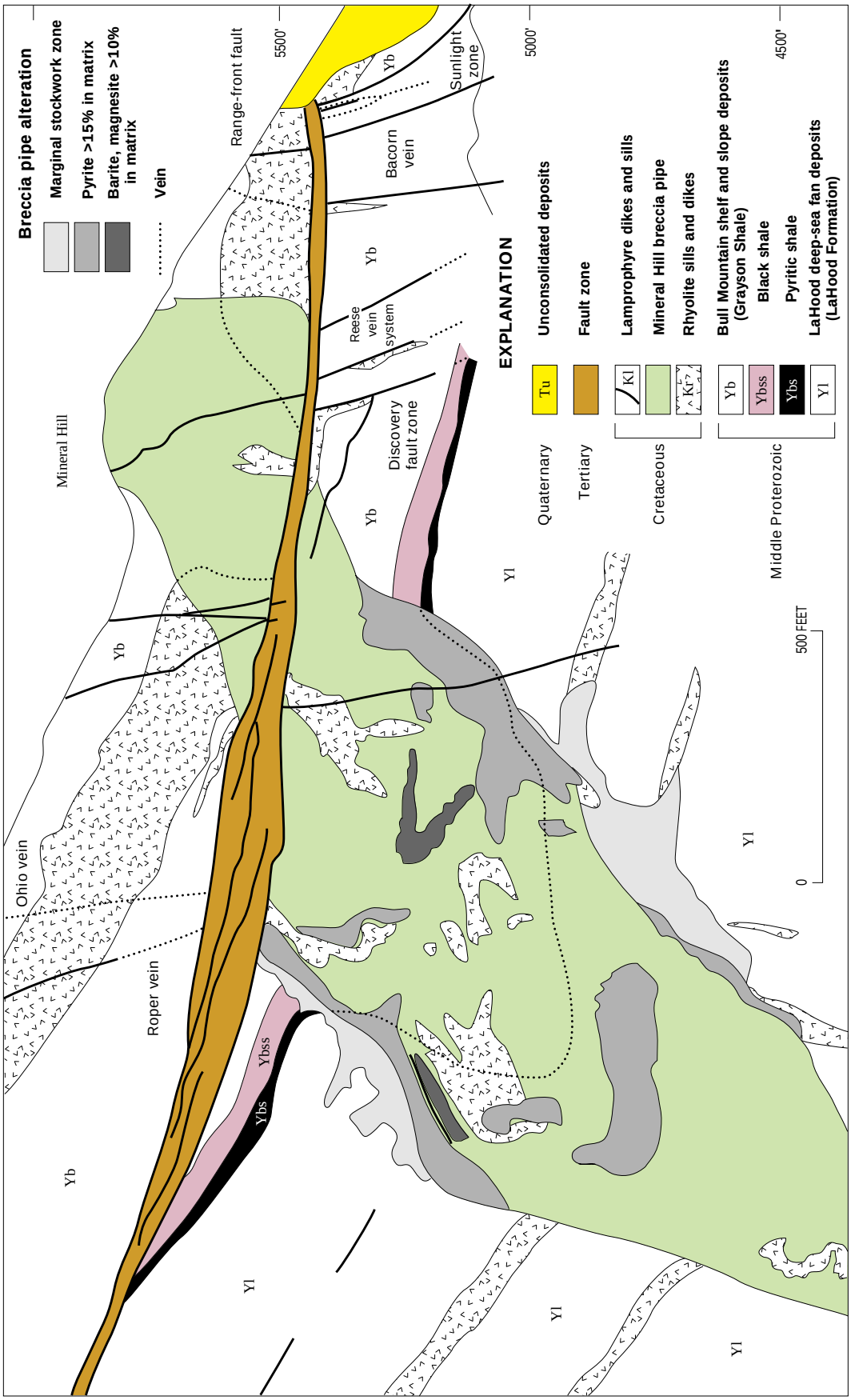

Figure 2. Geologic cross section of the Golden Sunlight breccia pipe. Location of section on figure 1. Heavy dotted lines in pipe show downdropped limit of distinctive stratigraphic units Yb, near the top of the pipe, and Ybs, lower in the pipe.

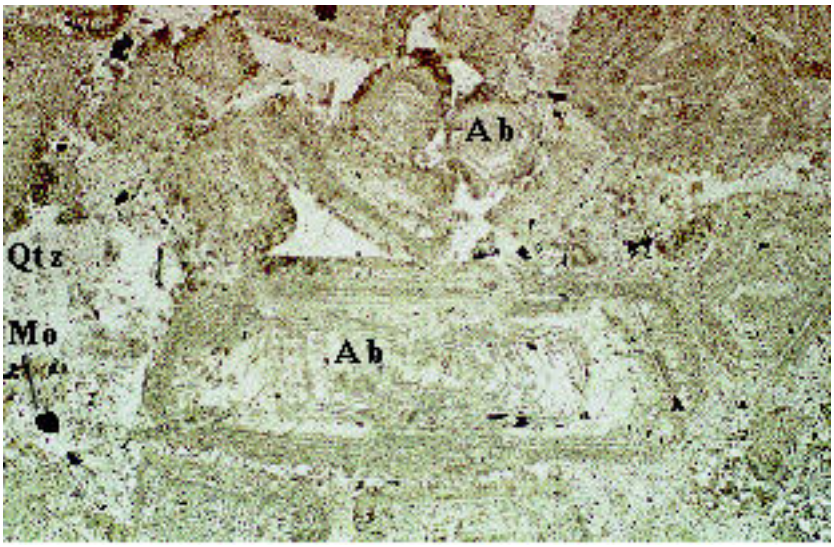

Figure 3. Photomicrograph in plane-polarized light of mineralized rhyolite (sample 90C6-2300′) from breccia pipe at the Golden Sunlight mine. Ab, albite to oligoclase phenocrysts; Otz, quartz; Mo, molybdenite. Field of view 4.2×3.0 mm.

RHYOLITE

Numerous sills, dikes, and irregular bodies of rhyolite porphyry (unit Kr, figs. 1 and 2) cut strata of the Belt Supergroup in the vicinity of the Golden Sunlight mine and are mineralized near the breccia pipe. At depth in the pipe, rhyolite porphyry forms the matrix of the breccia.

PETROLOGY

Most rhyolite is porphyritic, fine grained, and hydrothermally altered. Rhyolite in sills and dikes commonly contains fewer phenocrysts than rhyolite in the breccia pipe. Groundmass-to-phenocryst volumetric ratios greater than 1 to 1 are common in the sills, but ratios much less than 1 to 1 are common in the breccia pipe. Groundmass is composed of quartz and minor orthoclase. Phenocrysts are plagioclase, 1×2 mm to 3×8 mm. Oscillatory zoning and albite twinning are strongly developed in the phenocrysts, which are altered to a fine-grained mixture of sericite and minor epidote-group minerals. Initial composition of the phenocrysts is difficult to determine because of hydrothermal sericite. If the extinction angles between albite twins can be used to approximate the original composition, the phenocrysts were albite to oligoclase. Mafic minerals in the rhyolite are uncommon, but minor clots and irregularly shaped masses of biotite associated with sulfide minerals are noted. Whether or not any of this biotite is of primary igneous origin is uncertain. Accessory phases include apatite and zircon.

The rhyolite is commonly hydrothermally altered, with intensity increasing toward the mineralized breccia pipe. Alteration, in the form of potassium metasomatism, produced high K_2O concentrations (10.3 weight percent in sample 88GS-L, table 1) and resulted in formation of sericite from phenocrysts of plagioclase as well as creation of secondary orthoclase, cryptocrystalline quartz, and some calcite. Minor, primary biotite in least altered rhyolite is commonly replaced by fine-grained, secondary biotite in altered rhyolite. Sample 88GS-L (table 1), from the open pit of the mine, has plagioclase phenocrysts and groundmass replaced by fine-grained orthoclase and contains as much as 3 percent pyrite and 2 to 5 percent sericite. Sulfide minerals, principally pyrite and lesser molybdenite, and hematite typically occupy and replace the groundmass between feldspar grains (fig. 3). In strongly altered rhyolite, very fine grained pyrite replaces the plagioclase phenocrysts.

CHEMISTRY

Although hydrothermally altered in many places, samples of rhyolite were collected from the mine area in order to define its petrogenesis (fig. 4). Some previous workers suggested that the rhyolite was a latite (Wertz, 1971; Porter and Ripley, 1985), but our data do not support such a classification. Latite, as used by most petrologists, implies a relatively high calcium concentration. Rhyolite from the Golden Sunlight mine contain only traces of CaO. Consequently, Swanson (1989), using the alkali-silica diagram of LeMaitre (1984) and LeBas and others (1986), referred to the felsic rocks as rhyolite. If the R_1R_2 classification of De LaRoche and others (1980) is used, the least hydrothermally altered samples of this unit (samples 88GS-7 and 191-2025′; table 1) are rhyolite (fig. 5*A*). Least altered samples of rhyolite are alkali-calcic (fig. 5A), mildly peraluminous (fig. 5*B*), very sodic (fig. 5*C*), and Mg rich (fig. 5*D*). With increasing potassium metasomatism and introduction of pyrite, hematite, and molybdenite, the rhyolite is altered to an alkalic quartz syenite (fig. 5*A*) that is strongly peraluminous (fig. 5*B*), potassic to very potassic (fig. 5*C*), and Fe rich to very Fe rich (fig. 5*D*). Thirty-seven samples of the rhyolite from Wertz (1971) and three samples of the rhyolite from Swanson (1989) agree with the changes noted for our four samples. Because much of the linear trend for our samples of rhyolite (fig. 5*A*) is defined by altered rocks, and because there is little chemical variability in the fresh rhyolite, we cannot speculate about lines of descent or fractional crystallization paths of these felsic rocks.

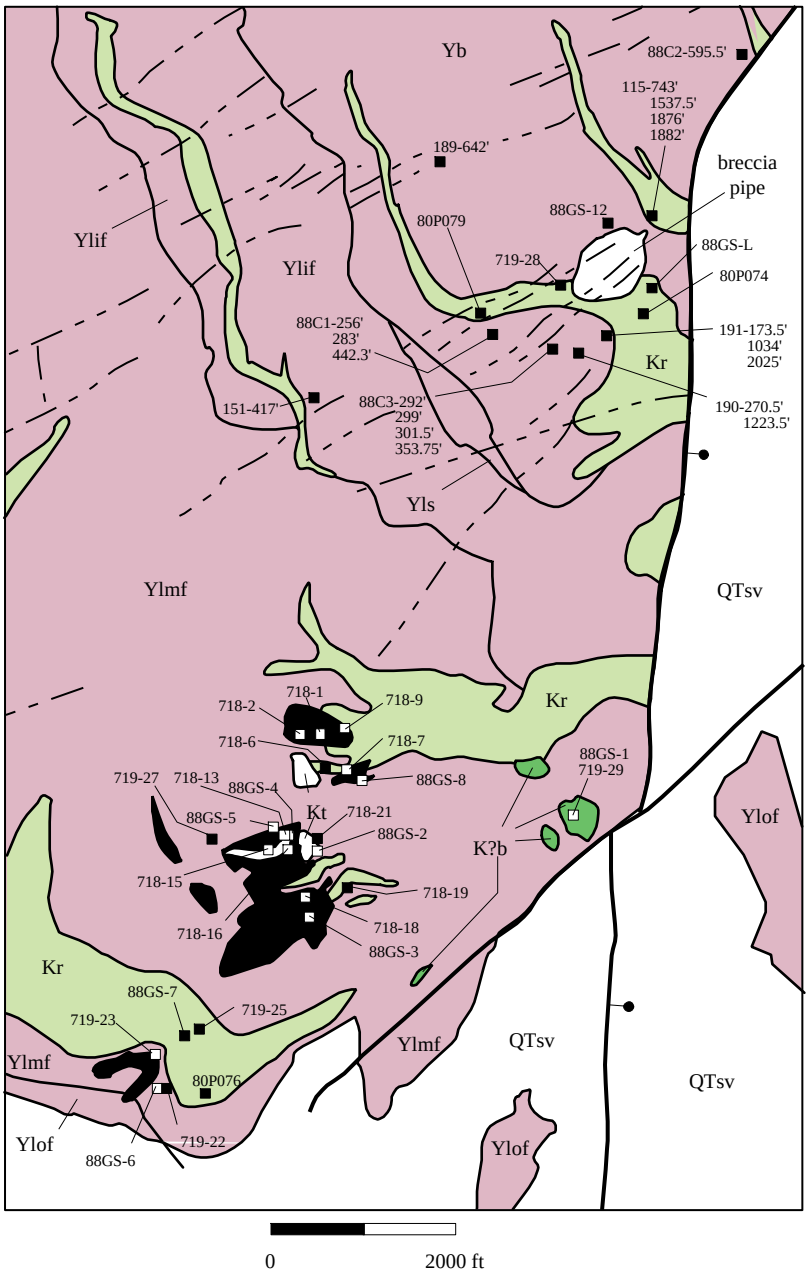

Figure 4. Sample locality map of the Golden Sunlight mine area. Map area shown on figure 1. Rock-unit abbreviations as in figure 1. Data for all samples listed are in table 1. Samples not shown on this figure include St. Paul Gulch shown on figure 1 and JC-1 and JC-2 from Jefferson Canyon, south of figure 1.

Rare-earth-element (REE) patterns (fig. 6) are LREE-enriched and have chondrite-normalized La/Yb ratios (La/Yb_{CN}) ratios of 10 in fresh to 40 in mildly metasomatized samples. Heavy rare-earth-element (HREE) parts of the profiles are notably flat. No europium anomalies are observed. La/Yb_{CN} ratios increase to as much as 50 in one strongly metasomatized sample. Whether or not this apparent LREE enrichment is due to true enrichment of LREE during mineralization cannot be proven by our data.

CHRONOLOGY OF RHYOLITE EMPLACEMENT

Rhyolite matrix from drill core (sample 90C6-2300′) that contains fragments of mineralized sedimentary rocks of the Belt Supergroup was processed to retrieve zircon for U-Th-Pb dating. Morphologically, the zircon varied from rounded, milky white grains to elongate, clear, euhedral crystals. Although the rounded zircon may be detrital grains contributed by the sedimentary rocks, the euhedral variety is

Table 1. Major-, minor-, and rare-earth-element geochemistry of igneous rocks in the Golden Sunlight mine area, southwestern Montana.

[Major-element chemistry by X-ray fluorescence by Dave Seims and J.E. Taggart. Minor-element chemistry by induction-coupled plasma spectrometry by D. Fey. Rare-earth-element chemistry by induction-coupled plasma spectrometry by A.L. Meier. FeO, H_2O, and CO_2 analyses by M.G. Kavulak. Leaders (--) indicate "not analyzed." Suite abbreviations: Bas, basalt; Ton, tonalite; Ton N, tonalite normalized; Lam 1, lamprophyre 1 having CO_2<5 percent; Lam 2, lamprophyre 2 having CO_2 between 5 and 9 percent; Lam 3, lamprophyre 3 having CO_2 between 10 and 14 percent; Lam 4, lamprophyre 4 having CO_2 between 15 and 20 percent; Lam N, lamprophyre normalized; Rhy, rhyolite; Rhy N, rhyolite normalized; R_1, calculated values for R_1R_2 plot; R_2, calculated values for R_1R_2 plot; A/CNK, calculated values for SiO_2 versus A/CNK plot; Fe number, calculated values for $(FeO^+0.89Fe_2O_3)/(FeO^+0.89\ Fe_2O_3^+MgO)$ versus SiO_2 plot; K number, calculated values for $K_2O/(K_2O^+Na_2O)$ versus SiO_2 plot; La/Yb_{CN}, chondrite normalized ratio of La/Yb; Eu/Eu*, calculated value of europium anomaly (numbers less than 1 indicate negative anomaly, numbers greater than 1 indicate positive anomaly). From ICP asnalyses, 88C3-301.5′ has minimum of 1.95 weight percent SO_3, 191-173.5′ has minimum of 0.49 weight percent SO_3, 88GS-8 has minimum of 0.18 weight percent SO_3, 88GS-12 has about 2.02 weight percent SO_3, and 88GS-L has about 1.35 weight percent SO_3]

Field no.	88GS-1	719-29	88GS-2	88GS-4	88GS-?	718-21	718-15	718-6	88C1-256′	88GS-5	88C3-292′	190-270.5′	88GS-3
Lab no.	D322303	Swanson	D322304	D322306		Swanson	Swanson	Swanson	D322313	D322307	D322316	D322324	D322305
Suite	Bas	Bas	Ton	Ton	Ton	Ton N	Ton N	Ton N	Lam 1	Lam 1	Lam 1	Lam 1	Lam 1
Major elements (weight percent)													
SiO_2	48.20	49.65	63.10	66.90	63.70	59.90	68.24	68.91	46.30	46.90	47.30	47.30	50.70
TiO_2	1.00	1.01	0.42	0.34	0.55	0.52	0.35	0.25	0.91	0.95	0.94	0.93	0.60
Al_2O_3	13.00	13.16	15.50	15.90	14.60	14.92	16.36	14.67	12.10	12.30	12.50	12.30	10.40
Fe_2O_3	3.54	--	2.59	1.80	1.04	--	--	--	5.56	5.09	6.41	6.31	3.44
Fe_tO	--	9.34	--	--	--	5.70	3.24	2.90	--	--	--	--	--
FeO	5.80	--	1.80	1.30	4.30	--	--	--	5.70	6.40	5.30	5.30	5.90
MnO	0.16	0.15	0.10	0.04	0.07	0.13	0.04	0.05	0.20	0.19	0.20	0.20	0.16
MgO	11.90	13.56	2.89	1.52	3.48	5.39	1.52	2.18	8.11	9.14	8.30	8.35	13.40
CaO	8.94	9.01	3.42	1.46	2.42	5.54	1.56	2.82	11.40	11.80	11.20	11.20	8.84
Na_2O	2.48	2.03	3.82	4.41	4.63	3.56	4.58	4.10	1.43	1.55	1.96	1.31	2.14
K_2O	1.55	1.73	3.62	3.77	1.40	3.53	3.76	3.91	4.02	3.60	3.52	4.12	3.15
P_2O_5	0.35	0.35	0.43	0.32	0.11	0.80	0.34	0.19	0.73	1.10	0.76	0.75	0.61
H_2O^+	2.10	--	1.00	1.40	2.30	--	--	--	1.20	0.78	1.20	1.70	0.43
H_2O^-	1.50	--	0.96	0.55	0.36	--	--	--	0.83	0.44	0.55	0.51	0.50
CO_2	0.04	--	0.19	0.02	0.73	--	--	--	1.80	0.03	0.38	0.50	0.06
Total	100.56	99.99	99.84	99.73	99.69	99.99	99.99	99.98	100.29	100.27	100.52	100.78	100.33
R_1	1691	1895	1874	1918	2110	1728	1940	2132	1315	1402	1299	1393	1614
R_2	1802	1895	813	544	718	1153	563	698	1859	1957	1855	1854	1814
A/CNK	0.59	0.61	0.95	1.14	1.08	0.76	1.14	0.91	0.44	0.44	0.46	0.46	0.45
Fe No.	0.43	0.41	0.59	0.66	0.60	0.51	0.68	0.57	0.57	0.55	0.57	0.57	0.40
K No.	0.38	0.46	0.49	0.46	0.23	0.50	0.45	0.49	0.74	0.70	0.64	0.76	0.60
La/Yb_{CN}	13.48	--	17.03	34.38	4.82	--	--	--	13.16	18.73	12.87	15.61	10.11
Eu/Eu*	0.92	--	1.00	0.95	0.81	--	--	--	0.94	0.87	0.91	0.96	0.92
Minor elements (ppm)													
Ba	550	700	1300	1400	330	1142	1270	934	780	870	790	780	780
Sr	580	717	1100	860	740	989	888	383	1200	1400	1500	1400	870
Y	19	21	14	10	18	17	10	9	21	20	21	21	14
Zr	--	114	--	--	--	155	175	126	--	--	--	--	--
Nb	7	--	16	13	4	--	--	--	7	10	13	11	<4
Sc	--	28	--	--	--	13	4	4	34	35	34	34	28
Cu	86	79	32	15	49	58	23	9	180	71	160	180	120
Pb	10	--	13	19	27	--	--	--	8	10	9	9	11
Zn	74	--	50	27	66	--	--	--	94	95	97	98	69
Ni	376	345	51	23	65	227	36	66	80	110	78	80	390
Cr	800	904	100	30	130	347	193	226	310	430	310	300	940
Co	56	79	15	9	18	58	23	9	48	51	49	49	57
Rare earth elements (ppm)													
La	28	--	48	51	15	--	--	--	41	50	42	44	18
Ce	58	--	82	81	30	--	--	--	78	98	77	85	33
Pr	6.8	--	8.1	7.6	3.4	--	--	--	8.3	10	8.3	8.8	3.7
Nd	28	--	30	27	15	--	--	--	35	45	35	37	16
Sm	4.4	--	4.8	4	3	--	--	--	5.6	7.4	5.9	6.3	2.9
Eu	1.2	--	1.4	0.96	0.8	--	--	--	1.6	1.9	1.6	1.8	0.88
Gd	3.3	--	3.5	1.8	3	--	--	--	4.5	5.6	4.5	4.9	2.9
Tb	0.56	--	0.51	0.4	0.45	--	--	--	0.75	1	0.79	0.8	0.43
Dy	3.1	--	3.1	2.1	3.4	--	--	--	4.1	4.6	4	4.4	2.5
Ho	0.57	--	0.58	0.38	0.64	--	--	--	0.7	0.85	0.84	0.84	0.53
Er	1.6	--	1.7	0.88	2	--	--	--	2.4	2.2	2.3	2.2	1.5
Tm	0.23	--	0.31	0.17	0.34	--	--	--	0.33	0.33	0.28	0.32	0.2
Yb	1.4	--	1.9	1	2.1	--	--	--	2.1	1.8	2.2	1.9	1.2

Table 1. Major-, minor-, and rare-earth-element geochemistry of igneous rocks in the Golden Sunlight mine area, southwestern Montana—*Continued*.

Field no.	88GS-6	88GS-8	189-642′	88C3-299′	151-417′	190-1223.5′	88C2-595.5′	88C3-353.75′	115-1876′	88C3-301.5′	115-1537.5′	115-1882′	191-1034′
Lab no.	D322308	D322310	D322323	D322317	D322329	D322325	D322315	D322319	D322321	D322318	D322320	D322322	D322327
Suite	Lam 1	Lam 2	Lam 2	Lam 2	Lam 2	Lam 2	Lam 2	Lam 2	Lam 2	Lam 3	Lam 3	Lam 3	Lam 3
Major elements (weight percent)													
SiO_2	55.40	45.70	44.00	44.60	45.00	45.10	45.50	45.90	47.90	42.30	42.80	43.20	46.70
TiO_2	0.65	0.78	0.85	0.83	0.68	0.73	0.71	0.56	0.76	0.81	0.83	0.47	2.54
Al_2O_3	12.00	11.70	11.20	11.40	11.10	9.84	10.70	8.97	13.40	11.20	11.20	7.74	10.60
Fe_2O_3	3.02	0.30	5.64	3.75	3.60	3.62	3.58	2.53	3.34	4.89	3.95	2.21	2.79
Fe_tO	--		--	--	--	--	--	--	--	--	--	--	--
FeO	5.80	15.10	11.30	5.40	4.90	5.20	5.20	5.50	5.20	4.30	5.30	5.10	4.60
MnO	0.15	0.26	0.25	0.14	0.15	0.14	0.15	0.14	0.13	0.18	0.15	0.12	0.12
MgO	7.98	6.29	6.35	9.39	7.84	10.10	11.10	15.70	5.34	8.34	8.55	16.60	9.46
CaO	8.61	9.13	7.77	7.77	8.82	9.96	7.08	6.54	6.65	8.30	8.25	4.95	5.82
Na_2O	2.40	1.74	1.73	1.46	1.78	1.10	1.64	1.22	1.64	1.59	1.40	1.69	1.89
K_2O	3.22	2.08	3.04	3.57	3.45	3.26	3.12	1.98	3.79	3.20	3.66	2.52	3.57
P_2O_5	0.53	0.92	0.67	0.94	0.76	0.81	0.59	0.32	0.54	0.98	0.98	0.41	0.55
H_2O^+	0.38	2.91	1.10	1.50	1.40	2.00	1.60	3.00	2.10	1.80	1.60	1.50	1.10
H_2O^-	0.49	0.09	0.86	0.73	1.00	0.77	1.20	1.40	0.42	1.00	0.63	0.95	0.72
CO_2	0.02	3.17	5.50	8.40	9.29	7.30	8.20	6.60	6.30	10.40	10.30	12.00	10.70
Total	100.65	100.17	100.26	99.88	99.77	99.93	100.37	100.36	97.51	99.29	99.60	99.46	101.16
R_1	1831	1491	1128	1352	1314	1597	1466	1930	1474	1242	1230	1478	1343
R_2	1552	1518	1366	1521	1550	1760	1518	1654	1239	1521	1526	1505	1300
A/CNK	0.52	0.54	0.55	0.56	0.49	0.42	0.57	0.56	0.71	0.53	0.53	0.53	0.60
Fe no.	0.52	0.71	0.72	0.48	0.51	0.46	0.43	0.33	0.61	0.51	0.51	0.30	0.43
K no.	0.57	0.54	0.64	0.71	0.66	0.75	0.66	0.62	0.70	0.67	0.72	0.60	0.65
La/Yb_{CN}	8.33	--	13.48	14.33	16.48	13.97	8.43	13.48	8.09	12.42	12.14	9.55	9.15
Eu/Eu*	0.91	--	0.96	0.88	0.92	0.92	1.06	0.94	1.01	0.98	0.83	1.11	0.87
Minor elements (ppm)													
Ba	830	--	690	930	900	620	840	550	840	140	810	580	820
Sr	580	--	1200	820	1300	660	730	500	740	860	2200	830	810
Y	17	--	18	18	16	16	15	13	16	16	17	10	12
Zr	--	--	--	--	--	--	--	--	--	--	--	--	--
Nb	<4	--	15	6	7	<4	4	<4	5	8	6	<4	<4
Sc	28	--	33	27	23	34	24	22	23	25	26	18	20
Cu	95	--	160	130	110	190	85	74	95	130	140	83	92
Pb	12	--	7	13	9	10	10	13	14	37	10	12	10
Zn	77	--	220	74	78	71	72	56	84	91	78	50	61
Ni	97	--	140	240	120	240	400	650	56	230	230	710	290
Cr	340	--	320	520	330	600	500	530	170	470	440	630	500
Co	41	--	80	44	40	43	47	59	33	44	45	57	42
Rare earth elements (ppm)													
La	21	--	38	34	44	29	25	24	24	35	36	17	19
Ce	40	--	72	67	86	59	49	49	47	72	73	31	37
Pr	4.3	--	7.6	7.3	8.8	6.5	5.3	5.5	4.9	7.9	8.4	3.4	3.9
Nd	19	--	32	35	36	29	24	24	22	36	35	14	18
Sm	3.3	--	5.2	5.5	6.2	5	4.1	3.9	3.8	5.8	6.1	2.4	2.8
Eu	0.99	--	1.6	1.5	1.7	1.4	1.3	1.1	1.2	1.7	1.5	0.85	0.88
Gd	3.3	--	4.8	4.7	4.8	4.1	3.2	3.1	3.3	4.5	4.7	2.2	3.4
Tb	0.57	--	0.72	0.69	0.73	0.64	0.6	0.53	0.56	0.73	0.72	0.27	0.43
Dy	3.4	--	4	3.5	4.2	3.4	3.5	2.7	3.2	3.6	4.1	2	2.7
Ho	0.6	--	0.67	0.69	0.69	0.66	0.71	0.56	0.64	0.8	0.67	0.4	0.5
Er	1.7	--	2.1	2.1	2	1.6	2.1	1.4	1.8	1.9	2.4	1.2	1.3
Tm	0.3	--	0.27	0.29	0.29	0.25	0.28	0.18	0.25	0.28	0.32	0.13	0.19
Yb	1.7	--	1.9	1.6	1.8	1.4	2	1.2	2	1.9	2	1.2	1.4

Table 1. Major-, minor-, and rare-earth-element geochemistry of igneous rocks in the Golden Sunlight mine area, southwestern Montana—*Continued*.

Field no.	88C1-283′	191-173.5′	719-23	718-16	718-9	718-7	718-13	718-1	718-18	718-2	719-27	719-22	88GS-12
Lab no.	D322314	D322326	Swanson	Swanson	Swanson	Swanson	Swanson	Swanson	Swanson	Swanson	Swanson	Swanson	D322311
Suite	Lam 4	Lam 4	Lam N	Lam N	Lam N	Lam N	Lam N	Lam N	Lam N	Lam N	Lam N	Lam N	Rhy
Major elements (weight percent)													
SiO_2	38.80	39.20	--	47.37	47.76	47.82	47.84	50.57	51.06	51.46	54.45	55.92	66.30
TiO_2	0.35	0.44	--	0.91	0.95	0.97	0.92	0.90	0.59	0.88	0.84	0.65	0.09
Al_2O_3	6.34	6.69	--	12.17	12.16	13.60	12.57	13.34	10.57	13.43	13.38	12.51	16.40
Fe_2O_3	1.59	1.79	--	--	--	--	--	--	--	--	--	--	2.99
Fe_tO	--	--	--	11.00	11.00	11.60	11.19	10.48	9.12	10.49	9.14	8.61	--
FeO	5.90	5.60	--	--	--	--	--	--	--	--	--	--	<0.01
MnO	0.13	0.12	--	0.20	0.20	0.22	0.20	0.20	0.16	0.20	0.16	0.16	<0.02
MgO	15.80	17.70	--	10.11	9.58	8.46	9.29	7.74	13.86	7.58	7.47	7.32	0.14
CaO	5.06	5.03	--	11.85	12.44	10.72	11.41	9.73	8.64	9.25	8.92	8.39	0.02
Na_2O	0.67	0.79	--	1.73	1.88	2.29	1.50	2.33	2.18	2.44	1.93	2.51	4.34
K_2O	3.06	1.74	--	3.28	2.80	3.30	3.69	3.95	3.22	3.52	2.64	3.31	6.65
P_2O_5	0.39	0.25	--	1.37	1.23	0.96	1.39	0.77	0.60	0.75	1.07	0.62	0.07
H_2O^+	1.00	2.00	--	--	--	--	--	--	--	--	--	--	0.68
H_2O^-	0.92	0.90	--	--	--	--	--	--	--	--	--	--	0.46
CO_2	20.00	15.50	--	--	--	--	--	--	--	--	--	--	<0.01
Total	100.01	97.75	--	99.99	100.00	99.94	100.00	100.01	100.00	100.00	100.00	100.00	98.17
R_1	1418	1711	--	1444	1528	1253	1456	1303	1604	1423	2048	1803	1243
R_2	1449	1547	--	2008	2045	1833	1928	1687	1819	1629	1587	1506	331
A/CNK	0.47	0.54	--	0.44	0.42	0.51	0.46	0.52	0.46	0.55	0.60	0.55	1.14
Fe no.	0.32	0.29	--	0.52	0.53	0.58	0.55	0.58	0.40	0.58	0.55	0.54	0.95
K no.	0.82	0.69	--	0.65	0.60	0.59	0.71	0.63	0.60	0.59	0.58	0.57	0.61
La/Yb_{CN}	4.90	10.37	--	--	--	--	--	--	--	--	--	--	20.87
Eu/Eu*	0.95	0.87	--	--	--	--	--	--	--	--	--	--	0.93
Minor elements (ppm)													
Ba	970	990	772	832	724	800	865	977	705	732	731	791	1200
Sr	510	500	505	1333	1166	1432	1282	1278	764	1016	809	521	700
Y	8	10	18	24	23	24	22	22	15	22	25	19	4
Zr	--	--	112	132	123	115	130	112	70	110	146	106	--
Nb	<4	<4	--	--	--	--	--	--	--	--	--	--	13
Sc	17	18	26	33	38	30	32	28	26	28	29	25	--
Cu	71	110	87	175	97	152	51	74	119	125	128	124	49
Pb	9	140	--	--	--	--	--	--	--	--	--	--	8
Zn	46	240	--	--	--	--	--	--	--	--	--	--	64
Ni	590	810	192	255	145	107	192	84	397	108	106	109	7
Cr	680	1000	345	197	400	393	397	282	906	284	290	375	2
Co	62	66	19	27	31	30	32	26	31	26	16	36	5
Rare earth elements (ppm)													
La	8	20	--	--	--	--	--	--	--	--	--	--	13
Ce	17	41	--	--	--	--	--	--	--	--	--	--	17
Pr	1.7	4.5	--	--	--	--	--	--	--	--	--	--	1.6
Nd	8.5	20	--	--	--	--	--	--	--	--	--	--	5.7
Sm	1.4	3.4	--	--	--	--	--	--	--	--	--	--	0.75
Eu	0.44	0.88	--	--	--	--	--	--	--	--	--	--	0.25
Gd	1.4	2.6	--	--	--	--	--	--	--	--	--	--	0.9
Tb	0.27	0.39	--	--	--	--	--	--	--	--	--	--	0.17
Dy	1.5	2.1	--	--	--	--	--	--	--	--	--	--	0.72
Ho	0.26	0.44	--	--	--	--	--	--	--	--	--	--	0.12
Er	0.91	1.1	--	--	--	--	--	--	--	--	--	--	0.46
Tm	0.11	0.14	--	--	--	--	--	--	--	--	--	--	0.05
Yb	1.1	1.3	--	--	--	--	--	--	--	--	--	--	0.42

Table 1. Major-, minor-, and rare-earth-element geochemistry of igneous rocks in the Golden Sunlight mine area, southwestern Montana—*Continued*.

Field no.	191-2025′	88GS-L	88GS-7	719-28	718-19	719-25
Lab no.	D322328	D322312	D322309	Swanson	Swanson	Swanson
Suite	Rhy	Rhy	Rhy	Rhy N	Rhy N	Rhy N
Major elements (weight percent)						
SiO_2	66.60	66.70	69.70	69.84	71.86	72.10
TiO_2	0.12	0.10	0.12	0.10	0.08	0.13
Al_2O_3	18.20	16.00	16.20	16.64	16.21	16.48
Fe_2O_3	2.26	1.99	1.30	--	--	--
Fe_tO	--	--	--	1.13	1.14	1.23
FeO	<0.01	<0.01	<0.01	--	--	--
MnO	<0.02	<0.02	0.06	--	0.04	0.01
MgO	0.77	0.15	0.16	0.16	0.08	0.19
CaO	0.10	0.01	0.45	0.01	0.19	0.11
Na_2O	3.08	2.09	5.36	3.47	6.33	4.81
K_2O	5.15	10.30	4.68	8.55	3.99	4.85
P_2O_5	0.05	0.02	0.02	0.10	0.08	0.08
H_2O^+	1.70	0.58	0.76	--	--	--
H_2O^-	0.84	0.60	0.58	--	--	--
CO_2	0.18	<0.01	0.27	--	--	--
Total	99.11	98.57	99.67	100.00	100.00	99.99
R_1	2076	1240	1608	1387	1571	1922
R_2	406	322	374	335	342	345
A/CNK	1.68	1.10	1.10	1.11	1.08	1.24
Fe no.	0.73	0.92	0.88	0.88	0.93	0.87
K no.	0.63	0.83	0.47	0.71	0.39	0.50
La/Yb_{CN}	14.33	51.74	10.79	--	--	--
Eu/Eu*	1.08	0.62	1.26	--	--	--
Minor elements (ppm)						
Ba	240	320	1700	1691	1471	762
Sr	550	320	590	387	1496	273
Y	3	<2	6	4	5	5
Zr	--	--	--	76	118	95
Nb	7	13	13	--	--	--
Sc	--	--	--	1	--	--
Cu	13	9	1	57	11	10
Pb	5	4	52	--	--	--
Zn	14	<2	31	--	--	--
Ni	13	4	3	37	20	30
Cr	6	2	5	195	238	216
Co	13	3	3	57	11	10
Rare earth elements (ppm)						
La	34	33	16	--	--	--
Ce	48	38	29	--	--	--
Pr	4.1	2.6	2.8	--	--	--
Nd	14	8.5	11	--	--	--
Sm	1.4	0.75	1.7	--	--	--
Eu	0.5	0.14	0.6	--	--	--
Gd	1.4	0.6	1.1	--	--	--
Tb	0.18	0.1	0.2	--	--	--
Dy	1.5	0.42	0.94	--	--	--
Ho	0.35	0.1	0.3	--	--	--
Er	1.1	0.28	0.93	--	--	--
Tm	0.22	0.05	0.07	--	--	--
Yb	1.6	0.43	1	--	--	--

interpreted to have crystallized at the time of rhyolite emplacement and formation of the breccia pipe. A concentrate of the clearest, most elongate zircon crystals—having length-to-width ratios of greater than 6 to 1—was handpicked for analysis. Unfortunately, even this zircon contains a large component of Precambrian radiogenic lead (table 2), probably present in the cores of old zircon upon which the younger crystals nucleated. Because of this inherited lead component, a precise age for the emplacement of rhyolite cannot be determined from this single analysis. However, the data can be used to approximately date the Precambrian component, which was likely derived from the basement source rock of the rhyolite magma. Assuming the rhyolite is approximately 80 Ma and making a linear extrapolation on a concordia diagram (fig. 7) from that age through the analytical point, an upper intercept age of ~2,600 Ma is determined. Such an age agrees well with other evidence for a Late Archean crystalline basement in southwestern Montana.

Zircon also was separated from three samples of rhyolite collected in the mine area and dated by fission-track methods (table 3) in an attempt to date the emplacement of the sills. Fission-track methods were employed because feldspar and biotite from the sills are too altered for ^{40}Ar-^{39}Ar techniques. Two outcrop samples (80P076 and 80P079) and one drill-core sample (80P074) were selected . A zircon fission-track date of 53.5±10.9 Ma was determined for drill-core sample 80P074, and dates of 53.1±7.2 Ma for outcrop sample 80P076 and 68.9±8.0 for sample 80P079 were determined. The fission-track date of a zircon is reset by temperatures in the range 170°–240°C over geological time scales. These dates obviously do not reflect the time of emplacement of the sills because the sills are older than the 77-Ma lamprophyre bodies that crosscut them.

The zircon fission-track dates may, however, record either localized heating and post-lamprophyre emplacement cooling or regional cooling during Laramide uplift and denudation. The oldest zircon fission-track date (68.9±8.0 Ma) comes from the topographically highest sample, which is consistent with simple uplift and cooling of the area starting in Late Cretaceous time. The topographically lowest samples, less than a kilometer lower, have much younger dates (53±7–10 Ma). If interpreted as evidence of simple uplift and cooling, these data would suggest an uplift rate of about 0.04 m per 1,000 years. This rate is very slow compared to uplift rates of 0.3–3 m per 1,000 years for Laramide uplifts elsewhere in the northern Rocky Mountains (Perry and others, 1992). Clearly, more fission-track samples are needed, at varying elevations, to fully understand our reconnaissance data.

BRECCIA PIPE AND ADJACENT STRATA

Within the pipe and the adjacent country rock, gold is concentrated as electrum in pyrite and within the telluride minerals calaverite, petzite, sylvanite, and krennerite (Porter and Ripley, 1985) in both veins and within zones of

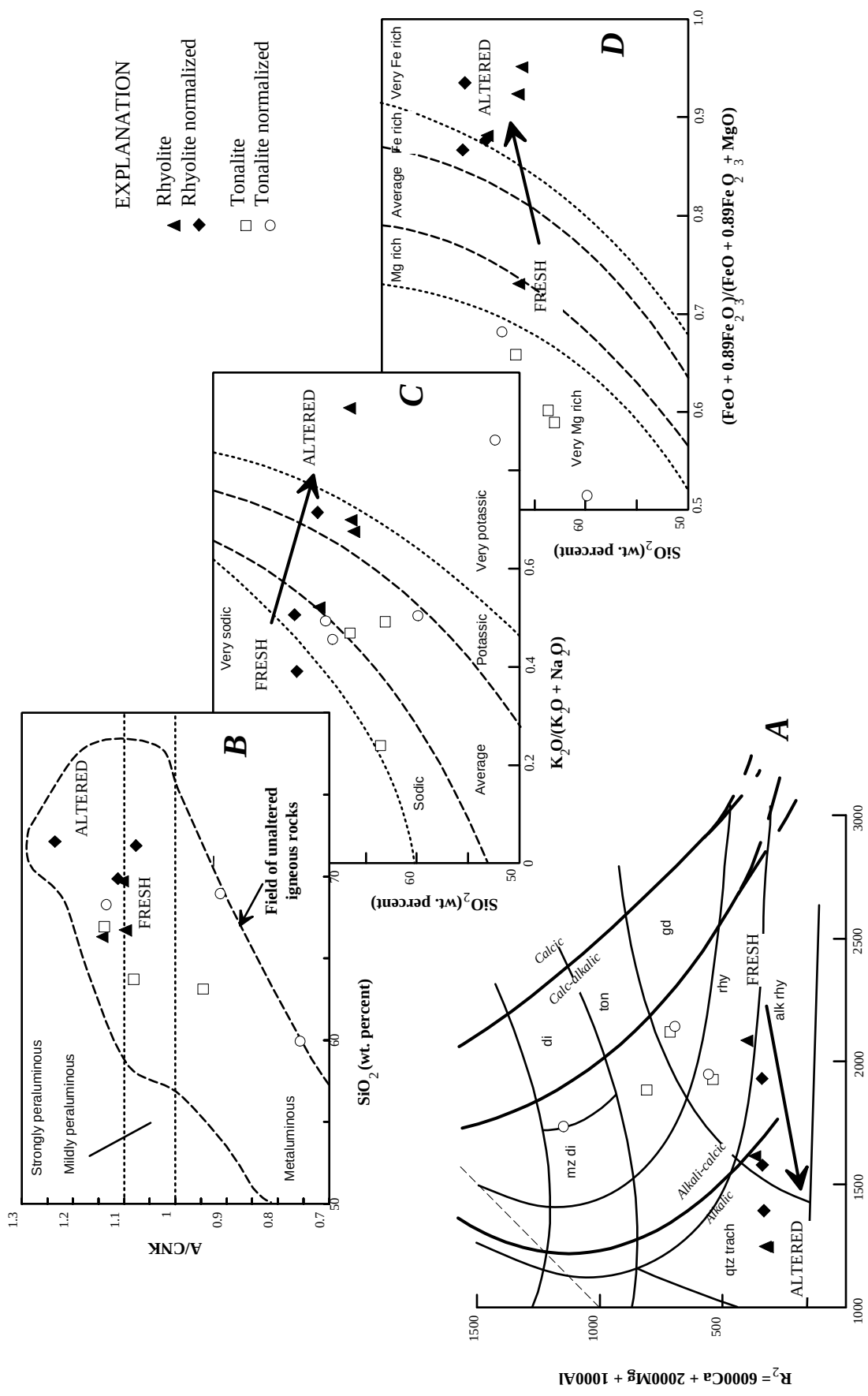

Figure 5. Major-element geochemistry plots of rhyolite and tonalite from the Golden Sunlight mine area. FRESH, rhyolite that is as fresh as we could collect in the vicinity of the mine; ALTERED, hydrothermally altered rhyolite in the vicinity of the mine; normalized, analyses from Swanson (1989), normalized on a volatile-free basis.*A*, R_1 versus R_2 plot (De LaRoche and others, 1980); di, diorite; mz di, monzodiorite; ton, tonalite; gd, granodiorite; rhy, rhyolite (plutonic equivalent is granite); alk rhy, alkali rhyolite (plutonic equivalent is alkali granite); qtz trach, quartz trachyte (plutonic equivalent is quartz syenite). Field of alkalinity modified slightly from DeWitt (1989).*B*, SiO_2 versus A/CNK plot; A/CNK, molar alumina/sum of molar calcium, sodium, and potassium; field of unaltered igneous rocks from DeWitt (unpub. data, 1994).*C*, $K_2O/(K_2O+Na_2O)$ versus SiO_2 plot; *x*-axis is "K number" listed in table 1; field boundaries from DeWitt (unpub. data, 1995). *D*, $(FeO+0.89Fe_2O_3)/(FeO+0.89\ Fe_2O_3+MgO)$ versus SiO_2 plot; *x*-axis is "Fe number" listed in table 1; field boundaries modified from DeWitt (1989).

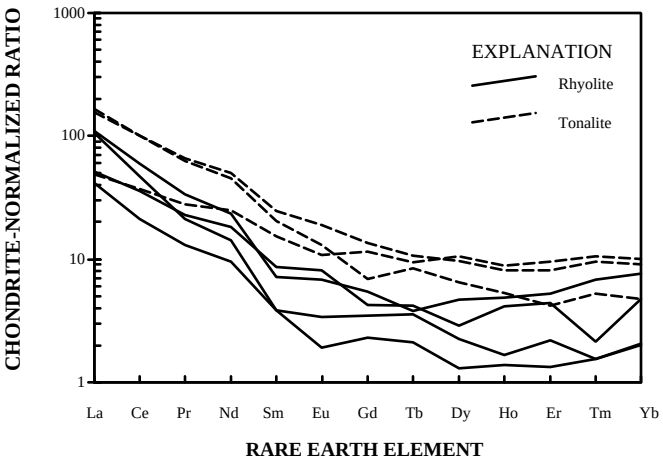

Figure 6. Chondrite-normalized rare-earth-element plot for rhyolite and tonalite in the Golden Sunlight mine area.

hydrothermally altered and silicified rock. Early quartz-pyrite-hematite veins (stage 1a of Porter and Ripley, 1985) are superseded by a period of copper-bismuth veins, some of which contain electrum (stage 1b). Lead-zinc veins (stage 2), tellurium-rich veins (stage 3), and late, barren barite-dolomite-magnesite veins (stage 4) complete the mineralizing process. Within the pipe, quartz, sericite, barite, and potassium feldspar are the common gangue. Magnesite is locally abundant near late mafic dikes (Alexander, 1955; Lindquist, 1966; Robinson, 1963; Schmidt and others, 1988, 1989; Tilling and others, 1968). Fragments of sedimentary rocks are typically bleached, silicified, and replaced by pyrite on their margins or along bedding planes. Secondary sericite is a common gangue in both the rhyolite and wallrocks. Much of the pyrite, hematite, chalcopyrite, and sphalerite is concentrated in the matrix, between fragments.

Deep in the pipe, molybdenite is volumetrically significant. Pyrite, hematite, and molybdenite in the deep parts of the pipe are concentrated in the groundmass of the rhyolite porphyry, between phenocrysts of oligoclase and albite. These early sulfide minerals also are cut by veinlets of quartz-pyrite-molybdenite-barite, and the groundmass and phenocrysts are silicified and replaced by lesser amounts of pyrite. The pipe is probably positioned above a hypabyssal stock related to an alkalic porphyry molybdenum system. Knowledge of the timing of emplacement of the breccia pipe may aid in refining exploration models for this type of deposit.

Hydrothermal minerals related to gold deposition proved difficult to date at the Golden Sunlight mine. Sericite from altered rhyolite was dated by the ^{40}Ar-^{39}Ar technique, but the results, reported at the end of the following section, are ambiguous. Therefore, we analyzed the lead isotopic composition of both unaltered and altered strata of the Belt Supergroup and altered and mineralized rhyolite in the pipe in order to limit the age of alteration and mineralization. We report those results in the following section.

CHRONOLOGY OF ALTERATION AND MINERALIZATION

An investigation of the lead isotope systematics of altered and unaltered sedimentary and igneous rock from the vicinity of the Golden Sunlight mine was undertaken in order to potentially determine: (1) the extent and nature of hydrothermal alteration, (2) the source of the lead in the rocks and ores, and (3) the approximate age of mineralization. Ideally, strata of the Belt Supergroup that shared a common initial lead isotopic composition and existed undisturbed as closed systems to U, Th, and Pb would have isotopic ratios that plot along ~1,400-Ma isochrons on $^{238}U/^{204}Pb$ versus $^{206}Pb/^{204}Pb$ and $^{232}Th/^{204}Pb$ versus $^{208}Pb/^{204}Pb$ diagrams. On the other hand, complete isotopic homogenization of preexisting lead plus any new lead introduced at the time of hydrothermal activity would serve to reset the chronometers and, if subsequently remaining closed systems, provide isochron ages that reflect the mineralization event. Incomplete retention of U, Th, or Pb, or inhomogeneity in initial lead isotopic composition might prevent calculation of precise ages but would still give some useful information about the general timing and conditions of mineralization.

Seven whole-rock and one pyrite sample defined as altered and three whole-rock samples defined as unaltered (G.A. Desborough, written commun., 1993) were analyzed for their U, Th, and Pb concentrations and Pb isotopic composition (table 4). Of the altered whole-rock samples, five (89C16-586.5′, 169-489′, 115-743′, 6100′ level, and 88C1-442.3′) are sericitized and (or) potassium-metasomatized equivalents of the LaHood Formation and contain cross-cutting quartz-pyrite veinlets and (or) disseminated pyrite. The other two altered whole-rock samples are rhyolite—one slightly altered with cross-cutting quartz-pyrite veinlets (90C6-2300′) and the other extensively sericitized and potassium metasomatized and containing abundant disseminated pyrite (G-010334). Pure pyrite separated from a vein in the slightly altered rhyolite (90C6-2300′PY) was also analyzed. The three unaltered whole-rock samples are black shale (89C10-585.9′ and St. Paul Gulch) and rhythmically banded

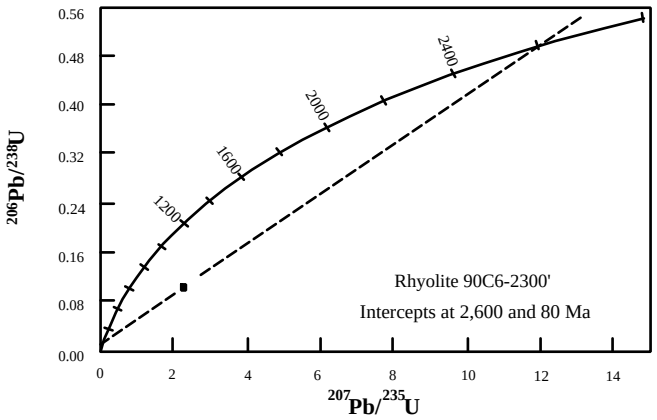

Figure 7. Concordia diagram for zircon from rhyolite (sample 90C6-2300′), Golden Sunlight mine.

Table 2. U-Th-Pb analytical data for zircon from rhyolite (sample 90C6-2300′), Golden Sunlight mine, southwestern Montana.

[Uncertainty in analytical data is calculated in the manner suggested by Ludwig (1991a); uncertainty in date (±2 sigma) is an estimated analytical uncertainty calculated according to Ludwig (1991b). Analyses by R.E. Zartman and Loretta Kwak]

Sample (mesh size)	U (ppm)	Th (ppm)	Pb (ppm)	Atomic composition of lead*				$^{206}Pb/^{238}U$ [Date (Ma)]	$^{207}Pb/^{235}U$ [Date (Ma)]	$^{207}Pb/^{206}Pb$ [Date (Ma)]	$^{208}Pb/^{232}Th$ [Date (Ma)]
				^{204}Pb	^{206}Pb	^{207}Pb	^{208}Pb				
90C6-2300' (–200+400)	524.8	382.4	57.96	0.0231	78.99	13.07	7.915	0.10098 [620±2]	2.2522 [1198±4]	0.16176 [2474±2]	0.01215 [244±2]

*Laboratory blank of 30 picograms lead with isotopic composition $^{206}Pb/^{204}Pb$ = 18.7, $^{207}Pb/^{204}Pb$ = 15.6, $^{208}Pb/^{204}Pb$ = 38.2 removed. No common lead correction has been applied to these ratios. Common lead correction used for zircon age calculations: $^{206}Pb/^{204}Pb$ = 14.31, $^{207}Pb/^{204}Pb$ = 14.94, $^{208}Pb/^{204}Pb$ = 33.99.

Table 3. Fission-track analytical data for zircon from rhyolite samples, Golden Sunlight mine area, southwestern Montana.

[Samples prepared for dating following the procedures of Naeser (1978). Irradiation performed in the U.S. Geological Survey TRIGA reactor with NBS-SRM 612 glass as a monitor. Ages calculated by the "zeta calibration" procedure of Hurford and Green (1983) using an experimentally determined zeta factor for zircon of 331.5±7.6 (1-sigma standard deviation). The number of tracks counted appears in parentheses under the corresponding track density]

Sample no.	Fossil track density (# counted)	Induced track density (# counted)	Monitor track density (10^6 tr/cm) (# counted)	Grains counted	Date (Ma)	95 percent confidence level (±)
80PO74	5.80 (850)	2.75 (403)	0.173 (1948)	7	53.5	10.9 *
80PO76	4.22 (732)	2.27 (394)	0.173 (1948)	6	53.1	7.2
80PO79	4.47 (1283)	1.85 (531)	0.173 (1948)	9	68.9	8.0

* In this determination, grain-to-grain variance is greater than can be accounted for by Poisson variability. Date calculated from weighted mean densities (fossil and induced) and the "±" from observed scatter.

siltite(?) (89C16-860.2′) of the LaHood Formation, all of which are devoid of secondary silicate minerals or hydrothermally introduced pyrite. These data together with two previously published analyses of presumably unaltered LaHood Formation from ~10 km southeast of the Golden Sunlight mine (Zartman, 1992) are presented in table 4.

The unaltered LaHood Formation samples can be compared to 1,400-Ma reference isochrons on $^{238}U/^{204}Pb$ versus $^{206}Pb/^{204}Pb$, $^{235}U/^{204}Pb$ versus $^{207}Pb/^{204}Pb$, and $^{232}Th/^{204}Pb$ versus $^{208}Pb/^{204}Pb$ diagrams constructed through initial $^{206}Pb/^{204}Pb$, $^{207}Pb/^{204}Pb$, and $^{208}Pb/^{204}Pb$ ratios of 16.20, 15.40 and 35.90, respectively (figs 8*A*, 8*B*, and 8*C*). These initial isotopic ratios were chosen as approximating the composition of much of the Belt Basin at the beginning of Belt Supergroup deposition (Zartman and Stacey, 1971). A close fit of the data to such isochrons might be taken as evidence for a relatively undisturbed condition of the unaltered rocks since their deposition. However, Zartman (1992) demonstrated that samples 12 and 13 from the Helena embayment of the Belt Basin do deviate appreciably from the above initial ratios, which he found to mainly characterize the more open Belt Basin to the west. Indeed, the scatter from the isochrons shown by the uncorrected data for these two samples—particularly manifest in the $^{235}U/^{204}Pb$ versus $^{207}Pb/^{204}Pb$ system—largely can be explained by the peculiar initial isotopic composition of the LaHood Formation. Accordingly, substantial corrections to at least samples 12 and 13 are needed in order to compare their positions to the 1,400-Ma isochrons (figs. 8*B*, 8*C*). Whether such corrections should also be applied to the other samples is not known, but initial lead systematics similar to those identified by Zartman (1992) would not improve the linearity of the unaltered array. Sample 11, the only other sample collected at a distance greater than 1 km from the Golden Sunlight mine, already plots significantly below the reference isochrons on the $^{238}U/^{204}Pb$ versus $^{206}Pb/^{204}Pb$ and $^{235}U/^{204}Pb$ versus $^{207}Pb/^{204}Pb$ diagrams (figs. 8*B*, 8*C*), so any downward correction of the point would further displace it from the reference isochron. Of course, sample 11 was itself collected from a small, abandoned mine adit and may have been

Table 4. Lead isotopic composition of rocks in the Golden Sunlight mine area, southwestern Montana.

[First part of hyphenated sample number refers to drill-hole number; second part refers to depth from which sample was taken. St. Paul Gulch, JC-1, and JC-2 are surface samples. Analyses by R.E. Zartman and Loretta Kwak]

Sample number	U (ppm)	Th (ppm)	Pb (ppm)	$^{206}Pb/^{204}Pb$	$^{207}Pb/^{204}Pb$	$^{208}Pb/^{204}Pb$
89C10-585.9′			330	17.852	15.608	37.418
89C16-860.2′	3.42	10.45	13.70	17.711	15.457	37.674
89C12-586.5′	5.72	8.63	8.06	18.377	15.541	37.581
169-489′	5.08	7.15	28.65	17.848	15.542	37.763
115-743′	3.88	9.73	4.66	18.450	15.531	38.330
6100′ level	6.89	21.77	220.20	17.770	15.514	37.751
88C1-442.3′	3.37	7.04	13.49	18.051	15.547	37.874
90C6-2300′	1.31	0.58	3.06	18.161	15.538	38.045
90C6-2300′PY	0.46	0.02	76.66	17.786	15.494	37.833
G-010334	1.34	1.40	8.39	18.009	15.561	37.910
St. Paul Gulch	5.86	10.05	14.64	20.143	15.778	38.900
JC-1	0.99	3.38	18.30	17.878	15.878	37.063
JC-2	0.94	2.99	5.44	18.989	15.867	37.925

Sample descriptions

89C10-585.9′	LaHood Formation, unaltered(?) black shale; Pb determined by energy-dispersive X-ray.
89C16-860.2′	LaHood Formation, unaltered rhythmically banded siltite.
89C12-586.5′	LaHood Formation, altered rhythmically banded siltite containing cross-cutting quartz-pyrite veinlets.
169-489′	LaHood Formation, laminated, K-rich, pyritic rock with fine-grained orthoclase as dominant mineral.
115-743′	LaHood Formation, altered with pyrite, sericite, quartz, orthoclase, and albite.
6100′ level	LaHood Formation, open pit of mine, bedded authigenic feldspar.
88C1-442.3′	LaHood Formation, altered with abundant pyrite and mineralogy similar to 115-743′.
90C6-2300′	Slightly altered rhyolite containing cross-cutting quartz-pyrite veinlets.
90C6-2300′PY	Pyrite from quartz-pyrite veinlets cutting rhyolite of sample 90C6-2300′.
G-010334	Altered rhyolite containing abundant pyrite, quartz, orthoclase, albite, and sericite.
St. Paul Gulch	LaHood Formation, black shale from abandoned mine adit.
JC-1	LaHood Formation, conglomeratic arkose, Jefferson Canyon, 10 km southeast of Golden Sunlight mine.
JC-2	LaHood Formation, arkose, Jefferson Canyon, 10 km southeast of Golden

disturbed by hydrothermal alteration related or unrelated to mineralization at Golden Sunlight mine. Based on this limited data set, we conclude that quite likely all rocks within and immediately adjacent to the Golden Sunlight mine underwent at least partial homogenization of their lead isotopes. Whether such effects extended as far as 1 km from the mine area is uncertain, but our limited evidence would suggest that, beyond that distance, lead isotopes were not disturbed by the mineralization event.

Calculation of best-fit lines for the eight altered samples on $^{232}Th/^{204}Pb$ versus $^{208}Pb/^{204}Pb$ and $^{238}U/^{204}Pb$ versus $^{206}Pb/^{204}Pb$ diagrams (figs. 8*A* and 8*C*) produces isochrons of much shallower slope than the 1,400-Ma reference isochrons. Particularly noteworthy is the model 3 isochron age of 84±18 Ma obtained for the $^{238}U/^{204}Pb$ versus $^{206}Pb/^{204}Pb$ plot (fig. 8*C*) using the ISOPLOT program of Ludwig (1991b). Model 3 ages assign scatter in excess of analytical uncertainty to variation in initial lead isotopic composition, an assumption that would be appropriate if complete homogenization had not taken place at the time of mineralization. The good agreement between this isochron age and other attempts to date the time of rhyolite intrusion and associated mineralization suggests to us that the altered samples do indeed reflect a largely reset chronometer. Considerably greater scatter of points from a linear array for the $^{232}Th/^{204}Pb$ versus $^{208}Pb/^{204}Pb$ plot (fig. 8*A*) results in a more poorly defined model 3 isochron age of 53± 83 Ma.

In considering the source of the lead associated with the gold mineralization, it is useful to compare the isotopic composition of average unaltered and average altered LaHood Formation lead at the time of mineralization. A match between the lead in both the unaltered and altered rock would support a hypothesis whereby most of this metal in the hydrothermally mineralized mine area was scavenged from the immediately surrounding country rock. Different isotopic compositions, on the other hand, would demand that either (1) the lead, if scavenged, does not represent an isotopically unbiased sampling of country rock, or (2) another source of lead, such as lower crustal rock that gave rise to the magma for the rhyolite, was at least partially involved in the mineralization process. Unweighted average lead isotope ratios (and 2σ uncertainties), calculated for the five unaltered samples and corrected to 80 Ma, yield $^{206}Pb/^{204}Pb$ = 18.38±1.86, $^{207}Pb/^{204}Pb$ = 15.70±0.32, $^{208}Pb/^{204}Pb$ = 37.8±1.24, but the presumably more appropriate weighted average ratios—dominated by sample 89C10-585.9′—yield $^{206}Pb/^{204}Pb$ = 17.89±0.47, $^{207}Pb/^{204}Pb$ = 15.61±0.08, $^{208}Pb/^{204}Pb$ = 37.43±0.31. The isochrons fit through the eight altered samples (figures 1and 2 and an equivalent $^{206}Pb/^{204}Pb$ vs. $^{235}U/^{204}Pb$ diagram) give initial lead-ratio intercepts of $^{206}Pb/^{204}Pb$ = 17.79±0.06, $^{207}Pb/^{204}Pb$ = 15.53±0.02, and $^{206}Pb/^{204}Pb$ = 37.79±0.19. Although the two sets of ratios are in modest agreement and, therefore, appear to permit the country-rock-source hypothesis, the present data are insufficient to accurately constrain the isotopic composition of the LaHood Formation as it may have existed at the time of rhyolite intrusion and mineralization.

Especially sensitive in making an isotopic match is $^{207}Pb/^{204}Pb$, which has a distinctly lower value for altered samples than unaltered samples. It can be argued, of course, that this mismatch is a reflection of biased sampling that has omitted low-U/Pb unaltered rocks. If the LaHood Formation and other Beltian rocks in the vicinity of the Golden Sunlight mine behaved essentially as closed systems with a uniform initial isotopic composition prior to Late Cretaceous alteration, an isochronous relationship would have existed between $^{206}Pb/^{204}Pb$ and $^{207}Pb/^{204}Pb$. Assuming the initial ratios at the time of LaHood deposition to be those determined by Zartman and Stacey (1971), permissible "close-approach" values of $^{206}Pb/^{204}Pb$ = 17.75 and $^{207}Pb/^{204}Pb$ = 15.54 do compare very well with the initial lead calculated for the altered samples.

An attempt was made to date fine-grained, hydrothermal sericite associated with pyrite and gold in the Golden Sunlight orebody by the ^{40}Ar–^{39}Ar technique. Sericite was separated from an altered and mineralized rhyolite sill (sample 88GS-11). Because the separation process involved partial digestion in HCl and HNO_3, the analyzed mineral (table 5) may have been slightly chemically altered . The resulting spectra (fig. 9) is disturbed and does not record a simple igneous or cooling history. The largest two gas fractions, with dates of 93 and 95 Ma, account for 66 percent of the gas from the sample, but the spectra declines in age up to the highest temperature gas fractions. We are hesitant to place much emphasis on the dates from 93 to 95 Ma because of the shape of the entire spectra.

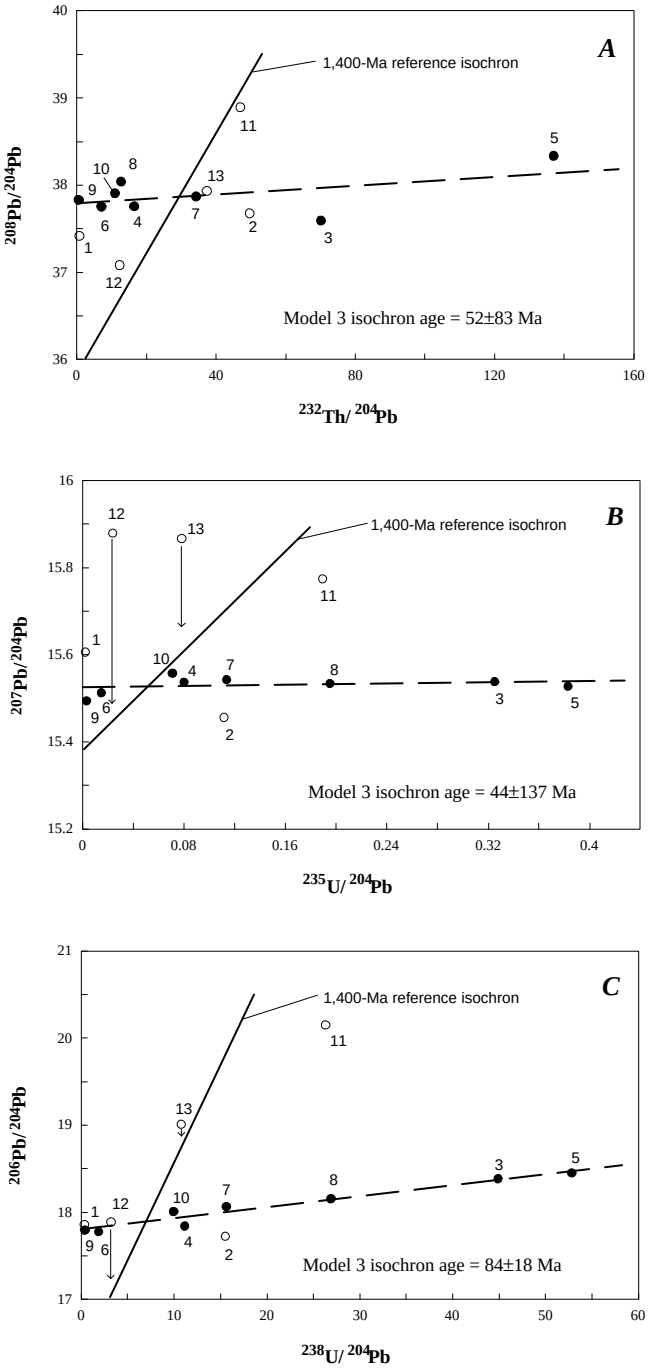

Figure 8. Lead evolution diagrams for samples from the Golden Sunlight mine area. Filled circles represent altered samples; open circles represent unaltered samples; 1,400-Ma reference isochron shown by thick, steeply inclined line in all diagrams. *A*, $^{232}Th/^{204}Pb$ versus $^{208}Pb/^{204}Pb$ plot. Model 3 isochron constructed for eight altered samples. *B*, $^{235}U/^{204}Pb$ versus $^{207}Pb/^{204}Pb$ plot. Model 3 isochron constructed for eight altered samples; arrows indicate direction that samples 12 and 13 should move to be corrected for lack of equilibration at 1,400 Ma. *C*, $^{238}U/^{204}Pb$ versus $^{206}Pb/^{204}Pb$ plot. Model 3 isochron constructed for eight altered samples; arrows indicate direction that samples 12 and 13 should move to be corrected for lack of equilibration at 1,400 Ma.

Table 5. ^{40}Ar-^{39}Ar data for sericite from rhyolite (sample 88GS-11), Golden Sunlight mine area, southwestern Montana.

[$^{40}Ar_c$, radiogenic ^{40}Ar corrected for mass discrimination and induced ^{40}Ar; ^{39}Arc, ^{39}Ar corrected for mass discrimination and radioactive decay; $\%^{40}Ar_{rad}$, percentage of radiogenic ^{40}Ar. Sample weight = 75 mg; J = 0.007283±0.25 percent. ^{40}Ar-^{39}Ar analyses by Ross Yeoman and L.W. Snee]

Temperature (°C)	$^{40}Ar_c$	$^{39}Ar_c$	F	% $^{40}Ar_{rad}$	% $^{39}Ar_{total}$	Date (Ma)	2 sigma uncertainty (Ma)
400	14.59479	2.25239	6.480	92.7	24.7	83.19	0.35
500	21.62990	2.89221	7.479	96.9	31.7	95.68	0.40
600	23.34362	3.18826	7.322	93.2	34.9	93.72	0.39
650	5.13684	0.70804	7.255	83.2	7.8	92.89	0.39
700	0.23069	0.03309	6.972	45.5	0.4	89.36	0.69
750	0.22523	0.04056	5.554	41.1	0.4	71.53	0.39
800	0.00764	0.00309	2.475	3.8	0.01	32.23	9.33
900	0.02506	0.00195	12.821	11.4	0.01	161.04	16.14
1000	0.01111	0.00158	7.032	8.3	0.01	90.10	10.30
1375	0.07121	0.00386	18.463	35.0	0.01	227.59	6.83
Total gas No plateau		7.1054			91.62	0.65	

INTERMEDIATE TO FELSIC PLUTONIC ROCKS

Small stocks and plugs cut the Belt Supergroup rocks in the mine area. Their contacts with rhyolite sills and lamprophyre are poorly exposed, but the plutonic rocks appear to cut all other rock units (figs. 1 and 4). In all likelihood, these intrusive rocks are related to emplacement of either the Boulder batholith or to intrusive activity associated with the Elkhorn Mountains Volcanic field.

PETROLOGY AND CHEMISTRY

These rocks do not appear to be genetically related to the rhyolite sills, as evidenced by their major- and minor-element geochemistry. The intrusive rocks have seriate, hypidiomorphic texture and contain moderate amounts of granophyre-myrmekite. Primary minerals, in decreasing percentages, are plagioclase, alkali feldspar, quartz, hornblende, biotite, and traces of clinopyroxene.

Chemically, these plutonic rocks range from monzodiorite to granite, but average tonalite in composition (fig. 5*A*). All unaltered rocks are alkali-calcic (fig. 5*A*), metaluminous to mildly peraluminous (fig. 5*B*), average to sodic (fig. 5*C*), and Mg rich to very Mg rich (fig. 5*D*). Where altered, the tonalitic rocks are strongly peraluminous (fig. 5*B*).

The suite of rocks have REE patterns (fig. 6) that are LREE enriched and have La/Yb_{CN} ratios of 17–34. HREE parts of the profiles are slightly concave upward. No europium anomalies are noted. The patterns plot generally above those for rhyolite sills in the area.

LAMPROPHYRES

Numerous lamprophyre sills and dikes cut the gold-mineralized breccia pipe at the Golden Sunlight mine and Middle Proterozoic sedimentary rocks in the surrounding area. Sills are more numerous than dikes. Lamprophyre bodies range from several centimeters to several meters thick but normally do not exceed 3 m. Many sills and dikes are not shown on figure 1 due to their small size. Contact-metamorphic effects from the lamprophyres are generally minor to nonexistent. The lamprophyre bodies are described in detail in this report because of their unusual chemistry, alteration, and possible tie to late stages of mineralization.

PETROLOGY OF CO_2-POOR LAMPROPHYRE

Lamprophyre dikes having low concentrations of CO_2 are dark gray where fresh and distinctly porphyritic. Large phenocrysts, averaging 4–10 mm across, of olivine and clinopyroxene are set in a fine-grained groundmass that also contains smaller phenocrysts of olivine and clinopyroxene (fig. 10). In decreasing amounts, the groundmass (fig. 11) is composed of clinopyroxene, sanidine, albite, biotite, opaque minerals, and apatite (fig. 11). Swanson (1989) noted that the lamprophyres average 72 percent fine- and intermediate-grained groundmass and 28 percent coarse-grained phenocrysts (average of 10 samples).

Pale-green, euhedral, strongly zoned diopsidic augite is the main coarse-grained phenocryst (fig. 12). Such large phenocrysts are as much as 1 cm or more in maximum dimension, but phenocrysts as small as 4 mm are present. Many

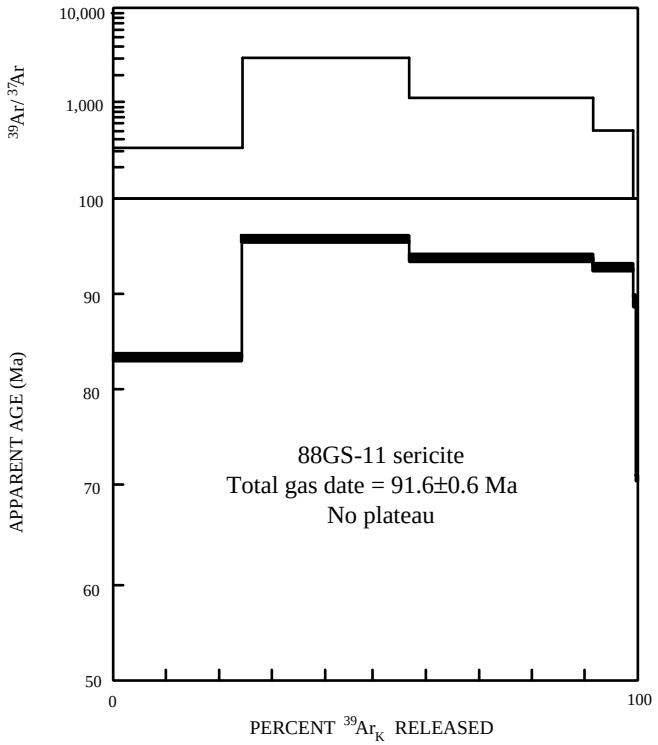

Figure 9. ^{40}Ar-^{39}Ar release spectra for sericite from rhyolite (sample 88GS-11), Golden Sunlight mine.

phenocrysts are strongly resorbed and embayed by groundmass minerals. In some grains, inclusions of carbonate(?) minerals and feldspar are aligned along zone boundaries that are parallel to crystal outlines (fig. 13). Diopsidic augite constitutes 20–25 percent of the coarse-grained phenocrysts and 15–20 percent of the smaller phenocrysts in the groundmass (fig. 14). Augite contains minor amounts of Cr (about 0.5 weight percent in sample 191-939).

Very pale green to colorless, euhedral to subhedral and broken, primarily unzoned forsteritic olivine (about $Fo_{85–90}$) is the second most abundant phenocryst. Most lamprophyres average 7 percent coarse-grained olivine. Some varieties contain as much as 5 percent finer grained phenocrysts, principally in the groundmass. Olivine averages several millimeters across but may be as large as 1–2 cm (fig. 15).

Euhedral, brownish-green biotite (much of it Mg rich) phenocrysts are subordinate to clinopyroxene and olivine and normally do not exceed 2 percent. Biotite may be several centimeters across but is usually 5 mm or less. Phenocrysts are typically embayed by groundmass minerals (fig. 16). Such phenocrysts contain 1,200–2,400 ppm Cr, 650–1,450 ppm Ni, 340–490 ppm V, and 2,100–2,300 ppm Ba (table 6).

The fine-grained (less than 0.01 mm) groundmass is composed of subequal amounts of diopsidic augite and sanidine and lesser amounts of biotite, albite, magnetite and ilmenomagnetite, carbonate minerals, and apatite. In rocks having an extremely fine grained groundmass, large phenocrysts are not embayed or altered on their edges. In rocks having a coarser grained groundmass, diopsidic augite or biotite are surrounded by thin selvages of biotite- and opaque-poor, sanidine-rich material (fig. 17). Diopsidic augite in the groundmass is pale green and euhedral to subhedral (fig. 18). Euhedral to subhedral, lath-shaped sanidine (Carlsbad twinned, low 2V) forms an interstitial mat to surrounding clinopyroxene (fig. 19). Minor amounts of euhedral, albite-twinned albite are associated with sanidine. The volume percent of magnetite for 10 CO_2-poor samples averages 1.5 percent, as determined with a hand-held magnetic susceptibility meter. Magnetite and ilmenomagnetite are disseminated throughout the groundmass. Biotite is present in three morphologies, as coronas of magnetite and ilmenomagnetite (fig. 20), as euhedral elongate grains between sanidine and albite (fig. 19), and as ophitic clots (up to 1 cm across) surrounding clinopyroxene and sanidine (fig. 21). Fine-grained carbonate minerals are interstitial to sanidine laths (fig. 22) and appear to be of primary, magmatic origin. Very fine grained, acicular apatite needles are disseminated through the groundmass but are principally within sanidine grains. Sparse sulfide minerals (chiefly pyrite) are noted (samples 88C3-301.5′, 88GS-8, and 191-173.5′) both in disseminated form and as microveinlets having alteration haloes.

Locally, the lamprophyre dikes are extremely heterogeneous. In one gently dipping dike(?) at the south end of Bull Mountain, the relative percentages of phenocryst minerals are highly variable over a thickness of about 6 ft. No regular pattern of zonation was observed. In certain parts of the body, no megascopic clinopyroxene or olivine are noted and biotite is the principal phenocryst. In other parts, just 1–2 cm away, large crystals (1–2 cm across) of diopsidic augite and subordinate olivine are the dominant phenocrysts and no biotite is visible.

CHEMISTRY OF CO_2-POOR LAMPROPHYRE

W.L. Coppinger and the Golden Sunlight mine staff originally noted the alkalic nature of the dikes, their primitive nature, and spatial association of some areas of high-grade gold in the breccia with the dikes. A study of 17 samples of the lamprophyre (Swanson, 1989) revealed many of the features of the mafic rocks but did not contain analyses for FeO, CO_2, H_2O^+, H_2O^-, or REE. Also, Swanson (1989) leached his samples with dilute HCl prior to analysis and normalized the resulting oxides to 100 percent. However, his normalized results can be used to augment our analyses if care is taken in interpretation of the data. Using the total alkali-silica (TAS) classification scheme of LeBas and others (1986), Swanson (1989) classified the majority of lamprophyres as trachybasalt and potassic trachybasalt (because $Na_2O < K_2O$). Several samples were basaltic andesite (or andesibasalt).

For our study, 19 additional samples were collected, five from the same outcrops as those sampled by Swanson (1989). Agreement between duplicate samples is very good. Chemically, the lamprophyres were subdivided into five

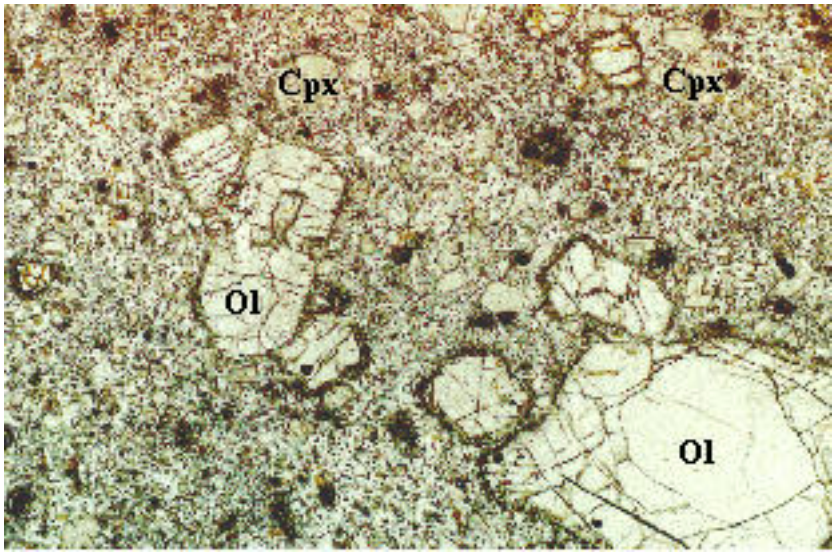

Figure 10. Photomicrograph in plane-polarized light of olivine and clinopyroxene phenocrysts in lamprophyre (sample 88GS-6). Ol, olivine; Cpx, clinopyroxene. Field of view 4.2×3.0 mm.

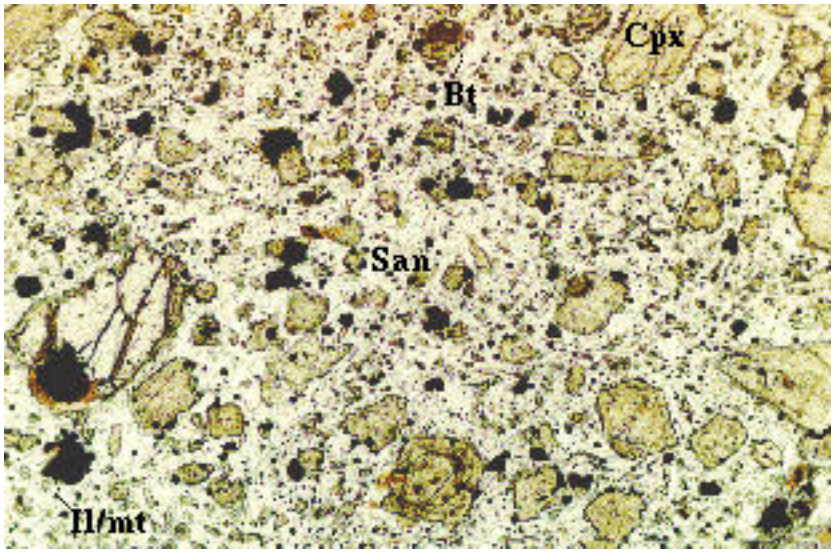

Figure 11. Photomicrograph in plane-polarized light of groundmass texture and minerals in lamprophyre (sample 88GS-3). Cpx, clinopyroxene; San, sanidine; Bt, biotite; Il/mt, ilmenomagnetite. Field of view 1.6×1.1 mm.

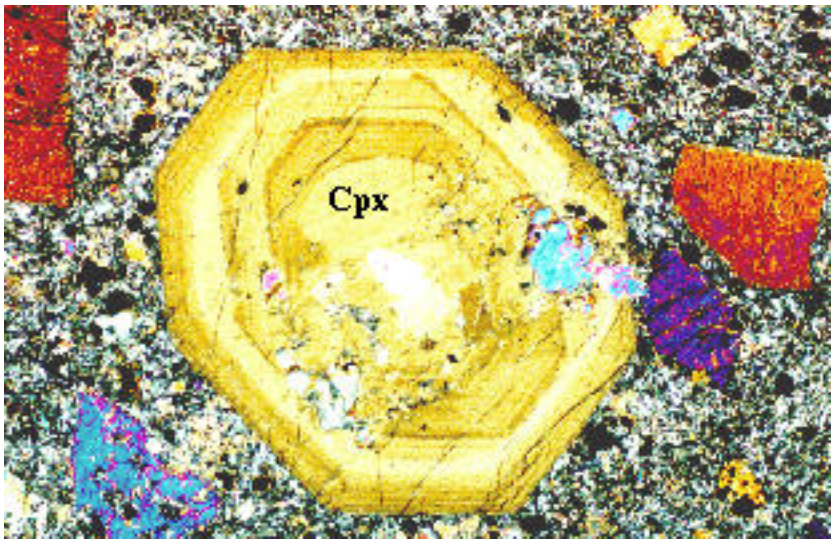

Figure 12. Photomicrograph of strongly zoned clinopyroxene phenocryst in lamprophyre (sample 88GS-5). Cpx, clinopyroxene; crossed nicols. Field of view 4.2×3.0 mm.

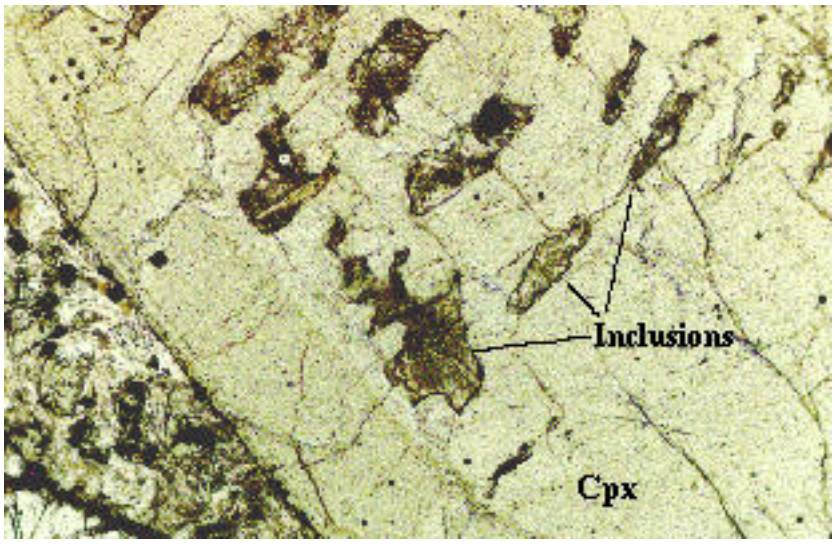

Figure 13. Photomicrograph in plane-polarized light of carbonate mineral(?)- and feldspar-rich inclusions in clinopyroxene phenocryst in lamprophyre (sample 88C3-292′). Cpx, clinopyroxene. Field of view 1.6×1.1 mm.

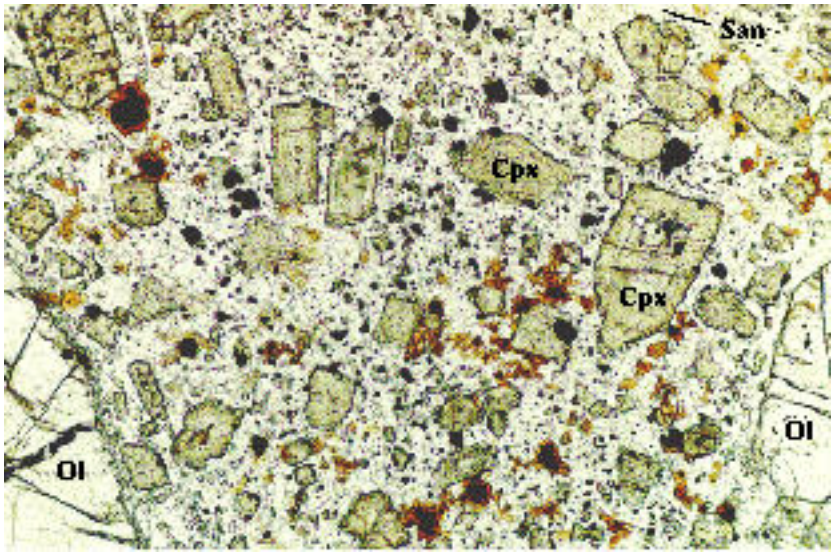

Figure 14. Photomicrograph in plane-polarized light of clinopyroxene grains in groundmass in lamprophyre (sample 88GS-3). Ol, olivine; Cpx, clinopyroxene; San, sanidine. Field of view 1.6×1.1 mm.

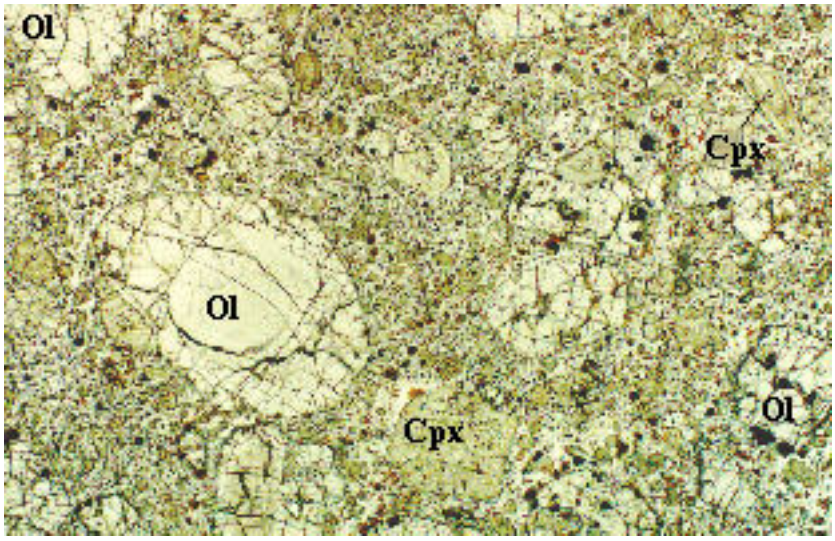

Figure 15. Photomicrograph in plane-polarized light of olivine phenocrysts in lamprophyre (sample 88GS-3). Ol, olivine; Cpx, clinopyroxene. Field of view 8.5×5.8 mm.

informal groups according to their CO_2 concentrations. Group 1 (labeled "lamprophyre 1" on figures) contains less than 2 weight percent CO_2; rocks in this group have not experienced CO_2 metasomatism. Group 2 rocks contain 3–9 percent CO_2, group 3 rocks contain 10–14 percent CO_2, and group 4 rocks contain 15–20 percent CO_2. Analyses from Swanson (1989) are treated as a separate group ("lamprophyre normalized" on figures).

Plots of SiO_2 versus major-element oxides (fig. 23) show much more scatter than would be expected from one cogenetic igneous population. Smooth trends of sample points are not apparent for many major-element oxides. MgO and K_2O versus SiO_2 especially show evidence of more than one population of lamprophyre, as will be discussed in following sections. H_2O concentrations of CO_2-poor lamprophyres are in the field of "common" basic igneous rocks (LeMaitre, 1976) or between there and the field of lamprophyres as defined by Rock (1987). Most trace-element concentrations for the CO_2-poor lamprophyres are similar to values reported for "calc-alkaline" kersantites (Streckeisen, 1979; Rock, 1984, 1989; LeMaitre, 1989).

Chemically, lamprophyres with less than 2 weight percent CO_2 (group 1) are predominantly alkali gabbro (fig. 24*A*) according to the classification of De LaRoche and others (1980). Two are olivine gabbro and one is a gabbro-diorite. Five of the samples from Swanson (1989) also are alkali gabbro. Apparently, the bulk composition of the parental magma was an alkali gabbro to olivine gabbro and was transitional from truly alkalic to alkali-calcic. The samples that plot as gabbro-diorite may represent a population that is distinct from the alkali gabbro, as is shown by their sub-alkalic nature and by their position on subsequent geochemical plots.

Table 6. Minor- and trace-element geochemistry of phlogopitic biotite phenocryst samples from lamprophyre bodies, Golden Sunlight Mine, southwestern Montana.

[All values in ppm, except Na_2O and MnO, which are reported in weight percent (wt %). Analyses by F.E. Lichte by incuction-coupled mass spectrometry]

Element	88C3-301.5′ (average of 3)	88GS-8 (average of 2)
Li	45	45
B	296	4
Na_2O	0.2 wt %	0.58 wt %
Sc	15	11
V	339	486
Cr	2413	1255
MnO	0.0 wt %	0.13 wt %
Co	103	113
Ni	1450	646
Cu	2.0	10.0
Zn	177	114
Ga	59	25
Ge	3.2	0.3
Rb	275	276
Sr	131	100
Zr	9.2	13.8
Cs	7.8	4.68
Ba	2310	2100
Tl	0.5	58.5
Pb	1.7	1.9
Bi	0.2	0.3
Th	0.3	0.2
U	0.1	2.4

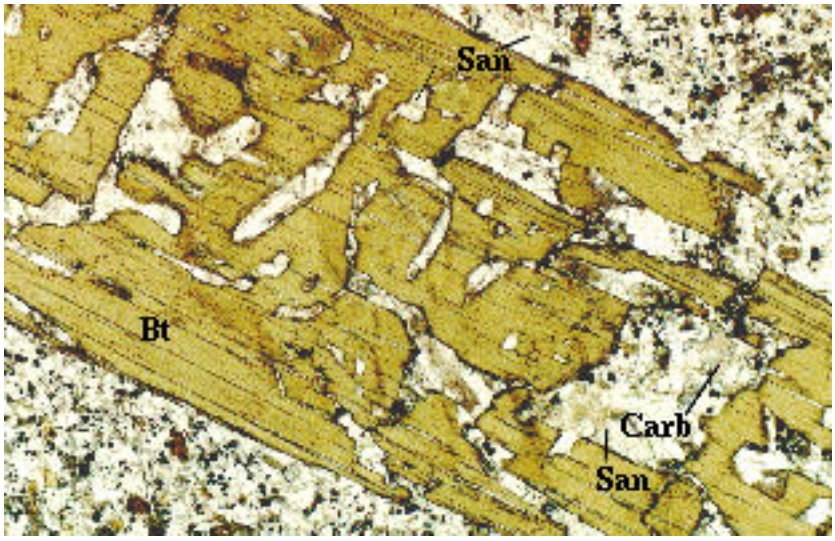

Figure 16. Photomicrograph in plane-polarized light of embayed biotite phenocryst in lamprophyre (sample 115-153.6′). Bt, biotite; San, sanidine; Carb, carbonate minerals. Field of view 4.2×3.0 mm.

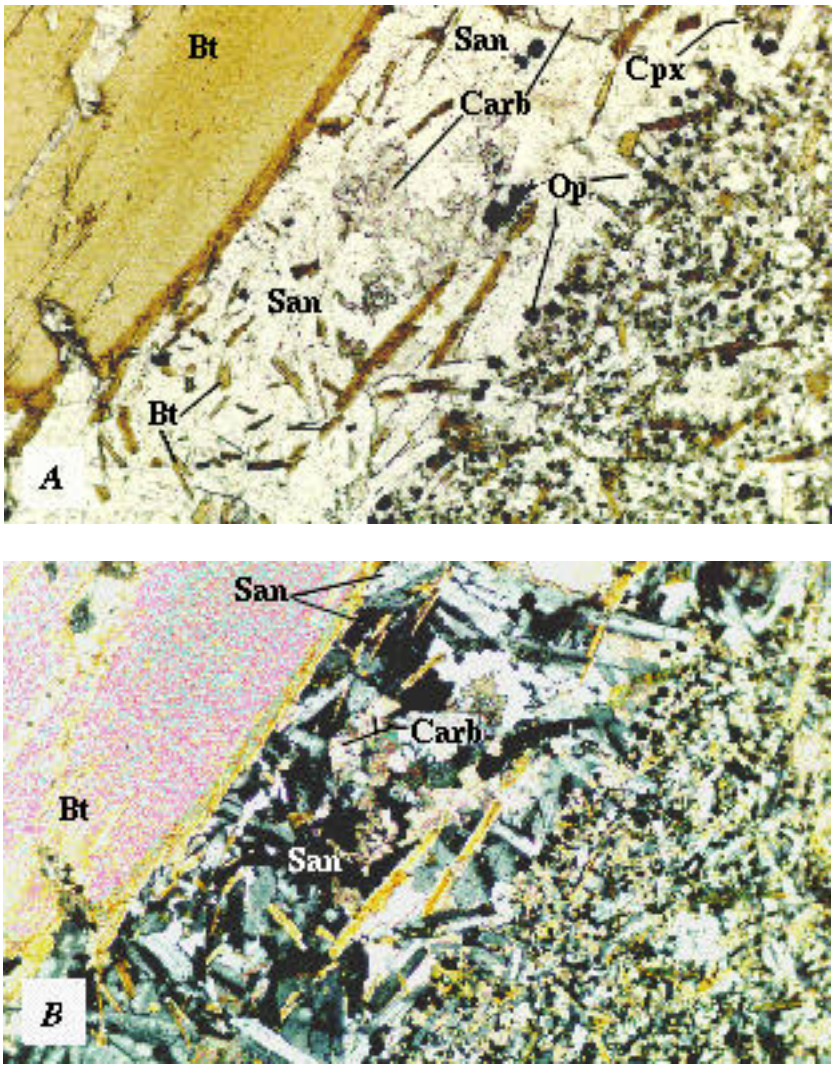

Figure 17. Photomicrographs of biotite phenocryst surrounded by opaque-mineral- and clinopyroxene-poor selvage of groundmass in lamprophyre (sample 189-194.5′). Selvage is nearly pure sanidine, and minor carbonate minerals and apatite. Away from selvage, groundmass contains average concentrations of opaque minerals and clinopyroxene. Bt, biotite; Cpx, clinopyroxene; San, sanidine; Carb, carbonate minerals; Op, opaque minerals. *A*, plane-polarized light; *B*, crossed nicols. Field of view 1.6×1.1 mm.

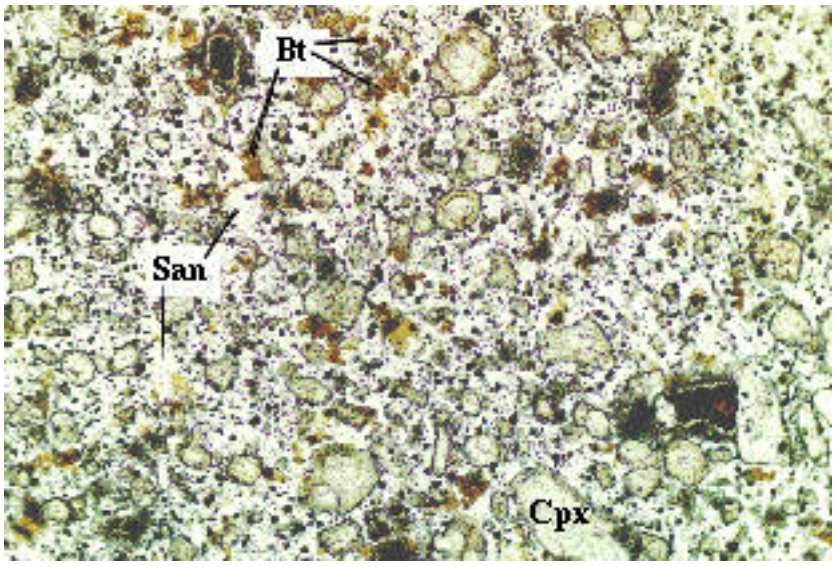

Figure 18. Photomicrograph in plane-polarized light of clinopyroxene in groundmass in lamprophyre (sample 88GS-6). Cpx, clinopyroxene; Bt, biotite; San, sanidine. Field of view 1.6×1.1 mm.

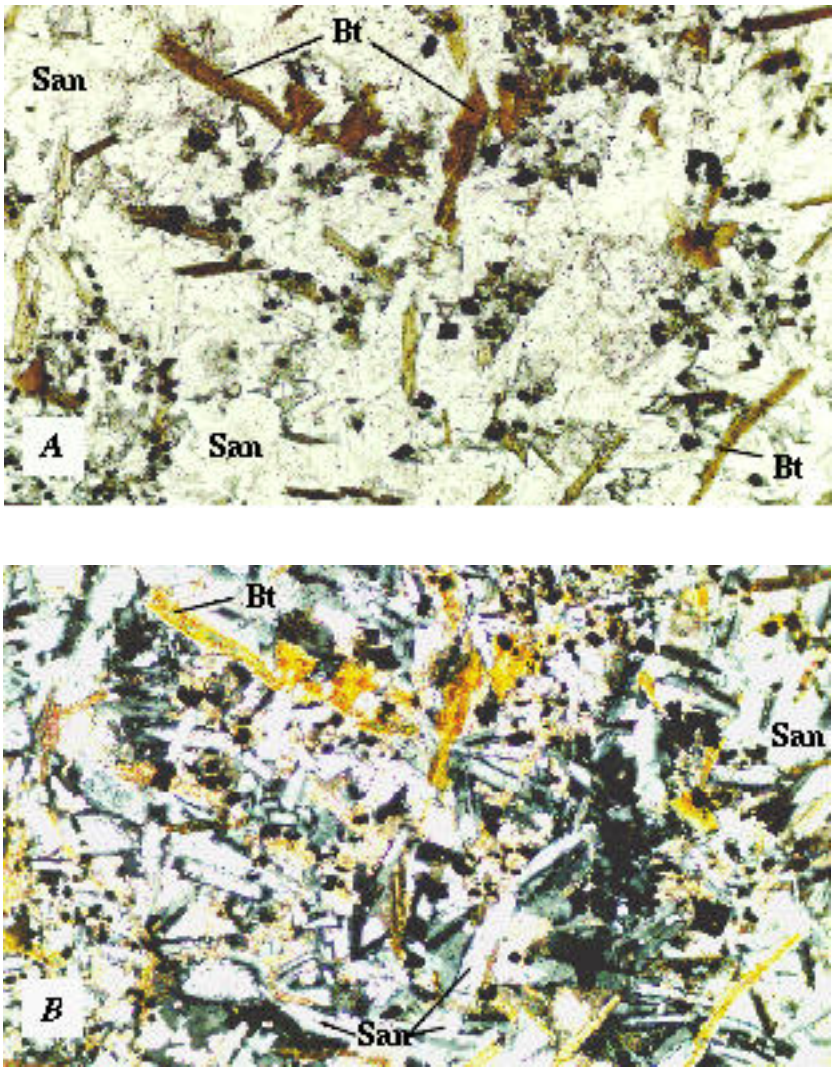

Figure 19. Photomicrographs of intergrown sanidine and biotite in groundmass in lamprophyre (sample 189-194.5′). Bt, biotite; San, sanidine. *A*, plane-polarized light; *B*, crossed nicols. Field of view 1.6×1.1 mm.

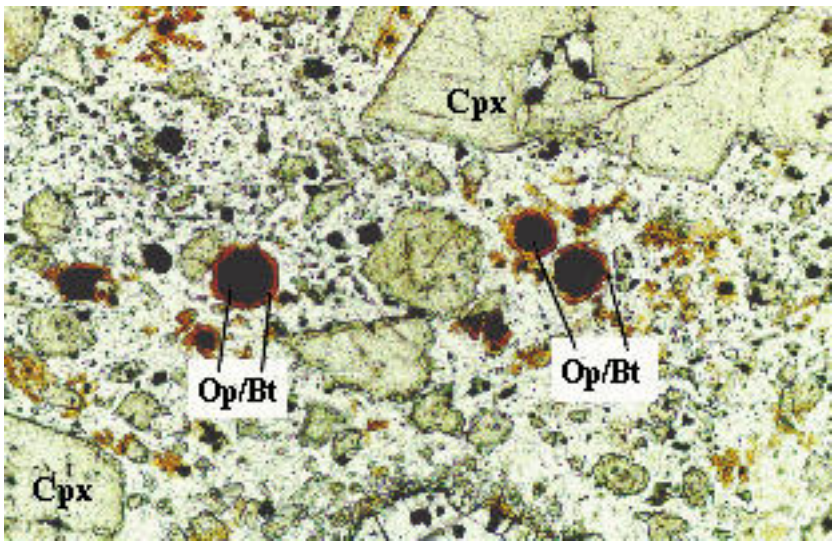

Figure 20. Photomicrograph in plane-polarized light of corona of biotite surrounding opaque mineral in lamprophyre (sample 88GS-3). Op/bt, opaque minerals surrounded by biotite; Cpx, clinopyroxene. Field of view 1.6×1.1 mm.

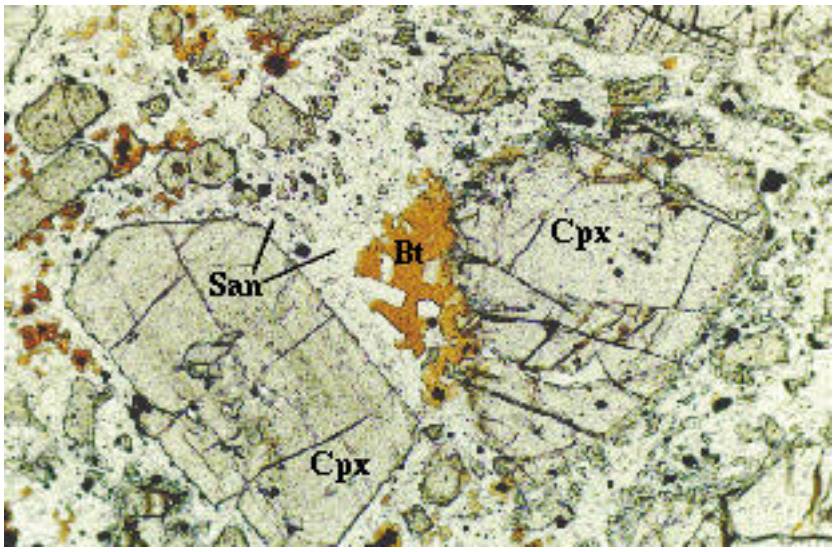

Figure 21. Photomicrograph in plane-polarized light of ophitic biotite in groundmass in lamprophyre (sample 88GS-3). Bt, biotite; Cpx, clinopyroxene; San, sanidine. Field of view 1.6×1.1 mm.

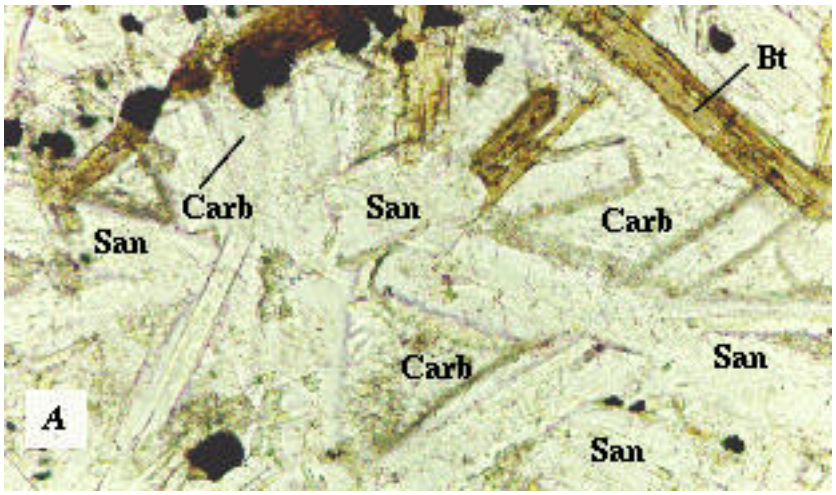

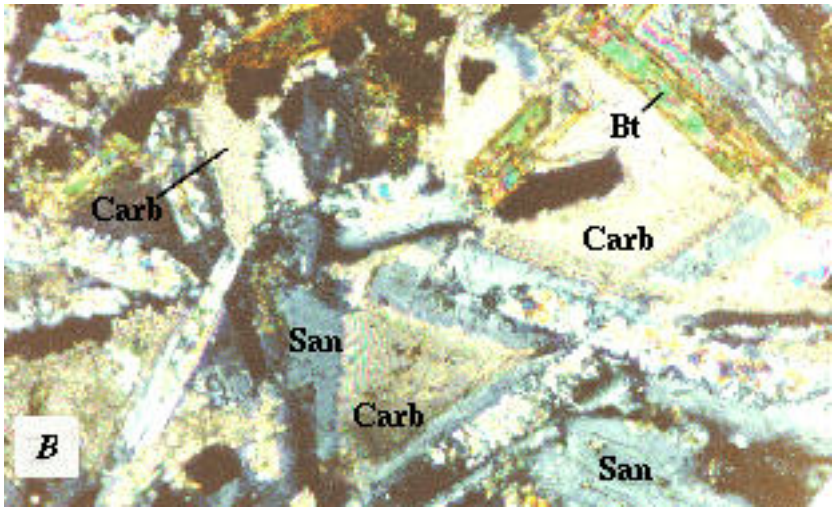

Figure 22. Photomicrographs of fine-grained carbonate mineral interstitial to groundmass sanidine in lamprophyre (sample 189-194.5′). Textural relations indicate that carbonate mineral is not alteration product of other mineral, but is of primary, magmatic origin. Bt, biotite; San, sanidine; Carb, carbonate minerals. *A*, plane-polarized light; *B*, crossed nicols. Field of view 0.4×0.25 mm.

The CO_2-poor alkali gabbro are metaluminous and plot in the field of unaltered igneous rocks (fig. 24*B*). Olivine gabbro and gabbro-diorite plot to the right of the alkali gabbro, outside the field of unaltered igneous rocks. Placement of the boundary of unaltered igneous rocks at these low SiO_2 concentrations is problematic—we do not place much emphasis on the fact that the olivine gabbro and gabbro-diorite plot outside the field boundary. All the lamprophyre bodies are very potassic (fig. 24*C*), but the olivine gabbro and gabbro-diorite are the least enriched in potassium. The alkali gabbro bodies have no strong iron enrichment (fig. 24*D*), but the olivine gabbro and gabbro-diorite are distinctly Mg rich. The "average" nature of the alkali gabbro is partly a function of their high concentrations of Fe_2O_3.

Are the olivine gabbro and gabbro-diorite more primitive than the alkali gabbro? Determination of magnesium numbers (Mg number) can aid in the classification of lamprophyres, but care must be exercised in interpretation of the data, as Mg number can be calculated in a number of ways. If Mg number is calculated as molar $Mg/(Mg+Fe^{2+})$, lamprophyres of group 1 range from 0.72 to 0.80. Alkali gabbro have lower Mg number (0.73 average) than gabbro-diorite (0.75). If Mg number is calculated as molar $Mg/(Mg+0.8(FeO_{total}))$, group 1 lamprophyres range from 0.63 to 0.77. Again, alkali gabbro have lower Mg number (0.64 average) than gabbro diorite (0.73 average). Frey and others (1978) suggest that primitive magmas that were in equilibrium with mantle peridotite and underwent little, if any, differentiation prior to solidification should have Mg number of 0.67 to 0.75. Rhodes (1981) favors the range 0.65–0.80. If Mg number is calculated as $Mg/(Mg+Fe^{2+})$, the lamprophyres appear primitive; if Mg number is calculated as $Mg/(Mg+0.8(Fe_{total}))$, the lamprophyres do not. We favor the interpretation that the lamprophyres may be related to primitive magmas but that the alkali gabbro bodies do not represent truly primitive magmas. The gabbro-diorite does, however, appear to be related to a primitive magma.

Concentrations of the compatible elements, Cr, Ni, Co, and Sc are also indicators of the primitive nature of magmas. Alkali gabbro of group 1 averages 337 ppm Cr, 87 ppm Ni, 49 ppm Co, and 34 ppm Sc. Gabbro-diorite of group 1 averages 640 ppm Cr, 243 ppm Ni, 49 ppm Co, and 28 ppm Sc. Rhodes (1981) suggested that primitive magmas having high Mg number should have concentrations of 200–500 ppm Cr, 90–700 ppm Ni, 25–80 ppm Co, and 15–30 ppm Sc. Gabbro-diorite has the requisite concentrations of all compatible elements, but Ni concentrations for alkali gabbro to olivine gabbro are slightly low. A plot of Mg number (calculated in both ways as discussed above) versus Co reveals that alkali gabbro to olivine gabbro of group 1 plots either within or slightly outside the field defined by Rhodes (1981) for primary, primitive magmas (fig. 25). Gabbro-diorite plots within the primitive field. A plot of magnesium number versus Sc, although not shown, is in agreement with the Mg number versus Co plot.

Pearce element-ratio plots (i.e., Ti/K vs. P/K), as used by Russell and Nicholls (1988), are constructed by many investigators of mafic igneous rocks; we do not favor their use for these lamprophyres. A fundamental precept of such plots is that a conserved constituent (element) must be in the denominator. That conserved constituent must be one whose concentration does not change during the crystallization process in order for the system change to be accurately portrayed (Russell and Nicholls, 1988). As an example, in most calcic to calc-alkalic gabbro norites and tholeiites, K is a conserved element because biotite or other potassium-bearing phases are not present. However, in alkalic gabbros and basalts, the presence of primary biotite phenocrysts affects the concentration of K_2O in derivative magmas and indicates that K is not a conserved element. Because few, if any, major elements appear to be conserved during the crystallization history of the alkalic, mafic magma at the Golden Sunlight mine, Pearce element-ratio plots were not utilized.

Chondrite-normalized rare-earth-element plots for group 1 lamprophyres show the separation of alkali gabbro and olivine gabbro versus gabbro-diorite (fig. 26). All rocks have LREE-enriched patterns having no Eu anomalies. Alkali gabbro and olivine gabbro plot above and distinctly separate from gabbro-diorite. Alkali gabbro and olivine gabbro are more LREE enriched than gabbro-diorite. La/Yb_{CN} ratios for the alkali gabbro and olivine gabbro average 15; the gabbro-diorite averages 9. Lack of any europium anomalies is expected in rocks from which plagioclase did not crystallize as a phenocryst.

Most of the variability of concentrations of the LREE is probably related to modal concentrations of apatite because apatite preferentially concentrates the light and intermediate REE. In the lamprophyres, the highest concentrations of REE are probably within apatite and biotite. But, because biotite normally does not selectively concentrate the LREE or HREE, it has little effect on fractionating the heavy versus the light REE. In a plot of La vs. P_2O_5, the dependence of La concentrations on modal percentage of apatite is clear (fig. 27). Alkali and olivine gabbro are enriched in La and P_2O_5 compared to gabbro-diorite and occupy the upper right-hand corner of the diagram.

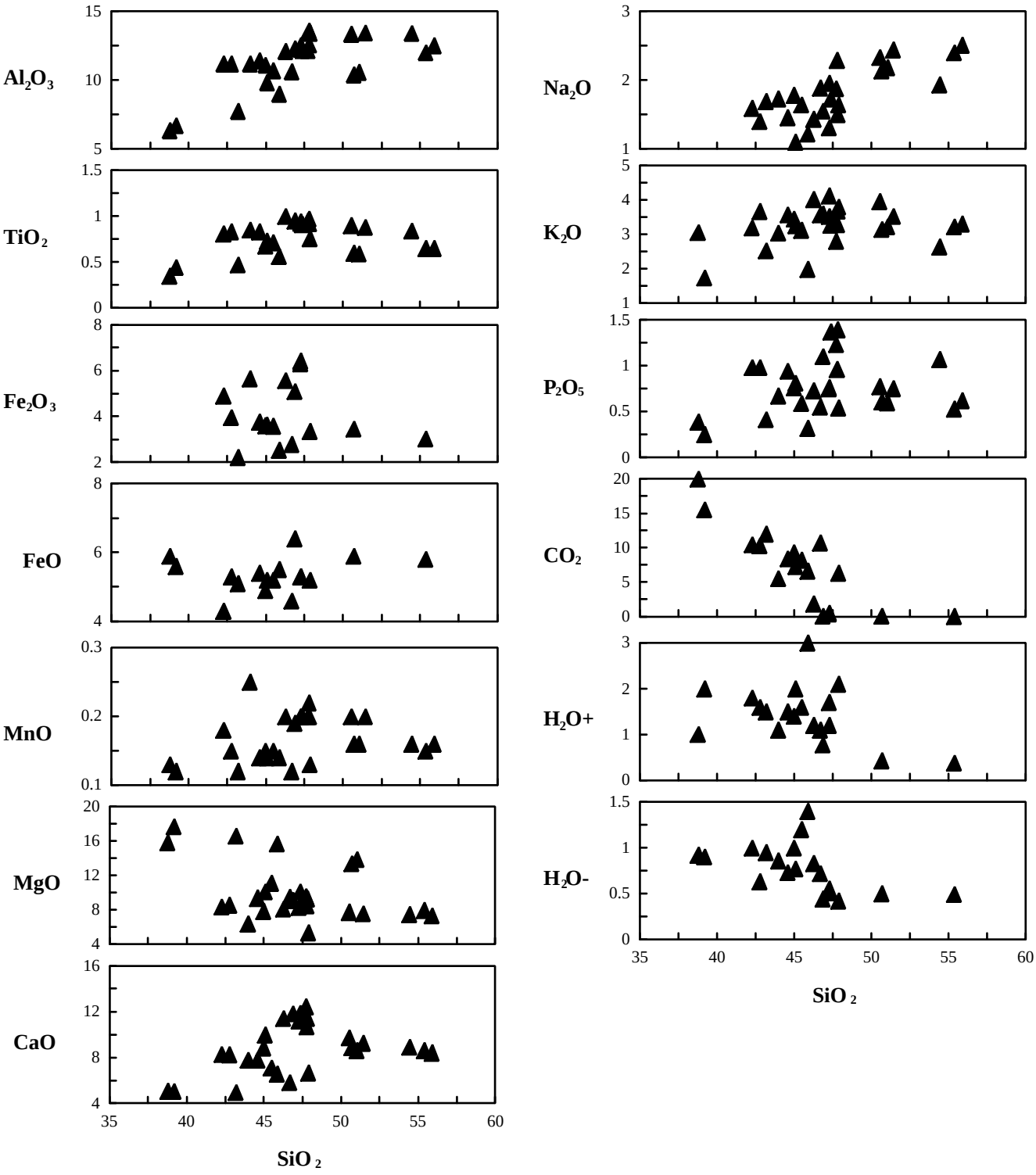

Figure 23. SiO_2 versus major-element-oxide plots (Harker diagrams) for all lamprophyre samples, Golden Sunlight mine area.

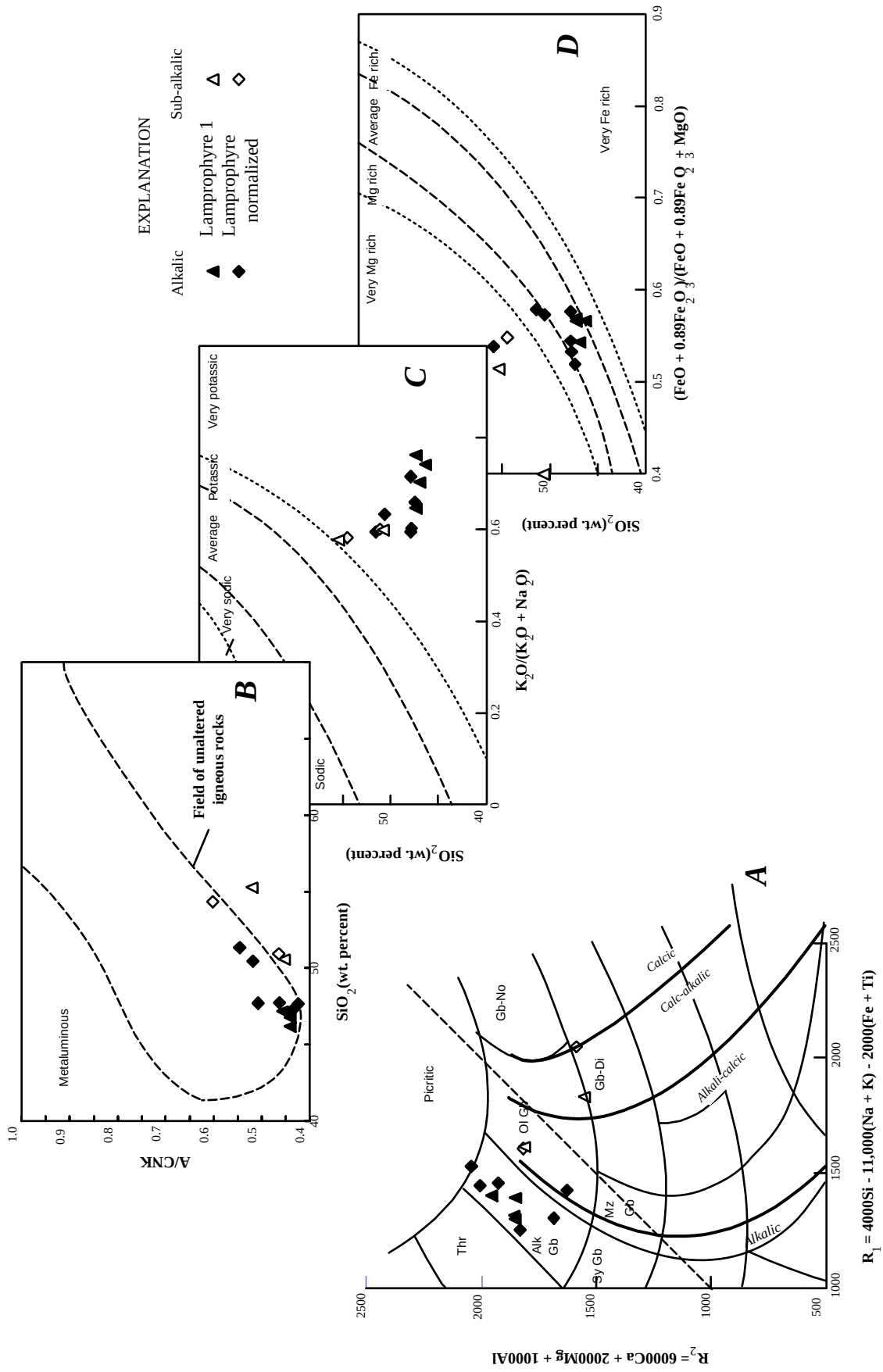

Figure 24. Major-element plots of CO_2-poor lamprophyre, Golden Sunlight mine. Alkalic lamprophyre, filled symbols. Sub-alkalic lamprophyre, open symbols. *A*, R_1 versus R_2 plot (De LaRoche and others, 1980); Picritic, picritic composition or ultramafic rocks; Thr, therallite; Alk Gb, alkali gabbro; Ol Gb, olivine gabbro; Gb-No, gabbro-norite; Sy Gb, syenogabbro; Mz Gb, monzogabbro; Gb-Di, gabbro-diorite. Fields of alkalinity modified slightly from DeWitt (1989). *B*, SiO_2 versus A/CNK plot; A/CNK, molar alumina/sum of molar calcium, sodium, and potassium. Field of unaltered igneous rocks from DeWitt (unpub. data, 1994). *C*, $K_2O/(K_2O+Na_2O)$ versus SiO_2 plot; *x*-axis is "K number" listed in table 1. Field boundaries from DeWitt (unpub. data, 1995). *D*, $(FeO+0.89Fe_2O_3)/(FeO+0.89\ Fe_2O_3+MgO)$ versus SiO_2 plot; *x*-axis is "Fe number" listed in table 1. Field boundaries modified from DeWitt (1989).

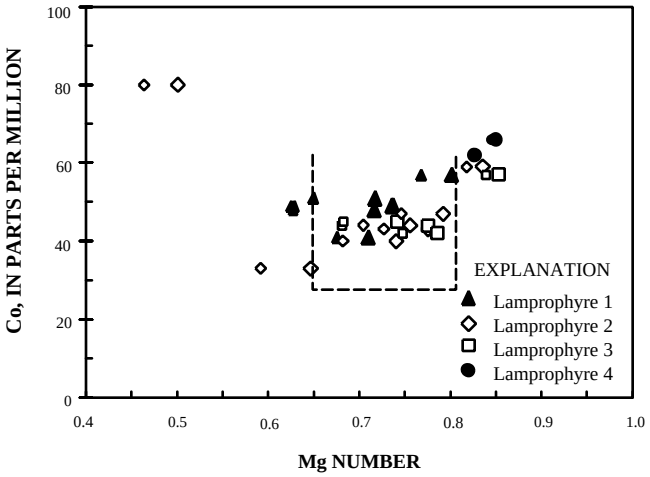

Figure 25. Mg number (magnesium number) versus Co diagram for all lamprophyres, Golden Sunlight mine area. Lamprophyre 1 contains less than 2 percent CO_2. Lamprophyre 2 has 5–9 percent CO_2. Lamprophyre 3 has 10–14 percent CO_2. Lamprophyre 4 has 15–20 percent CO_2. Large symbols have Mg numbers calculated on basis of $Mg/(Mg + Fe^{2+})$. Small symbols have Mg number calculated on basis of $Mg/(Mg + 0.8(Fe_{total}))$. Dashed region is limits of "primitive magmas" from Frey and others (1978) and Rhodes (1981).

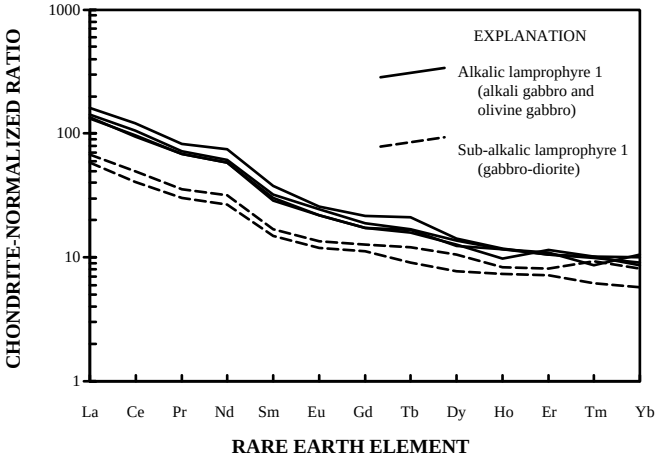

Figure 26. Chondrite-normalized rare-earth-element plot for alkalic and sub-alkalic CO_2-poor lamprophyre, Golden Sunlight mine area.

GEOCHRONOLOGY OF CO_2-POOR LAMPROPHYRE

Two samples of biotite-bearing lamprophyre were collected for age determinations. Phenocrysts of phlogopitic biotite were separated from each for isotopic analyses. One biotite (sample 81P120 collected by Walter Bauer from drill core DDH30-6, 644-646′) was from the Ohio adit, which was destroyed during open-pit mining. The other (88GS-8) was from the southern end of Bull Mountain (fig. 1). A conventional K-Ar date of 79.8±2.8 Ma (two-sigma uncertainty) was determined for biotite from 81P120 (table 7). Biotite

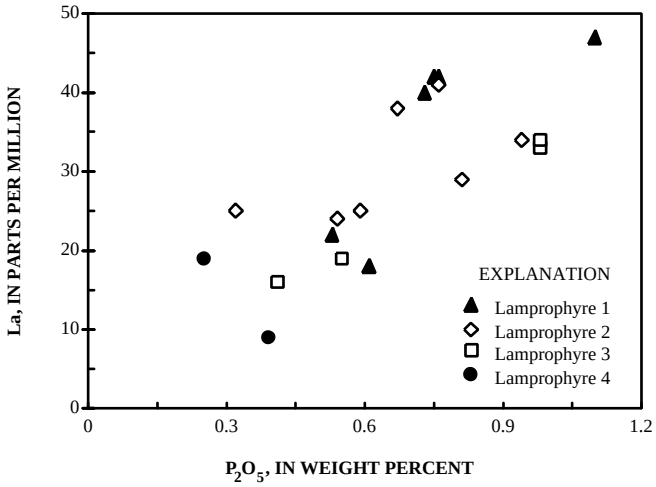

Figure 27. P_2O_5 versus La plot for alkalic and sub-alkalic lamprophyres, Golden Sunlight mine. Lamprophyre 1 contains less than 2 percent CO_2. Lamprophyre 2 has 5–9 percent CO_2. Lamprophyre 3 has 10–14 percent CO_2. Lamprophyre 4 has 15–20 percent CO_2.

from 88GS-8 was analyzed by ^{40}Ar-^{39}Ar techniques (table 8) and yielded a slightly disturbed spectra (fig. 28) having a ^{40}Ar-^{39}Ar total gas date of 76.4±0.7 Ma (two-sigma uncertainty). A plateau date of 76.9±0.4 Ma is defined by 78 percent of the gas. The slightly older conventional K-Ar date of 79.8 Ma for biotite from 81P120 is probably the result of small impurities in the mineral separate because no excess argon is apparent in the spectra for biotite from 88GS-8 (fig. 28). We interpret the somewhat disturbed spectra of biotite from 88GS-8 to indicate cooling below about 375°C for the phlogopitic biotite phenocrysts and, hence, emplacement of the dikelike body.

PETROLOGY OF CO_2-RICH LAMPROPHYRE

A complete transition, from CO_2-poor lamprophyre, to CO_2-rich lamprophyre, exists within the sills and dikes at the Golden Sunlight mine. Both in drill cores and in outcrop, the lamprophyres range from CO_2 poor (CO_2 concentrations of ≤ 0.3 weight percent, and H_2O_{tot} concentrations ≤ 0.9 weight percent) to CO_2 rich (CO_2 = 20.0 weight percent, H_2O_{tot} = 1.9 weight percent for sample 88C1-283′). Petrographic and X-ray diffraction studies indicate an unusual alteration-mineral assemblage associated with CO_2 metasomatism that is characterized by Mg-rich carbonate minerals. Our findings expand on the observations of Swanson (1989), who noted chlorite and opaque minerals replacing olivine but who did not work extensively with the CO_2-rich rocks.

CO_2 metasomatism has partially to completely replaced phenocrysts of light-apple-green diopsidic augite with dolomite and minor magnesite (fig. 29). Both centimeter-size phenocrysts and groundmass clinopyroxene may be replaced. In fewer than 10 percent of all samples, clinopyroxene phenocrysts are replaced by dolomite and quartz (sample 115-1876′).

Table 7. K-Ar analytical data for biotite from lamprophyre (sample 81P120), Golden Sunlight mine area, southwestern Montana.

[Analyzed by R.F. Marvin, H.H. Mehnert, and E.L. Brandt (Branch of Isotope Geology, Denver, Colo., Report 674). Date in this table differs from that in original report because of change in λ_e. Sample location: lat 45°54′10″N., long 112°00′40″W. (sec. 19, T. 2 N., R. 3 W., Black Butte 7Ω-minute quadrangle, Jefferson County, Montana). $\lambda_b = 4.962\times10^{-10}$/yr; $\lambda_e = 0.572\times10^{-10}$/yr; atomic abundance of $^{40}K = 1.167\times10^{-4}$]

K_2O (wt %)	^{40}Ar (moles/gram)	^{40}Ar (%)	$^{40}Ar/^{40}K$	Date (Ma)	2-sigma uncertainty (Ma)
9.395 avg	10.88×10^{-10}	94	0.00467	79.8	2.8

Table 8. ^{40}Ar-^{39}Ar data for biotite from lamprophyre (sample 88GS-8), Golden Sunlight mine area, southwestern Montana.

[$^{40}Ar_c$, radiogenic ^{40}Ar corrected for mass discrimination and induced ^{40}Ar; $^{39}Ar_c$, ^{39}Ar corrected for mass discrimination and radioactive decay; $\%^{40}Ar_{rad}$, percentage of radiogenic ^{40}Ar. Sample weight = 64.8 mg; J = 0.007846±0.25 percent. ^{40}Ar-^{39}Ar analyses by Ross Yeoman and L.W. Snee]

Temperature (°C)	$^{40}Ar_c$	$^{39}Ar_c$	F	$\%\ ^{40}Ar_{rad}$	$\%\ ^{39}Ar_{total}$	Date (Ma)	2-sigma uncertainty (Ma)
500	0.06014	0.01960	3.07	31.10	0.30	42.97	12.42
600	0.14907	0.07687	1.94	60.70	1.30	27.26	2.00
650	0.18598	0.04930	3.77	61.90	0.80	52.62	4.52
700	0.31994	0.05558	5.76	50.00	0.90	79.69	1.10
750	0.65532	0.11281	5.81	86.80	1.90	80.40	0.90
800	1.53368	0.26699	5.74	94.40	4.50	79.53	0.86
850	3.93491	0.69505	5.66	96.60	11.70	78.40	0.60
900	5.40134	0.97444	5.54	98.10	16.40	76.80	0.44
950	5.27044	0.93903	5.61	96.80	15.80	77.74	0.42
1000	3.56740	0.63658	5.60	92.90	10.70	77.63	0.60
1050	4.30633	0.77321	5.57	93.40	13.00	77.16	0.54
1150	7.15876	1.30517	5.49	95.30	22.00	76.01	0.42
1300	0.11408	0.02193	5.21	74.80	0.40	72.17	18.12
Total gas			5.51			76.36	0.70
Plateau age						76.94	0.48

Plateau from 900°C to 1,150°C contains 78.1 percent of the gas.

Forsteritic olivine (about $Fo_{85–90}$) has a variety of alteration products that change, somewhat, with increasing CO_2 concentration. In CO_2-poor rocks, olivine is cracked and partially replaced by limonite(?) and cream-white magnesite. These alteration products are also present in rocks with higher CO_2 concentrations, but are successively replaced by magnesite, sericite, and minor biotite (figs. 30 and 31). In extremely CO_2-rich rocks, only magnesite remains. Sample 88C1-283′ (the most CO_2 rich lamprophyre) originally contained abundant phenocrysts of olivine (fig. 32) and minor clinopyroxene. That olivine is now replaced by magnesite, minor dolomite, and a trace of talc or sericite. Cream-colored replacement products of olivine phenocrysts in sample 191-173.5′ are chiefly magnesite and minor dolomite, with much lesser amounts of quartz (X-ray diffraction data). Similarly, sample 88GS-10, which was collected from a lamprophyre dike in the mine pit, was rich in olivine phenocrysts. Iron-stained, red-brown pseudomorphs are now predominantly magnesite, minor talc and siderite, and traces of quartz.

Biotite phenocrysts are largely unaffected by CO_2 metasomatism and retain their embayed outlines. Minor amounts of sericite replace biotite in extremely CO_2 rich samples. Chlorite has replaced biotite in some samples but does not exceed several percent of individual grains.

The groundmass minerals, with the exception of clinopyroxene, are much less replaced than the large phenocrysts. Clinopyroxene in the groundmass is extensively replaced by dolomite and minor magnesite and limonite(?). Sanidine, which constitutes the bulk of the groundmass, is normally fresh but can be replaced by a mat of sericite. In extremely CO_2 rich samples, sanidine is replaced by micrometer-size orthoclase(?) and quartz (fig. 33). Biotite in

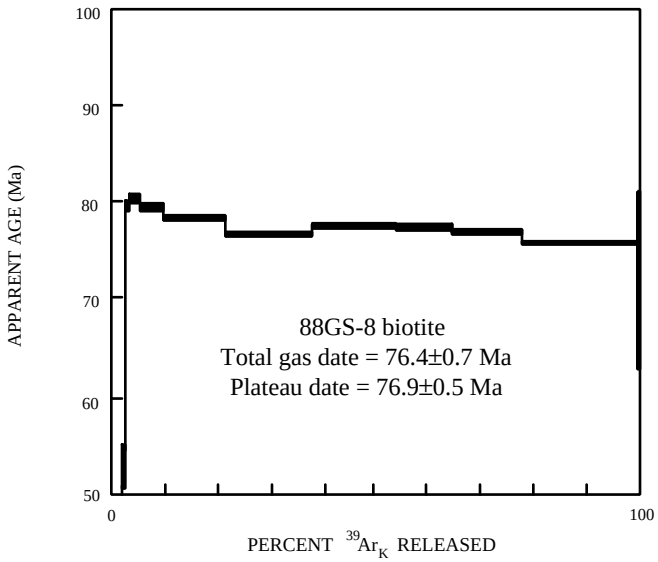

Figure 28. ^{40}Ar-^{39}Ar release spectra for biotite from lamprophyre (sample 88GS-8), Golden Sunlight mine. Plateau date of 76.9±0.5 Ma.

the groundmass remains fresh. The concentration of magnetite in the groundmass, which averages 1.5 percent in CO_2-poor samples, diminishes to less than 0.01 percent in CO_2-rich lamprophyre. Relicts of magnetite and ilmenomagnetite are replaced by limonite(?). White material filling globular structures (Rock, 1984) that were originally vesicles or amygdules is a mixture of quartz and plagioclase feldspar. Although Porter and Ripley (1985) reported clay minerals in altered lamprophyres, we observed none in the samples examined in this study.

The alteration assemblage of the lamprophyres is somewhat unusual: magnesite, dolomite, sericite, and minor quartz and chlorite. Velde (1968), in a review of metasomatized lamprophyres, noted the common assemblage of carbonate minerals, chlorite, actinolite, montmorillonite, quartz, and talc replacing olivine. Our samples lack many of these minerals and are especially noteworthy because of the general lack of calcite. Carbonate minerals mentioned by Rock (1984) in "calc-alkaline" lamprophyres include calcite, dolomite, ankerite, and siderite, in approximate decreasing percentages. At the Golden Sunlight mine, carbonate minerals replacing olivine and clinopyroxene are not primary. Minor, fine-grained carbonate minerals in the groundmass, however, do appear to be of primary, magmatic origin.

Based on the preceding petrographic observations, the major, unbalanced replacement reactions in the lamprophyres include:

$$\text{Olivine} + CO_2 \rightarrow 95\%\ \text{magnesite} \pm 5\%\ \text{sericite}$$
$$Mg_{1.8}Fe_{0.2}SiO_4 + CO_2 \rightarrow MgCO_3 \pm K_2Al_6Si_6O_{20}(OH)_4 \quad (1)$$

$$\text{Clinopyroxene} + CO_2 \rightarrow 80\%\ \text{dolomite} + 15\%\ \text{magnesite} + 5\%\ \text{quartz}$$
$$Ca(Mg_{0.8}Fe_{0.2})Si_2O_6 + CO_2 \rightarrow Ca_{0.4}Mg_{0.6}CO_3 + MgCO_3 + SiO_2 \quad (2)$$

$$\text{Sanidine} + H_2O \rightarrow 100\%\ \text{sericite}$$
$$KAlSi_3O_8 + H_2O \rightarrow K_2Al_6Si_6O_{20}(OH)_4 \quad (3)$$

$$\text{Sanidine} \rightarrow \text{quartz(?)} + \text{orthoclase(?)} KAlSi_3O_8 \rightarrow SiO_2 + KAlSi_3O_8 \quad (4)$$

Reaction 1, which cannot be balanced using the percentages of reaction products (predominantly magnesite), indicates that MgO, SiO_2 , and FeO are in excess and that K_2O and Al_2O_3 have been added to the pseudomorphs. Reaction 2, which also cannot be balanced because of the

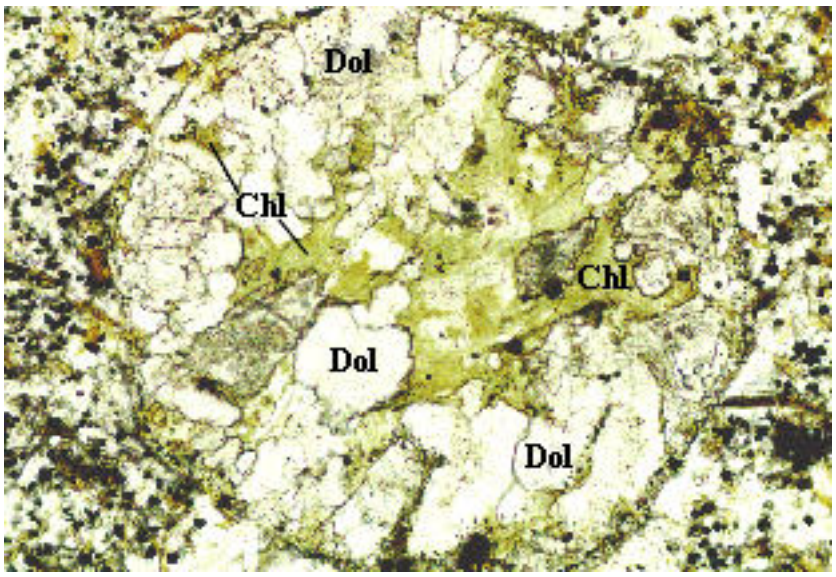

Figure 29. Photomicrograph in plane-polarized light of clinopyroxene phenocrysts replaced by dolomite and chlorite in lamprophyre (sample 189-194.5′). Chl, chlorite; Dol, dolomite. Field of view 1.6×1.1 mm.

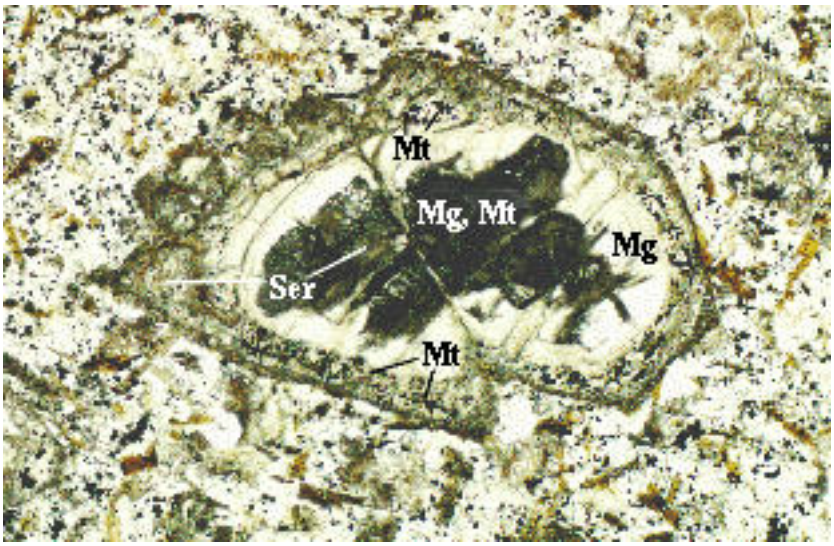

Figure 30. Photomicrograph in plane-polarized light of olivine phenocryst replaced by sericite, magnesite, and magnetite in lamprophyre (sample 190-1223.5′). Mg, magnesite; Mt, magnetite; Ser, sericite. Field of view 1.6×1.1 mm.

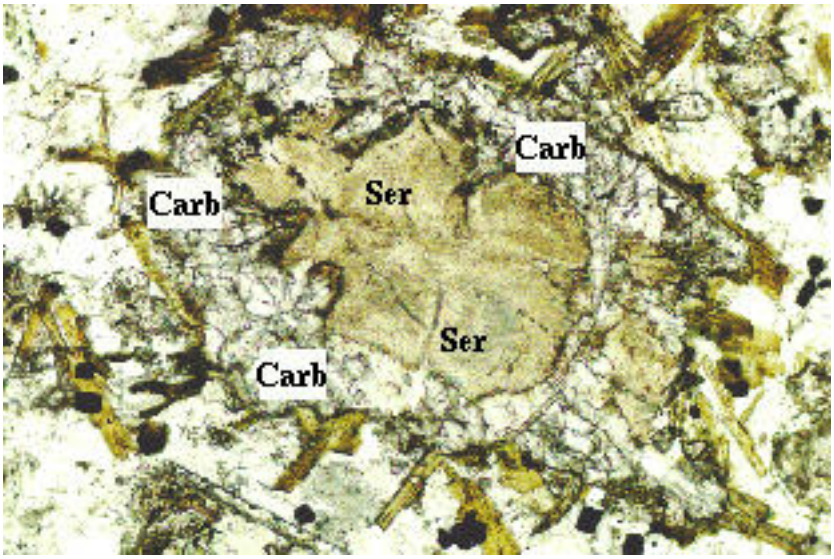

Figure 31. Photomicrograph in plane-polarized light of olivine phenocryst replaced by biotite and carbonate minerals in lamprophyre (sample 191-1034′). Ser, sericite; Carb, carbonate minerals, especially magnesite and dolomite. Field of view 1.6×1.1 mm.

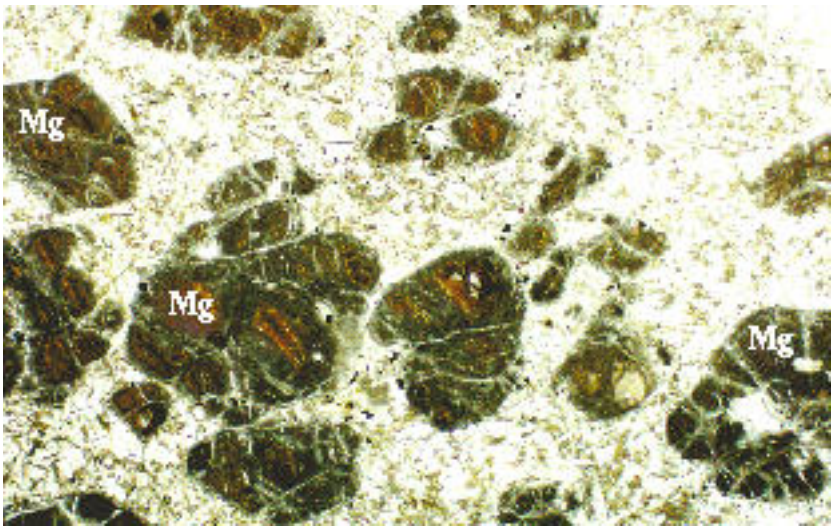

Figure 32. Photomicrograph in plane-polarized light of olivine-rich lamprophyre (sample 88C1-283′) showing complete replacement of olivine by magnesite. Mg, magnesite. Field of view 8.5×5.8 mm.

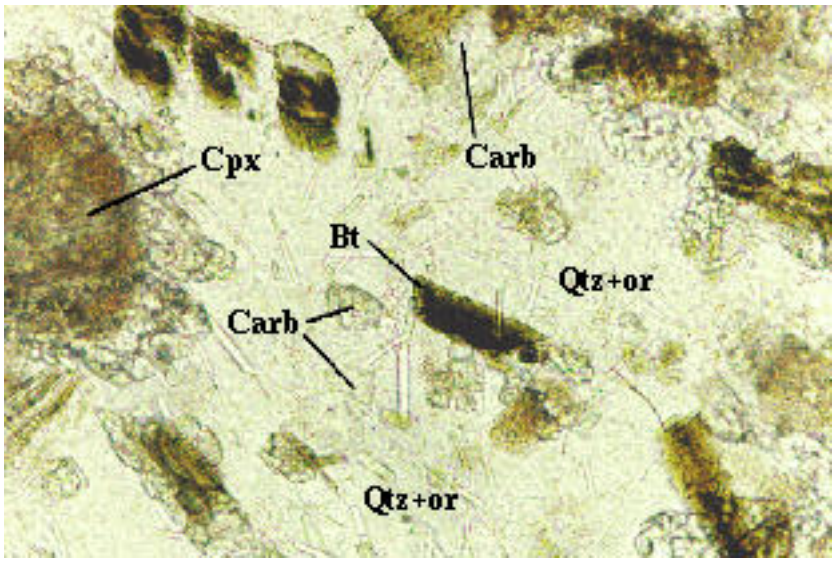

Figure 33. Photomicrograph in plane-polarized light of sanidine replaced by micrometer-size quartz and orthoclase(?) in lamprophyre (sample 88C1-283′). Cpx, clinopyroxene variable replaced by carbonate minerals; Carb, carbonate minerals; Bt, biotite; Qtz + or, quartz(?) plus orthoclase(?). Field of view 0.4×0.25 mm.

predominance of dolomite, reveals that CaO, MgO and SiO_2, and probably FeO, are in excess. Although quartz is a reaction product identified in thin sections, the low percentages present (normally less than 5 percent) are not enough to balance the reaction. Reaction 3 comes the closest to being balanced because only Al_2O_3 must be added to the system. Reaction 4 indicates that SiO_2 has been added to the system.

Importantly, point counts of CO_2-rich rocks indicate that the higher the concentration of CO_2, the higher the percentage of relict phenocrysts of olivine. Rocks containing less than 5 percent CO_2 average 6 percent olivine. Rocks having 5–9 percent CO_2 have 10–13 percent olivine, and rocks having 10–14 percent CO_2 have 16–20 percent altered and replaced olivine. Lamprophyres with 15–20 percent CO_2 have 25–28 percent totally replaced olivine phenocrysts. Therefore, the greatest affect of CO_2 metasomatism was replacement of olivine.

Volume change does not appear to have been significant during CO_2 metasomatism. Replaced phenocrysts of both olivine and clinopyroxene retain their aspect ratios and average sizes. No phenocrysts are flattened, compressed, or expanded. Groundmass plagioclase retains its characteristic interstitial form and is not decreased or increased in size. Groundmass biotite and sanidine also do not deviate from their form and aspect where replaced. Therefore, volume change, on a significant scale, has not taken place during metasomatism.

CHEMISTRY OF CO_2-RICH LAMPROPHYRE

The addition of CO_2 to lamprophyres at the Golden Sunlight mine has resulted in apparent enrichment of some elements and apparent depletion of others (figs. 34 and 35). Both alkalic (alkali gabbro and olivine gabbro) and sub-alkalic (gabbro-diorite) varieties of lamprophyre have similar apparent enrichment and depletion trends, and those trends are clearly separable on most multielement plots. With increasing CO_2 concentration, TiO_2, Fe number, Al_2O_3, Sr, K_2O, CaO, and P_2O_5 decrease in apparent concentration for both types of lamprophyre (fig. 34*A*–*G*). Scatter within some element plots is greater than within others, but the following trends are clear. On all plots, sub-alkalic lamprophyre samples plot at lower concentrations than do alkalic lamprophyre samples. At the highest CO_2 concentrations, separation of the two trends is more difficult because the trends tend to converge. With increasing CO_2 concentration, Cr, Ba, Ni, and MgO increase in apparent concentration for both lamprophyres (fig. 35*B*–*E*). Alkalic lamprophyre samples plot at lower concentrations than sub-alkalic samples, with the exception of Ba. Cobalt variation is somewhat enigmatic (fig. 35*A*) because sub-alkalic lamprophyres show an apparent increase and some alkalic lamprophyres exhibit an apparent decrease.

These patterns of apparent enrichment and depletion are deceptive because they appear to suggest addition of such refractory elements as Co, Cr, and Ni to the lamprophyres during CO_2 metasomatism. As noted in the section on mineralogy, both groups of lamprophyres have higher concentrations of relict olivine phenocrysts as CO_2 concentration increases. Therefore, the apparent enrichment trends may be only a function of original phenocryst concentration. A test of this possibility lies in the relationships between Ni, MgO, and percentage of olivine phenocrysts.

Point counts of replaced olivine phenocrysts in CO_2-rich lamprophyres were made in order to assess the apparent enrichment patterns of Ni, Cr, and MgO. As expected in rocks containing olivine phenocrysts, Ni concentration in our samples is highly correlated (r = 0.97) with modal percent olivine (fig. 36*A*). The regression of figure 36*A* was

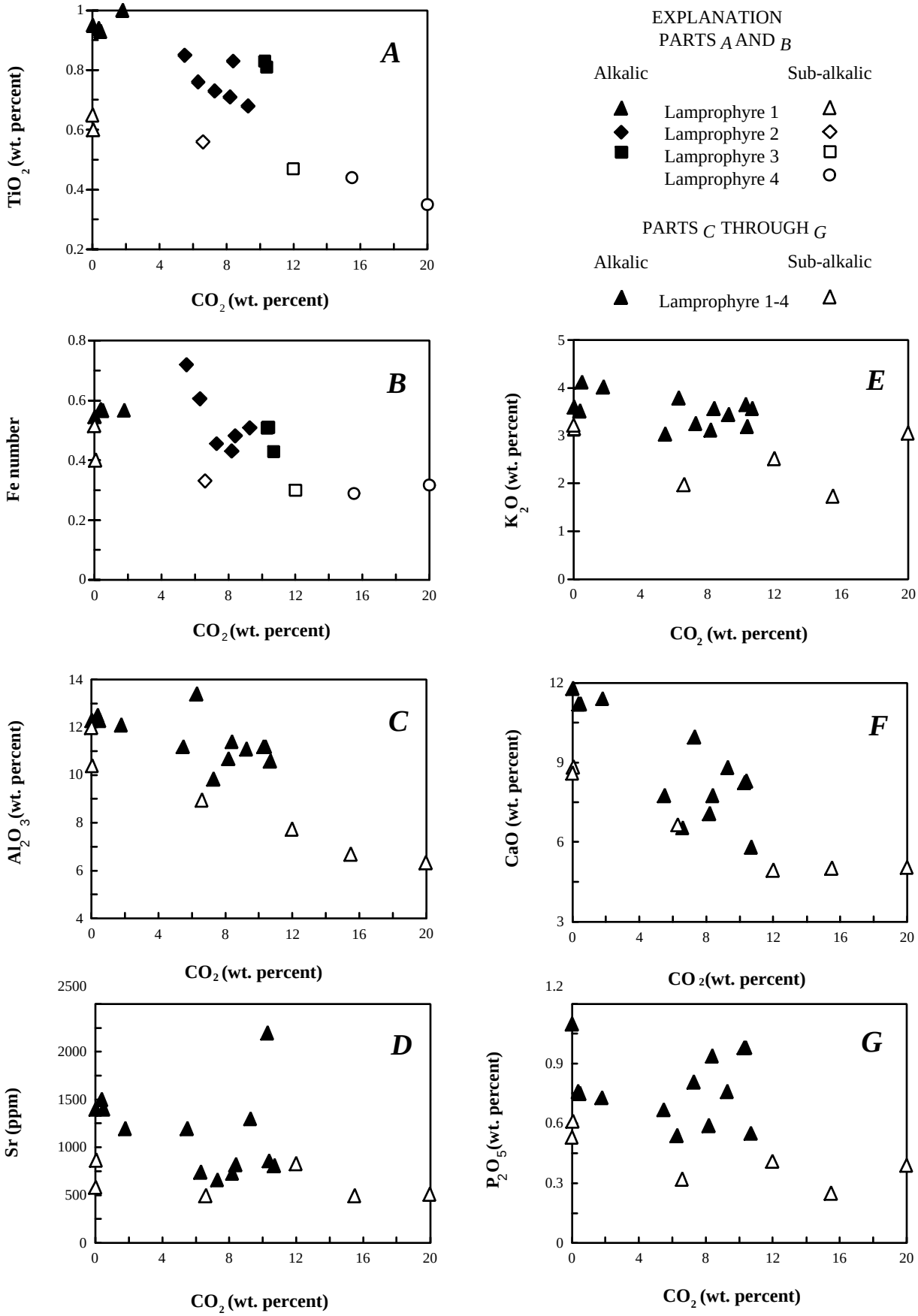
EXPLANATION
PARTS A AND B
Alkalic
Sub-alkalic
Lamprophyre 1
Lamprophyre 2
Lamprophyre 3
Lamprophyre 4
PARTS C THROUGH G
Alkalic
Sub-alkalic
Lamprophyre 1-4
A
B
C
D
E
F
G
TiO2 (wt. percent)
Fe number
Al2O3 (wt. percent)
Sr (ppm)
K2O (wt. percent)
CaO (wt. percent)
P2O5 (wt. percent)
CO2 (wt. percent)

constructed using both alkalic and sub-alkalic groups. However, the sub-alkalic group may define a regression of equal slope but higher *y*-intercept, as suggested by the limited data. This finding is substantiated by other element plots (figs. 26, 34, and 35). Ni is also highly correlated (r = 0.96) with MgO concentration (fig. 36*B*). These high correlations indicate that Ni, Cr, and MgO were not added to the lamprophyres during CO_2 metasomatism. Rather, rocks originally rich in olivine phenocrysts (and, hence, Ni and, to a lesser extent, Cr) were the most susceptible to replacement by magnesite and dolomite because of the instability of olivine during CO_2 metasomatism. Most of the apparent enrichment and depletion trends (figs. 34 and 35) are therefore mixing lines between olivine-rich lamprophyre (high MgO, Ni, Cr, Co) and olivine-poor lamprophyre (low MgO, Ni, Cr, Co).

Compositions of CO_2-metasomatized samples can be compared to fresh samples (fig. 37). The major-element composition of the CO_2-rich samples is expressed in the De LaRoche plot as lowered R_2 values, but little change in R_1 values (fig. 37*A*). From originally an alkali gabbro, most samples of the alkalic lamprophyre change to syenogabbro or monzogabbro. Sub-alkalic olivine gabbro changes to gabbrodiorite. These changes indicate that some combination of Ca, Mg, and Al were lost from the system to account for the lowered R_2 values. The largely unchanged R_1 values indicate that, although the sum of Si, Na, K, Fe, and Ti remained constant, individual components could have been lost or gained. CO_2 metasomatism resulted in slightly higher A/CNK ratios, but markedly lower SiO_2 concentrations (fig. 37*B*), approximately constant K_2O/K_2O+Na_2O at decreasing SiO_2 (fig. 37*C*), and lower Fe numbers at decreased SiO_2 (fig. 37*D*).

REE patterns in CO_2-rich lamprophyres have LREE enrichments similar to CO_2-poor lamprophyre, but the curves for CO_2-rich rocks plot successively below those for CO_2-poor rocks (fig. 38). The patterns are consistent with decreasing concentrations of apatite in CO_2-rich rocks (fig. 27). No REE mobility is suggested by the data, just lower concentrations of REE in more olivine-rich rocks.

Figure 34 (previous page). CO_2 versus other component plots for alkalic and sub-alkalic lamprophyres showing apparent depletion trends. *A*, CO_2 versus TiO_2; *B*, CO_2 versus Fe number; *C*, CO_2 versus Al_2O_3; *D*, CO_2 versus Sr; *E*, CO_2 versus K_2O; *F*, CO_2 versus CaO; *G*, CO_2 versus P_2O_5. *A* and *B* have lamprophyre 1–4 broken down by different plotting symbols. The remainder of the plots distinguish only between alkalic and sub-alkalic lamprophyres. Individual groups (1–4) can be distinguished on the basis of their CO_2 concentration. Lamprophyre 1 contains less than 2 percent CO_2. Lamprophyre 2 has 5–9 percent CO_2. Lamprophyre 3 has 10–14 percent CO_2. Lamprophyre 4 has 15–20 percent CO_2.

ELEMENT GAINS AND LOSSES DURING CO_2 METASOMATISM

The apparent enrichment and depletion trends (figs. 34 and 35) are therefore controlled by two factors: (1) compositional variation of the original lamprophyre; and (2) addition of CO_2. Those rocks having low CO_2 concentrations represent samples of both groups of lamprophyres, none of which has been CO_2 metasomatized. The CO_2-poor rocks are neither the most primitive nor the most evolved; they are merely those rocks that have totally escaped the metasomatic process. CO_2-rich rocks are those olivine-rich lamprophyres that were most susceptible to replacement because of the inherent instability of all phenocrysts in general and olivine phenocrysts in particular. The concentration of CO_2 in both groups of lamprophyres is not a function of the "completeness or intensity" of alteration but rather the percentage of olivine phenocrysts that existed and that could react with the CO_2-rich phase.

In order to quantify the true element enrichments and depletions, point counts were made of CO_2-rich lamprophyres that contained 15–20 percent CO_2. Pre-metasomatism whole-rock chemical compositions were calculated from the modes using published mineral chemistries of forsteritic olivine, diopsidic augite, sanidine, biotite, magnetite, ilmenite, apatite, and albite from alkalic basalt and alkalic gabbro (Deer, Howie, and Zussman, 1977). Comparison of the resulting, "primary" chemistries (table 9) with CO_2-rich analyses (table 1) allows a semiquantitative estimation of which elements and oxides were depleted during CO_2 metasomatism.

Calculation of the percent of each oxide removed or added during metasomatism is dependent on two factors: (1) knowledge of the chemistry of the mineral phases, and (2) accurate point counts of the pre-metasomatism phases. Because chemistries of the mineral phases were picked from published analyses of similar rocks, there is a large potential uncertainty in this factor. We checked this uncertainty by using the published chemistries to recalculate compositions of CO_2-poor samples from the modal mineral percentages of those samples. Our published analyses and the recalculated analyses were in excellent agreement. Therefore, our assumed mineral chemistries do not contribute significantly to uncertainties in the percentages of oxides removed or added during CO_2 metasomatism. Accurate point counts of all minerals in the rocks containing 15–20 percent CO_2, however, were more difficult to obtain. Particularly for trace minerals such as apatite and albite, and for low-percentage minerals such as ilmenite, the uncertainty of the percentage of TiO_2, P_2O_5 that were lost is high. Greatest confidence can be placed on the percentages of SiO_2, Al_2O_3, Fe_2O_3, FeO, MgO, CaO, Na_2O, and K_2O that were lost because accurate point counts were possible for relict olivine, clinopyroxene, magnetite, and for fresh biotite, sanidine, and albite.

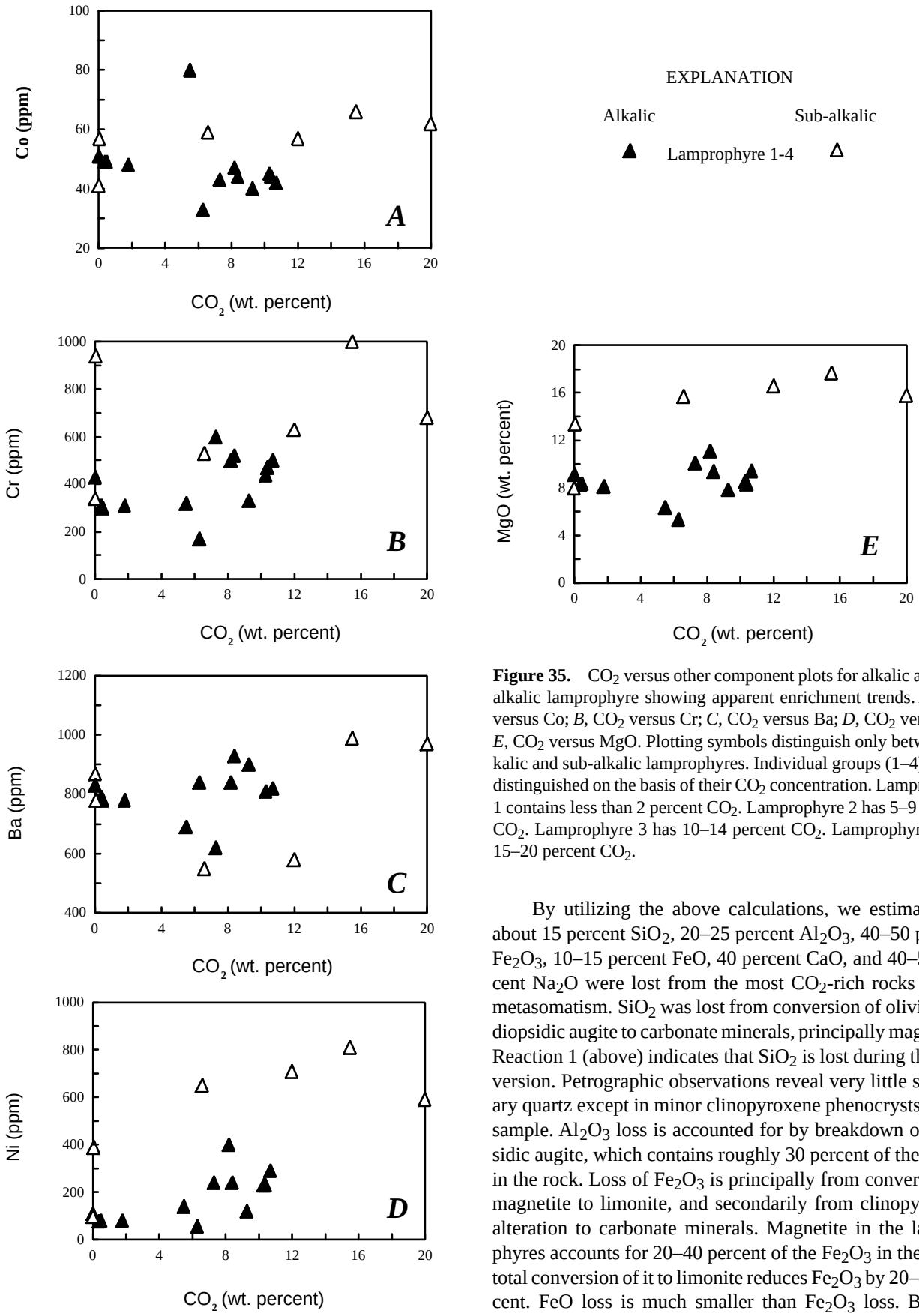

Figure 35. CO_2 versus other component plots for alkalic and sub-alkalic lamprophyre showing apparent enrichment trends. *A,* CO_2 versus Co; *B,* CO_2 versus Cr; *C,* CO_2 versus Ba; *D,* CO_2 versus Ni; *E,* CO_2 versus MgO. Plotting symbols distinguish only between alkalic and sub-alkalic lamprophyres. Individual groups (1–4) can be distinguished on the basis of their CO_2 concentration. Lamprophyre 1 contains less than 2 percent CO_2. Lamprophyre 2 has 5–9 percent CO_2. Lamprophyre 3 has 10–14 percent CO_2. Lamprophyre 4 has 15–20 percent CO_2.

By utilizing the above calculations, we estimate that about 15 percent SiO_2, 20–25 percent Al_2O_3, 40–50 percent Fe_2O_3, 10–15 percent FeO, 40 percent CaO, and 40–50 percent Na_2O were lost from the most CO_2-rich rocks during metasomatism. SiO_2 was lost from conversion of olivine and diopsidic augite to carbonate minerals, principally magnesite. Reaction 1 (above) indicates that SiO_2 is lost during the conversion. Petrographic observations reveal very little secondary quartz except in minor clinopyroxene phenocrysts in one sample. Al_2O_3 loss is accounted for by breakdown of diopsidic augite, which contains roughly 30 percent of the Al_2O_3 in the rock. Loss of Fe_2O_3 is principally from conversion of magnetite to limonite, and secondarily from clinopyroxene alteration to carbonate minerals. Magnetite in the lamprophyres accounts for 20–40 percent of the Fe_2O_3 in the rocks; total conversion of it to limonite reduces Fe_2O_3 by 20–40 percent. FeO loss is much smaller than Fe_2O_3 loss. Because

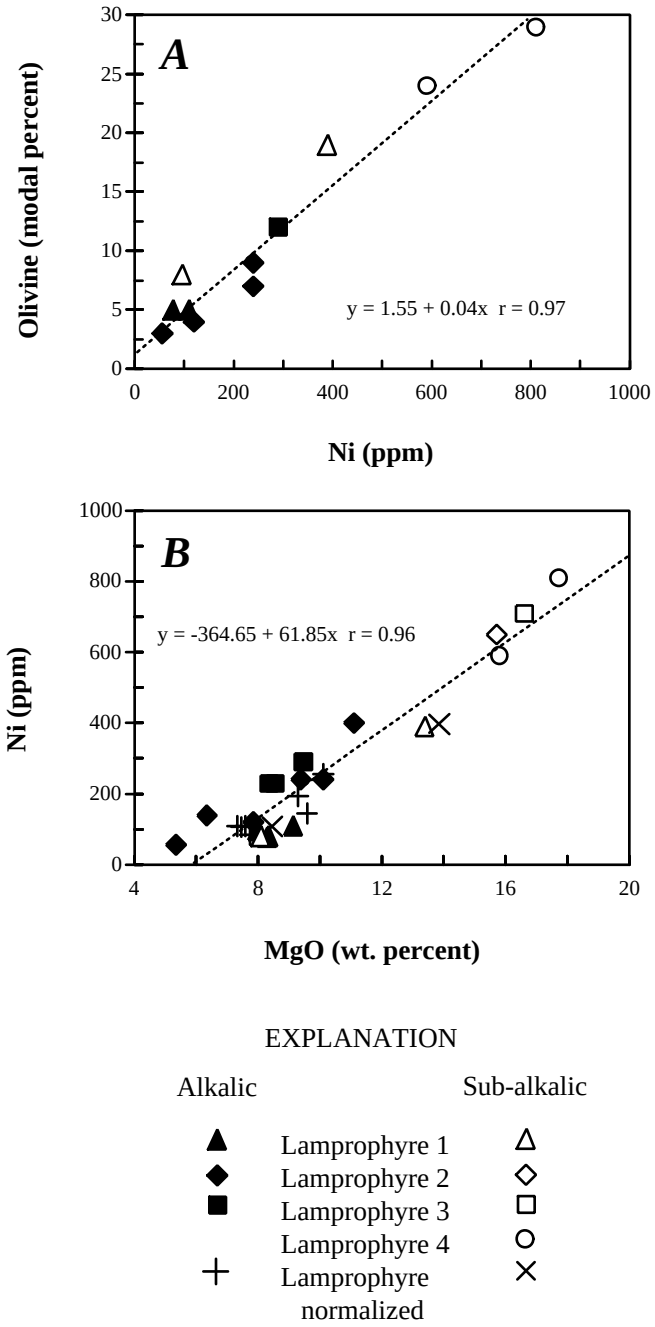

Figure 36. Plots illustrating relationships between Ni, MgO, and percentage of modal olivine in alkalic and sub-alkalic lamprophyre. *A*, Ni versus modal olivine; *B*, MgO versus Ni. Equations are linear regressions through all data points in each diagram. Lamprophyre 1 contains less than 2 percent CO_2. Lamprophyre 2 has 5–9 percent CO_2. Lamprophyre 3 has 10–14 percent CO_2. Lamprophyre 4 has 15–20 percent CO_2.

clinopyroxene contains most of the FeO in the rock, its breakdown to carbonate minerals liberates most of the FeO. Some FeO is reincorporated in siderite, but much remains in the rock in the form of iron oxide stains around other minerals and as FeO in limonite. CaO loss is chiefly by breakdown of diopsidic augite because clinopyroxene accounts for more than 85 percent of the CaO in the rock. Much of the CaO liberated by breakdown of clinopyroxene is retained in the carbonate minerals dolomite and magnesite, but reaction 2 (above) indicates that Ca is in excess. Na_2O loss is facilitated by breakdown of clinopyroxene because diopsidic augite contains roughly 20 percent of the Na_2O in the rock. Breakdown of groundmass albite may aid in the loss, but petrographic observations do not support this possibility.

K_2O, although showing some loss in sample 191-173.5′ (table 9), is probably conserved during metasomatism because biotite phenocrysts are not altered and sanidine in the groundmass is fresh or only replaced by sericite. Also, replacement of olivine phenocrysts by sericite and biotite is evidence that potassium-bearing minerals were being formed, not destroyed during CO_2 metasomatism. Changes in P_2O_5 and TiO_2 are more difficult to assess because of the uncertainty of point counts. Petrographic observations do not indicate a decrease in the amount of apatite needles in the groundmass, so P_2O_5 probably is not substantially decreased.

Table 9. Recalculated, CO_2-free compositions of CO_2-metasomatized lamprophyre samples, Golden Sunlight mine area, southwestern Montana.

Oxide	Recalculated composition based on modal mineralogy	CO_2-rich analysis of altered sample	Percentage of CO_2-rich oxide in recalculated composition
Sample 88C1-283′			
SiO_2	46.44	38.80	83
TiO_2	0.77	0.35	45
Al_2O_3	8.49	6.34	75
Fe_2O_3	3.05	1.59	52
FeO	6.62	5.90	89
MgO	16.93	15.80	93
CaO	8.46	5.06	60
Na_2O	1.32	0.67	50
K_2O	3.08	3.06	99
P_2O_5	0.42	0.39	93
H_2O^+		1.00	
H_2O^-		0.92	
CO_2		20.00	
Sample 191-173.5′			
SiO_2	46.62	39.20	84
TiO_2	0.71	0.44	62
Al_2O_3	8.12	6.69	82
Fe_2O_3	2.97	1.79	60
FeO	7.00	5.60	80
MgO	18.64	17.70	95
CaO	7.84	5.03	64
Na_2O	1.30	0.79	61
K_2O	3.00	1.74	58
P_2O_5	0.42	0.25	60
H_2O^+		2.00	
H_2O^-		0.90	
CO_2		15.50	

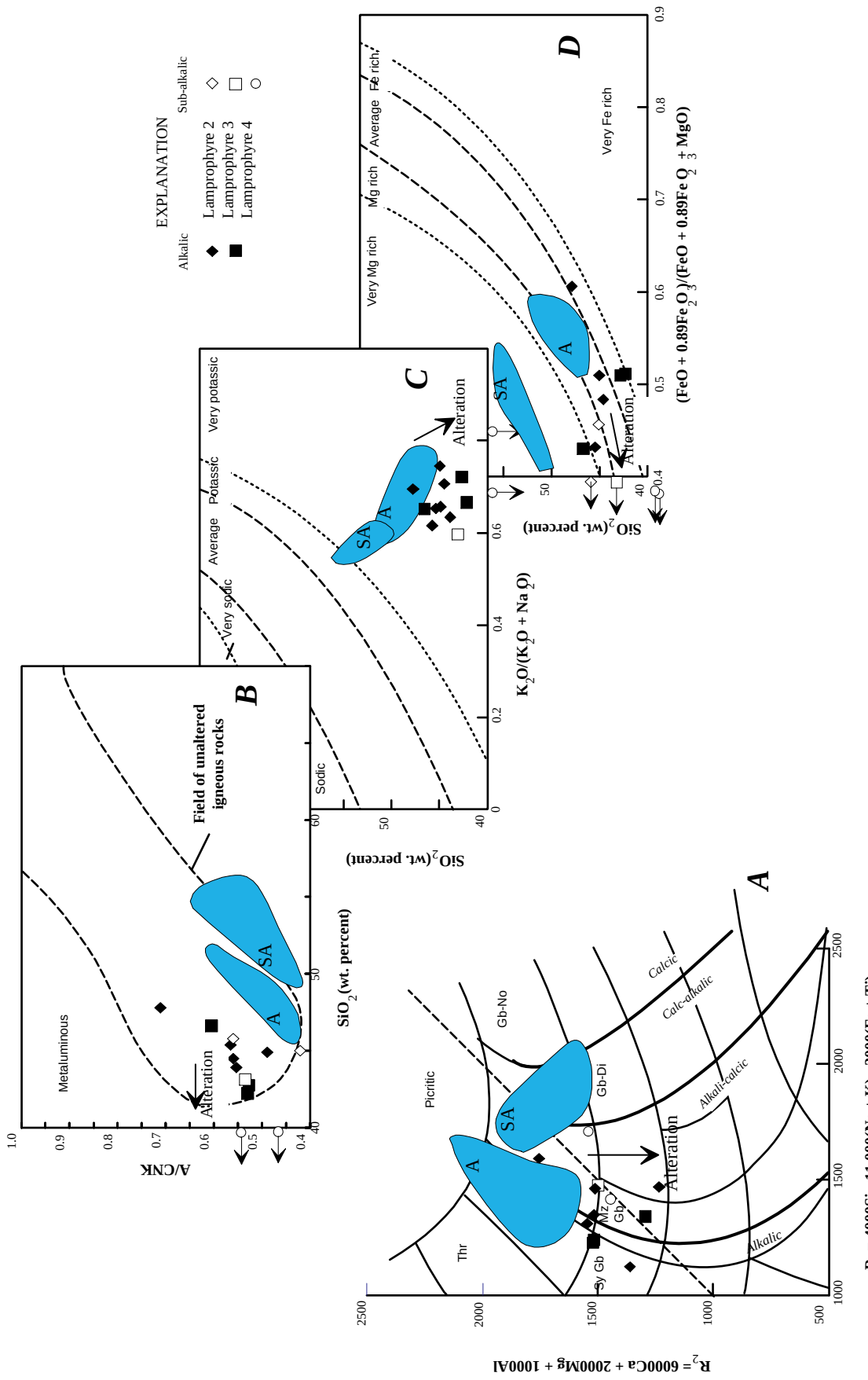

Figure 37. Major-element plots of CO_2-rich lamprophyre, Golden Sunlight mine. Alkalic lamprophyre in filled symbols. Sub-alkalic lamprophyre in open symbols. Fields of CO_2-poor alkalic (A) and sub-alkalic (SA) lamprophyre from figure 24 shown for comparison. Heavy arrows show direction that samples moved during alteration.*A*, R_1 versus R_2 plot (De LaRoche and others, 1980); Picritic, picritic composition or ultramafic rocks; Thr, therallite; Gb-No, gabbro-norite; Sy Gb, syenogabbro; Mz Gb, monzogabbro; Gb-Di, gabbro-diorite; fields of alkalinity modified slightly from DeWitt (1989).*B*, SiO_2 versus A/CNK plot; A/CNK, molar alumina/sum of molar calcium, sodium, and potassium; field of unaltered igneous rocks from DeWitt (unpub. data, 1994). Samples that plot to the left of the diagram are shown on the left border and have light arrows leading to the left.*C*, $K_2O/(K_2O+Na_2O)$ versus SiO_2 plot; *x*-axis is "K number" listed in table 1; field boundaries from DeWitt (unpub. data, 1995). Samples that plot below the diagram are shown on the bottom border and have light arrows leading down. *D*, $(FeO+0.89Fe_2O_3)/(FeO+0.89\ Fe_2O_3+MgO)$ versus SiO_2 plot; *x*-axis is "Fe number" listed in table 1; field boundaries modified from DeWitt (1989). Samples that plot to the left of the diagram are shown on the left border and have light arrows leading to the left.

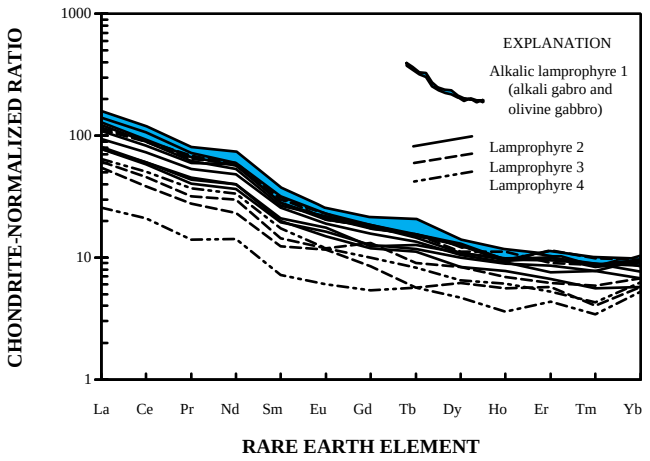

Figure 38. Chondrite-normalized rare-earth-element plot for CO_2-rich lamprophyre. Field for alkalic, CO_2-poor lamprophyre shown for comparison.

TiO_2 may decrease from alteration of ilmenite to limonite, but some TiO_2 that is liberated may be reincorporated in groundmass biotite or in sericite and biotite replacing olivine.

MgO shows no measurable decrease in rocks with the highest CO_2 concentrations (table 9). Although reactions 1 and 2 support magnesium loss, the mass balance does not. Perhaps more magnesite is present in pseudomorphs of clinopyroxene than we estimated through optical and X-ray techniques.

True losses (and some possible gains in addition to CO_2) of constituent elements and oxides can be shown in multielement plots (fig. 39). In these plots, CO_2-poor and CO_2-rich lamprophyres are plotted as well as the recalculated analyses from the most CO_2-rich samples. All plots reveal the distinction between alkalic and sub-alkalic lamprophyres. Most plots indicate which elements and oxides were lost or gained during CO_2 metasomatism. In the discussion that follows, most emphasis is placed on the alkalic lamprophyres because we have more analyses of them. For all plots, we show the field containing CO_2-poor alkalic lamprophyre samples. Also, a plus indicates recalculated compositions of CO_2-rich alkalic lamprophyres having 6–20 percent CO_2. The region between the field and the plus corresponds to the primary igneous composition of lamprophyres before CO_2 metasomatism. Samples that plot outside that trend have gained or loss constituents during metasomatism.

In the TiO_2 versus K_2O plot (fig. 39*A*), there is little variation in K_2O concentration indicated by data points from CO_2-rich samples outside the trend from CO_2-poor, alkalic lamprophyre to recalculated compositions of CO_2-rich alkalic lamprophyres. However, some points, especially lamprophyre with the highest CO_2 concentration, plots at TiO_2 concentrations much lower than the recalculated point. We interpret this plot to indicate little loss of K_2O during CO_2 metasomatism, but probable loss of TiO_2. Points representing sub-alkalic lamprophyres plot at much lower TiO_2 and K_2O concentrations than alkalic lamprophyres.

The MgO versus CaO plot (fig. 39*B*) shows the original control of olivine and clinopyroxene phenocrysts on the composition of the rock. At highest MgO concentrations, CaO is low and is explained by the greater percentage of olivine phenocrysts to olivine plus clinopyroxene phenocrysts. As MgO decreases from more than 16 percent to about 10 percent, clinopyroxene phenocrysts increase and CaO increases. From about 10 percent to 8 percent MgO, both the percentage of clinopyroxene phenocrysts decreases rapidly and CaO shows a parallel decrease. Notably in this plot, samples of CO_2-rich lamprophyre plot at lower CaO concentrations than the trend from CO_2 poor to recalculated compositions. We interpret this dispersion, in combination with the recalculated chemical compositions, to show major CaO loss during metasomatism. Minor MgO gain during alteration may be suggested by the plot, but the scatter is within our uncertainties of point counts and recalculated chemistries.

A similar trend that can be explained by the percentage of clinopyroxene phenocrysts is apparent in the Al_2O_3 versus CaO plot (fig. 39*C*). Highest Al_2O_3 concentrations are for the most evolved, most sanidine and albite rich rocks. Highest CaO concentrations correspond to less evolved, clinopyroxene-rich rocks. Lowest CaO and Al_2O_3 concentrations are for olivine-rich rocks. All samples from CO_2-rich rocks plot below the igneous trend and substantiate CaO loss. Al_2O_3 loss is suggested by the shift of CO_2-rich samples to lower concentrations.

K_2O versus P_2O_5 (fig. 39*D*) reveals a similar, crescent shape for the igneous trend from olivine-rich rocks at low K_2O and low P_2O_5 concentrations, through clinopyroxene-rich rocks at high K_2O and intermediate P_2O_5 concentrations, to olivine- and clinopyroxene-poor rocks at low K_2O and high P_2O_5 values. A slight loss of P_2O_5 may be indicated by the data. Sub-alkalic lamprophyres plot at much lower concentrations of both oxides than do alkalic lamprophyres.

Some alkalic lamprophyre samples indicate strontium gain during CO_2 metasomatism (fig. 39*E*), but many retain their original values despite major loss of CaO. Much of the strontium must be in albite and clinopyroxene, but a major component could be in sanidine as well. Because we do not fully understand the sites in which strontium is residing, we cannot assess its gain or loss in the system.

The decrease in CaO concentrations is largely independent of P_2O_5 variation (fig. 39*F*). This factor is explained by calcium loss being effected through clinopyroxene, not apatite, replacement. However, this plot (and fig. 39*D*) does suggest minor P_2O_5 loss.

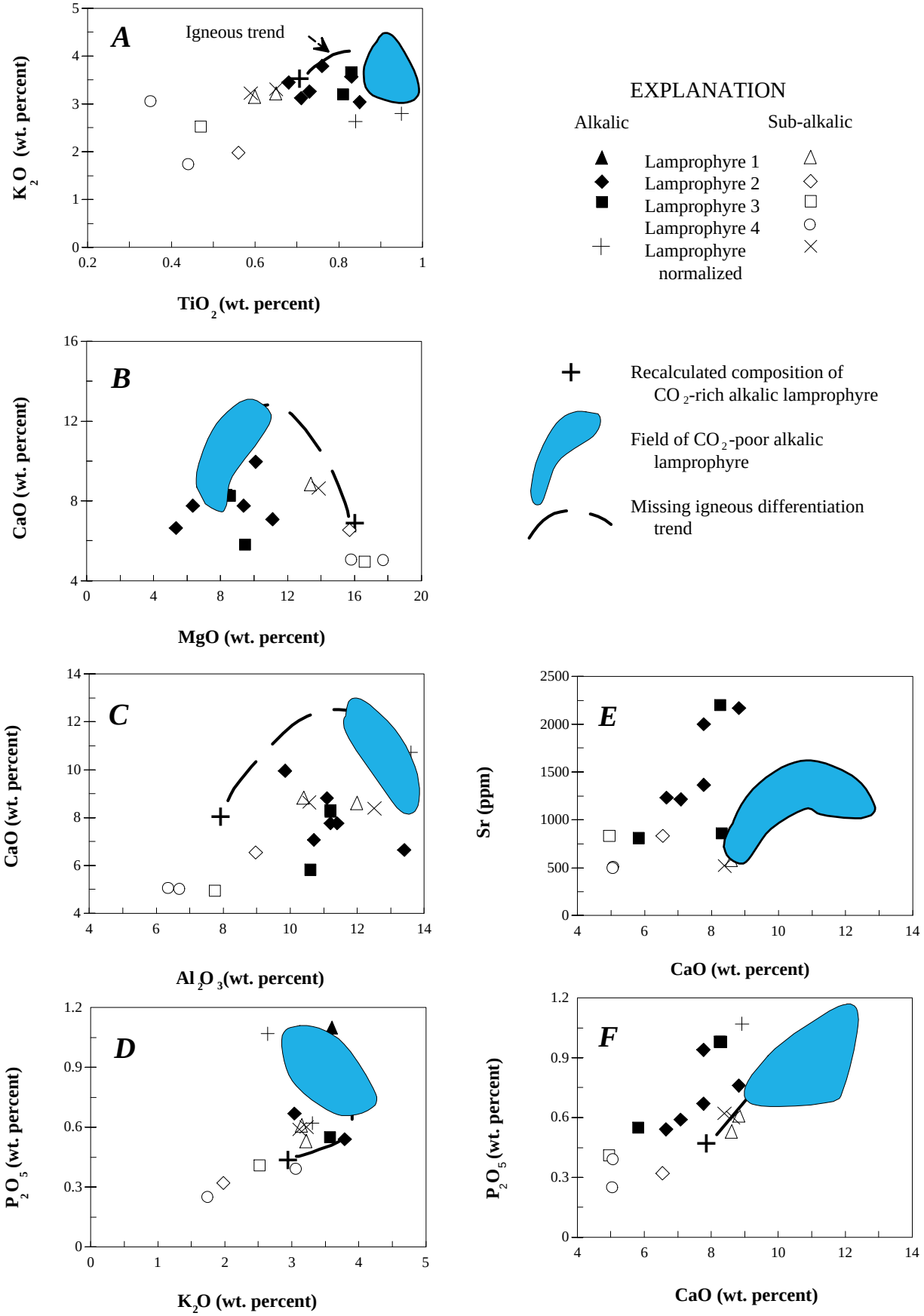
A
Igneous trend
K2O (wt. percent)
TiO2 (wt. percent)
EXPLANATION
Alkalic
Sub-alkalic
Lamprophyre 1
Lamprophyre 2
Lamprophyre 3
Lamprophyre 4
Lamprophyre normalized
B
CaO (wt. percent)
MgO (wt. percent)
Recalculated composition of CO2-rich alkalic lamprophyre
Field of CO2-poor alkalic lamprophyre
Missing igneous differentiation trend
C
CaO (wt. percent)
Al2O3(wt. percent)
E
Sr (ppm)
CaO (wt. percent)
D
P2O5 (wt. percent)
K2O (wt. percent)
F
P2O5 (wt. percent)
CaO (wt. percent)

GOLD ANALYSES OF LAMPROPHYRE AND OTHER IGNEOUS ROCKS

Although lamprophyre dikes clearly cut the mineralized breccia pipe, their spatial association with late shear zones and veins that produced high-grade gold during the period of early mining has led to speculation concerning a possible genetic relationship between gold deposition and lamprophyre emplacement. Also, the presence of magnesite as gangue in the breccia pipe and as replacement products of olivine and clinopyroxene in the lamprophyres may suggest that the latest stages of gold mineralization were coincident with lamprophyre emplacement. In their review of "calc-alkaline" lamprophyres, Rock and Groves (1988) suggest that lamprophyres may be an under-appreciated clan of rocks related to gold mineralization. As a test of the lamprophyre-gold model, all the samples of both lamprophyre groups collected at the Golden Sunlight mine were analyzed for gold, as were the other rock types for which we report major- and minor-element chemistry.

Of the 21 samples of lamprophyre, all but two have less than 0.05 ppm Au (table 10). Two samples of pyrite-bearing (about 2–3 percent pyrite) lamprophyre (88C1-301.5′, and 191-173.5′) have 0.1 and 0.05 ppm Au, respectively. Any suggestion of a genetic link between lamprophyre emplacement and gold mineralization is difficult to support with our data. Of three samples of rhyolite, only one, which contains pyrite (88GS-12), had a detectable concentration of gold (0.05 ppm Au). This sample, however, came from immediately adjacent to the breccia pipe (fig. 4) and should not be used to suggest that some of the rhyolite sills contained gold related to their emplacement. Wertz (1971) also suggested that rhyolite bodies removed from the breccia pipe were exceptionally low in base and precious metals.

Porter and Ripley (1985) observed that the lamprophyres they studied lacked sulfide minerals. Two of our core samples and one outcrop sample contain 2–3 percent pyrite in veinlets and as disseminations (88C1-301.5′, 191-173.5′, 88GS-8). We speculate that this sulfide mineralization is related to emplacement of the lamprophyre bodies and is younger than the breccia pipe mineralization. With our present data, however, we cannot rule out the possibility that the latest stages of breccia pipe formation overlapped in time with lamprophyre emplacement. Another, less likely, possibility is that lamprophyre magma entrained small amounts of auriferous pyrite from the breccia pipe or remobilized sulfur, gold, and iron from country rock on its ascent.

Table 10. Gold concentrations of igneous rocks in the Golden Sunlight mine area, southwestern Montana.

[0.05 ppm = 50 ppb; N, not detected at value shown. Analyses by B.H. Roushey]

Rock type	Sample no.	Au (ppm)
Basalt	88GS-1	N0.05
Tonalite	88GS-2	N0.05
Tonalite	88GS-4	N0.05
Rhyolite	88GS-7	N0.05
Rhyolite	88GS-12	0.05
Rhyolite	88GS-L	N0.05
Lamprophyre	88GS-3	N0.05
Lamprophyre	88GS-5	N0.05
Lamprophyre	88GS-6	N0.05
Lamprophyre	88GS-8	N0.05
Lamprophyre	88C1-256′	N0.05
Lamprophyre	88C1-283′	N0.05
Lamprophyre	88C2-559.5′	N0.05
Lamprophyre	88C3-292′	N0.05
Lamprophyre	88C3-299′	N0.05
Lamprophyre	88C3-301.5′	0.10
Lamprophyre	88C3-353.75′	N0.05
Lamprophyre	115-1537.5′	<0.05
Lamprophyre	115-1876′	N0.05
Lamprophyre	115-1882′	N0.05
Lamprophyre	151-417′	<0.05
Lamprophyre	189-642′	N0.05
Lamprophyre	190-642′	N0.05
Lamprophyre	190-1223.5′	<0.05
Lamprophyre	191-173.5′	0.05
Lamprophyre	191-1034′	N0.05
Lamprophyre	191-2025′	N0.05

MODEL FOR CO_2 METASOMATISM

Petrographic and chemical evidence reveal that addition of large amounts of CO_2 to lamprophyres in the Golden Sunlight mine area resulted in profound mineralogic and chemical changes to the rocks. Phenocrysts of olivine and clinopyroxene and groundmass clinopyroxene were extensively replaced by magnesite, dolomite, and minor sericite and biotite. Groundmass sanidine and albite were largely stable during the CO_2 metasomatism but were locally converted to sericite and mixtures of quartz and orthoclase. Shapes and sizes of relict phenocrysts and the unchanged texture and size of groundmass minerals indicates that volume change was insignificant during metasomatism. Mineral chemistries and modal data for the most CO_2-rich lamprophyres indicate that 40–50 percent of the Fe_2O_3, CaO, and Na_2O; 20–25 percent of the Al_2O_3; and 10–15 percent of the SiO_2 and FeO were removed during addition of 15–20 weight percent CO_2. Concentrations of MgO, K_2O, Cr, Ni, and possibly Co remained unchanged during metasomatism.

Figure 39 (previous page). Multielement plots illustrating differentiation and alteration trends in lamprophyre. *A*, TiO_2 versus K_2O; *B*, MgO versus CaO; *C*, Al_2O_3 versus CaO; *D*, K_2O versus P_2O_5; *E*, CaO versus Sr; *F*, CaO versus P_2O_5. Field of CO_2-poor alkalic lamprophyre shown for comparison. Heavy, curved and dashed line connects CO_2-poor alkalic lamprophyre with recalculated composition of original, non-metasomatized alkalic lamprophyre.

We believe that the most plausible explanation for the above observations is that a magmatic CO_2-rich fluid or gas enriched in alkali-earth elements attacked olivine and clinopyroxene phenocrysts in the mafic magma as the groundmass minerals were crystallizing during dike emplacement. The CO_2-rich fluid most likely exsolved from the primary magma upon cooling. Fine-grained, euhedral, interstitial carbonate minerals within the groundmass that are not replacement products indicate that fairly large amounts of CO_2 were dissolved in the magma before solidification. Although we lack isotopic data that could substantiate a genetic link, we believe that this CO_2-rich fluid or gas was derived from the original partial melting event in the mantle that generated the alkalic lamprophyre magma. Except for the possible addition of minor amounts of Sr to the system, we see no evidence of the types of element enrichments typically found in carbonatite settings (i.e., LREE, Cu, Na, P, etc.). Therefore, the lamprophyre dikes do not appear to be related to a more complex, but unexposed, igneous center.

A further indication that CO_2 metasomatism was an integral part of the magmatic history, and not of a later, unrelated alteration, is the paucity of CO_2-poor lamprophyre samples having high MgO and modal olivine. Our sampling of surface outcrops and drill core indicates that, for the most part, only CO_2-rich samples contain relicts of olivine greater than 5 volume percent. In other words, if the lamprophyre magma contained abundant olivine, that olivine is invariably transformed into carbonate minerals. The more primary olivine the magma contained, the greater the present percentage of carbonate minerals. If CO_2 metasomatism had been a later, unrelated event, or one controlled by structures or fractures, the pattern of olivine replacement would not be so predictable.

The existence of CO_2-poor lamprophyre grading into CO_2-rich lamprophyre in drill-core samples is explained by original variability in phenocryst percentages. In drill hole C3, lamprophyre samples at 299′ depth (table 1) contain 8 percent CO_2. Lamprophyre sampled at 292′ depth (table 1) contains 0.4 percent CO_2. Petrographically, sample 299 has 10 percent olivine, but sample 292 contains about 5 percent olivine. More olivine was present in sample 299, so more was replaced by the CO_2-rich fluid or gas phase in the magma. What at first looks like a possible structural control to CO_2 metasomatism turns out to be a compositional control imparted by the phenocrysts.

Abundant sanidine in the groundmass of the dikes indicates emplacement temperatures of the lamprophyre dikes of at least 700°C. This temperature is notably higher than the maximum temperature of 600°C suggested by Rock (1984) for typical lamprophyre magmas and suggests that intrusives at the Golden Sunlight mine may not be "typical" lamprophyres. Based on the phenocryst assemblage (olivine and clinopyroxene and lack of plagioclase and orthopyroxene), Swanson (1989), using the summary of Edgar (1987), suggested that phenocrysts crystallized at depths between about 24 and 41 km and temperatures of about 1,210°–1,270°C. Without a critical comparison of the chemistry of the sample quoted by Edgar (1987) and the lamprophyre bodies at the Golden Sunlight mine, we cannot evaluate whether the experimental results are directly applicable.

What became of the elements that were depleted from the lamprophyres during CO_2 metasomatism? No extensive alteration envelopes related to the mafic dikes are currently recognized in the vicinity of the Golden Sunlight mine, nor are there extensive vein networks that could contain the deposited products of the CO_2-rich gas or fluid. If the depleted elements were transported away from the lamprophyre bodies in a CO_2-rich hydrothermal fluid, that fluid, upon cooling, would precipitate epidote, quartz, calcite, and trace albite in the approximate ratios 6:2.5:1.5:trace. Because we do not see this vein or alteration assemblage at the Golden Sunlight mine, we can infer only that the depleted elements were carried farther upward or outward from the immediate area that we sampled.

Hypotheses have been proposed for the formation of some lamprophyre magma involving direct melting of normal mantle peridotite under high P_{CO_2} conditions with or without "zone refining" (Velde, 1971; Rock, 1984). Other models have suggested that lamprophyres result from 1–20 percent partial melting of mantle lherzolite. Regardless of which model(s) are appropriate, most workers agree that alkalic rocks of this composition had their ultimate source in the mantle. Rapidly changing physical and chemical conditions of the lamprophyre magma are indicated by strongly zoned and partially resorbed clinopyroxene phenocrysts and strongly embayed biotite phenocrysts. These changes probably took place during rapid ascent of the magma to the surface. The validity of any specific models for the lamprophyre dikes at the Golden Sunlight mine is uncertain until additional isotopic studies, especially Rb-Sr, C, and Sm-Nd, can be undertaken.

The separation on nearly all multielement plots of alkalic lamprophyres (alkalic gabbro and olivine gabbro) from sub-alkalic lamprophyres (gabbro-diorite) indicates to us that the two lamprophyres are probably derived from separate, though possibly related, magmas. Whether or not one group is older than the other is not known. Both have CO_2-metasomatized variants and both have similar apparent and real element enrichment and depletion trends. Were these two groups formed independently in the mantle, only to arrive at the same place in the upper crust? Did the two groups evolve from a common parent magma in the mantle? Only further, more detailed data will answer these questions.

Another possible, but we think less probable, model for CO_2 metasomatism involves incorporation of CO_2 from reaction with limestone and dolomite in the Proterozoic or Paleozoic strata in the area. Major thrusting of Precambrian Belt Supergroup rocks over Paleozoic to Mesozoic sedimentary and volcanic strata during the Late Cretaceous took place in the vicinity of the Golden Sunlight mine (Schmidt and others, 1988). Any thrusts are now buried by Cenozoic

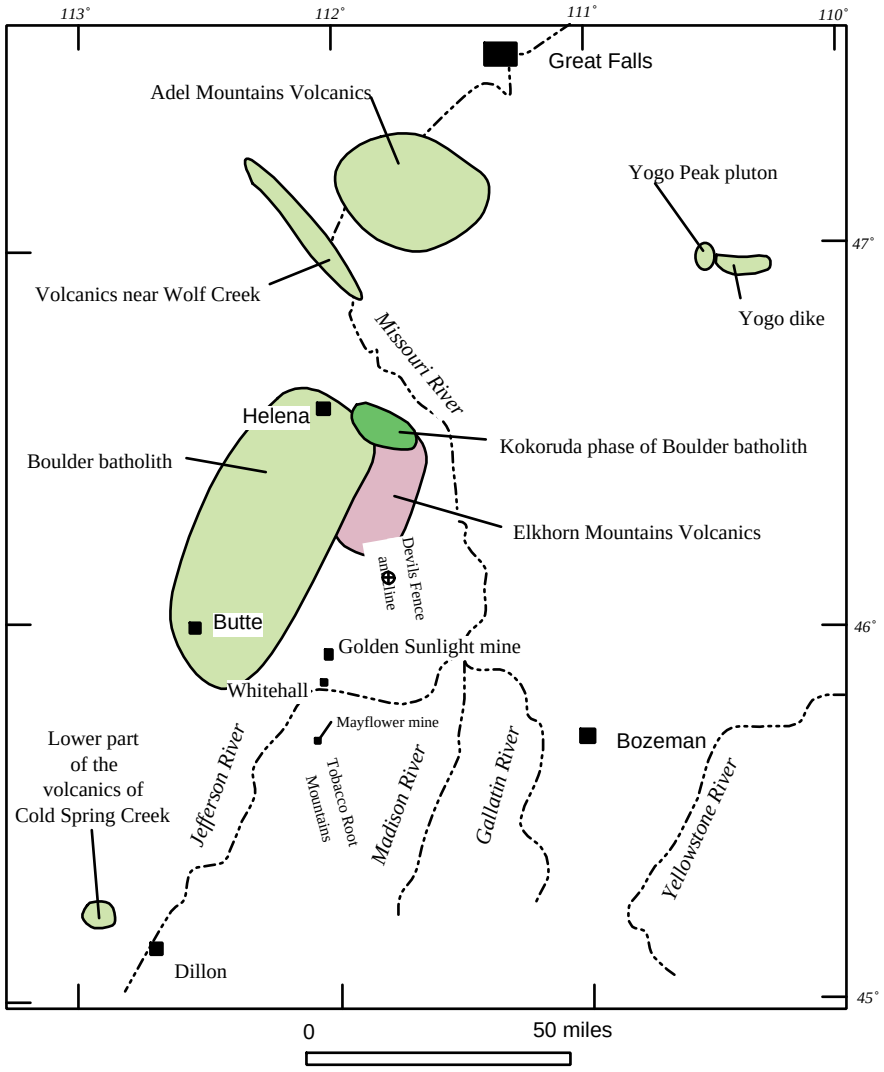

Figure 40. Location map of southwestern Montana showing localities and rock units discussed in text. Drill hole on Devils Fence anticline shown by plus sign inside circle.

deposits south of the Golden Sunlight mine. One fault at the Mayflower mine in the northern Tobacco Root Mountains (fig. 40) juxtaposes Belt Supergroup rocks and rocks as young as Late Cretaceous (Elkhorn Mountains Volcanics), but it may be a reverse fault. A major transverse (east-west-striking) fault zone has been mapped (Alexander, 1955; Robinson, 1963; Schmidt and others, 1988) south of Whitehall that could be interpreted as a tear fault between thrust plates. The aggregate eastward transport of the block occupied by the Golden Sunlight mine was at least 15 km. Possible evidence for major thrusting is provided by a 4,525 m (14,846 ft) drill hole on the Devils Fence anticline approximately 30 km northeast of the mine (Burton and others, 1991; Ballard and others, 1994). There, a major thrust, possibly the Lombard, was suggested at a depth of 2,130 m, which juxtaposed upper plate Belt Supergroup rocks of the Spokane, Greyson, and Newland Formations with Cretaceous Elkhorn Mountains Volcanics and the Slim Sam and Blackleaf Formations. The presence of Cretaceous strata was interpreted, partly, on the basis of Cretaceous dinoflagellates, which W.J. Perry, Jr., M.J. Pawlewicz, T.A. Daws, T.S. Dyman, and G.A. Desborough (written commun., 1995) consider to be a possible contaminant from bentonite drilling mud that contained Cretaceous fossils. Stratigraphy of the sedimentary rocks in question, the presence of porcellenite beds, and minor diabasic sills in the sedimentary rocks suggest that the rocks below the possible thrust may be part of the Belt Supergroup.

CORRELATION OF LAMPROPHYRES AND RHYOLITE WITH ROCKS IN SURROUNDING AREAS

Rocks as mafic or alkalic as the lamprophyres at the Golden Sunlight mine are not widely known in southwestern Montana. However, slightly more evolved basaltic to andesitic volcanic rocks in surrounding areas could be related to the lamprophyres. Felsic volcanic rocks are quite widespread in southwestern Montana, and some could be related to the sills of rhyolite that are so numerous in the mine area. We suggest the following correlation, based on analysis of chemical data (Ruppel, 1963; Schmidt, 1978; Lambe, 1981; Rutland, 1985; Ivy, 1988) from intrusive and extrusive rocks from south of Great Falls to north of Dillon (fig. 40).

Rocks that are chemically similar to the alkalic lamprophyres are augite trachybasalt found in the Adel Mountains Volcanics in the Wolf Creek area north of Helena (Schmidt, 1978). Although not as mafic as the lamprophyres (fig. 41*A*), the trachybasalt is alkalic to alkali-calcic and ranges in chemical composition from trachybasalt to latite and easily could be related to the lamprophyres by fractional crystallization. A relationship through fractional crystallization would also explain the trends away from the alkalic lamprophyres in alumina saturation (fig. 41*B*) and iron enrichment (fig. 41*D*). The trend toward a more sodic nature (fig. 41*C*) is not well explained by fractional crystallization, however. The trachybasalt flows lack olivine phenocrysts, but contain abundant augite in a groundmass of labradorite, sanidine, magnetite, and apatite. A Late Cretaceous paleomagnetic pole age (Gunderson and Sherif, 1991) for the Adel Mountain Volcanics agrees with the 77-Ma date determined by ^{40}Ar-^{39}Ar analyses for biotite from one lamprophyre in this study. The best estimate by Harlan and others (1991) for the age of flow units in the Adel Mountain Volcanics is 75–76 Ma, which is also in reasonable agreement with the 77-Ma biotite date.

The one picritic (ultramafic) analysis of the Yogo Peak pluton also is similar in chemistry to the alkalic lamprophyres (fig. 41*A*). In terms of alumina saturation (fig. 41*B*) and alkalinity (fig. 41*C*), the analysis of the pluton is more similar to the alkalic lamprophyres than are the analyses of the Adel Mountains Volcanics. Additional geochemical data would aid in our interpretation of chemical similarity to the data of Embry (1987). Existing geochronologic data (Marvin and others, 1973) suggest an age of 50 Ma age for the Yogo Peak pluton, so the lamprophyre at the Golden Sunlight mine does not appear to be time correlative to the Yogo Peak pluton.

Rocks that are chemically most similar to the sub-alkalic lamprophyres are the majority of flows in the informally named unit 8 of the Elkhorn Mountains Volcanics (Rutland, 1985). These calc-alkalic andesitic basalts to andesites are slightly more felsic than the gabbro-diorite at the mine (fig. 41*A*), but have similar alumina saturations (fig. 41*B*), are very potassic (fig. 41*C*), and are very Mg rich (fig. 41*D*). Unit 8 of the Elkhorn Mountains Volcanics averages 440 ppm Cr, 113 Ni, and 681 ppm Sr, and has REE_{CN} profiles that are LREE enriched and have no Eu anomalies (Rutland, 1985)—these values are very similar to the sub-alkalic lamprophyres (fig. 42). Estimated ages for the Elkhorn Mountains Volcanics are 77–79 Ma (Tilling and others, 1968), which are in agreement with the 77-Ma biotite date. Basalt flows in the Elkhorn Mountains Volcanics just west of the mine (Prostka, 1966) have a modal mineralogy similar to the alkalic lamprophyre, but chemical analyses are lacking for these flows.

Other units (fig. 41) that have chemical similarity to the sub-alkalic lamprophyres are rocks that intrude the Elkhorn Mountains Volcanics (Klepper and others, 1971) and some flow units from the lower part of the volcanics of Cold Spring

Figure 41 (following page). Major-element plots of Cretaceous-Tertiary mafic rocks in western Montana. Fields of alkalic (A) and sub-alkalic (SA) lamprophyre at the Golden Sunlight mine shown for comparison. Adel, Adel Mountains Volcanics; data from Schmidt (1978). Wolf Creek, volcanics near Wolf Creek that are possibly correlative with Adel Mountains Volcanics; data from Schmidt (1978). Kokoruda, Kokoruda phase of the northern part of the Boulder batholith; data from Smedes (1966). Yogo dike, sapphirine-bearing Yogo dike; data from Clabaugh (1952) and Dahy (1991). Yogo Peak, Yogo Peak pluton; data from Embry (1987). Boulder batholith (mafic), mafic rocks that predate the main part of the Boulder batholith; data from Lambe (1981). Elkhorn Volcanics, unit 8, informal unit 8 of the Elkhorn Mountains Volcanics, which corresponds to the upper part of the volcanics (Smedes, 1966; Klepper and others, 1971); data from Rutland (1985). Elkhorn intrusives, intrusive rocks that cut the Elkhorn Mountains Volcanics; data from Klepper and others (1971). Cold Spring, lower, lower part of the volcanics of Cold Spring Creek; data from Ivy (1988). *A*, R_1 versus R_2 plot (De LaRoche and others, 1980); Picritic, picritic composition or ultramafic rocks; Thr, therallite; Gb-No, gabbro-norite; T Bas, trachybasalt; Lat Bas, latibasalt; And-Bas, andesitic basalt (gabbro-diorite is plutonic equivalent); T And, trachyandesite; Lat, latite (monzonite is plutonic equivalent); Lat-And, lati-andesite (monzodiorite is plutonic equivalent); And, andesite (diorite is plutonic equivalent); Q Tr, quartz trachyte; Q Lat, quartz latite; Dac, dacite (tonalite is plutonic equivalent); R dac, rhyodacite. Fields of alkalinity modified slightly from DeWitt (1989). Samples that plot to left of diagram are shown on left margin and have arrows leading to the left. *B*, SiO_2 versus A/CNK plot; A/CNK, molar alumina/sum of molar calcium, sodium, and potassium; field of unaltered igneous rocks from DeWitt (unpub. data, 1994). Samples that plot below the diagram are shown on the bottom border and have arrows leading down. *C*, $K_2O/(K_2O+Na_2O)$ versus SiO_2 plot; *x*-axis is "K number" listed in table 1; field boundaries from DeWitt (unpub. data, 1995). Samples that plot below the diagram are shown on the bottom border and have arrows leading down. *D*, $(FeO+0.89Fe_2O_3)/(FeO+0.89Fe_2O_3+MgO)$ versus SiO_2 plot; *x*-axis is "Fe number" listed in table 1; field boundaries modified from DeWitt (1989). Samples that plot to the left of the diagram are shown on the left border and have arrows leading to the left. Samples that plot in the very Mg-rich field, below plot (C), have arrows leading to the left or up.

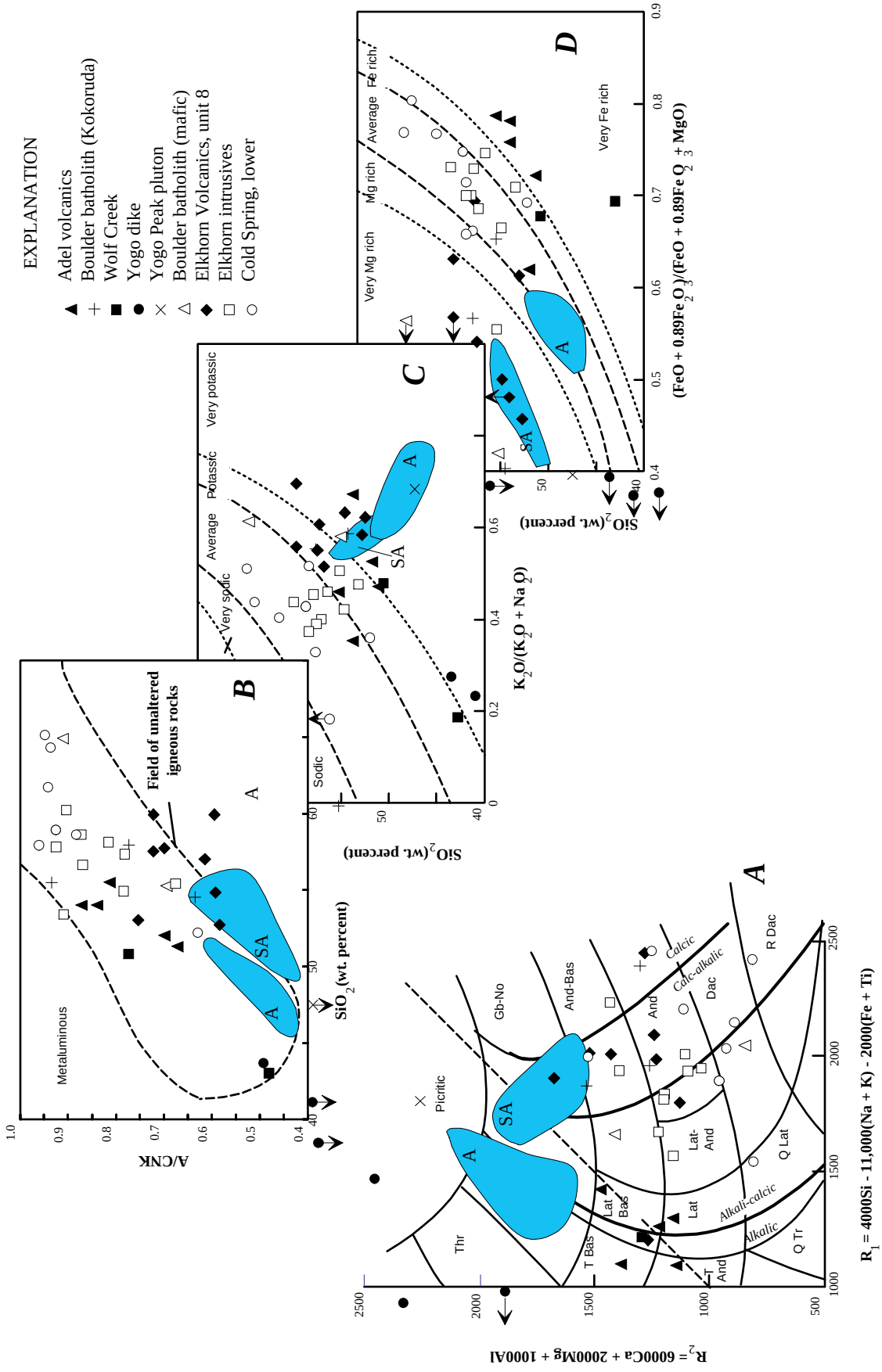
EXPLANATION
Adel volcanics
Boulder batholith (Kokoruda)
Wolf Creek
Yogo dike
Yogo Peak pluton
Boulder batholith (mafic)
Elkhorn Volcanics, unit 8
Elkhorn intrusives
Cold Spring, lower
A
B
C
D
SA
Field of unaltered igneous rocks
Metaluminous
A/CNK
SiO2 (wt. percent)
Very Mg rich
Mg rich
Average
Fe rich.
Very Fe rich
Very potassic
Potassic
Average
Very sodic
Sodic
SiO2 (wt. percent)
K2O/(K2O + Na2O)
(FeO + 0.89Fe2O3)/(FeO + 0.89Fe2O3 + MgO)
Picritic
Gb-No
And-Bas
And
Dac
R Dac
Thr
T Bas
Lat Bas
Lat
Lat-And
Q Lat
T And
Q Tr
Alkalic
Alkali-calcic
Calc-alkalic
Calcic
R2 = 6000Ca + 2000Mg + 1000Al
R1 = 4000Si - 11,000(Na + K) - 2000(Fe + Ti)

Creek near Bannack (Ivy, 1988). ^{40}Ar–^{39}Ar dates of hornblende from flows and ash flows in the volcanics of Cold Spring Creek are 76–78 Ma (Ivy, 1988), in agreement with the 77-Ma biotite date. Although a direct age-equivalent correlation cannot be proven with existing data between lamprophyre bodies at the Golden Sunlight mine and other mafic rocks in southwestern Montana, the data do indicate that mafic, alkalic plutonism and volcanism was taking place in western Montana in Late Cretaceous time. Further work will undoubtedly refine the correlations suggested by this work.

Rocks similar in age and chemistry to the rhyolite sills at the Golden Sunlight mine are present in the informally named units 7, 9, and 11 of the Elkhorn Mountains Volcanics (Rutland, 1985). Alkali-calcic lati-andesite to rhyodacite welded tuff units plot on a trend that would intersect the freshest felsic sills at the mine (fig. 43). Unit 11 is the most similar to rhyolite at the mine in terms of alumina saturation (fig. 40*B*), alkali enrichment (fig. 43*C*), and iron enrichment (fig. 43*D*). Limited analyses of units 7 and 9 may obscure their similarity to rhyolite at the mine. The most evolved of the rhyolites in unit 7 have Sr, Zr, and Fe numbers that are similar to those of the freshest rhyolite sills at the mine. Samples of rhyolitic welded tuff from the middle part of the Elkhorn Mountains Volcanics (Smedes, 1966) are also similar in major element composition to the sills at the mine.

If the rhyolite sills at the mine are temporally and genetically related to emplacement of voluminous ash-flow deposits of unit 7, 9, or 11 of the Elkhorn Mountains Volcanics, the source for both sills and tuffs may have been within the crust, as suggested by Rutland (1985). If basaltic flows of unit 8 are temporally and genetically related to emplacement of lamprophyre dikes, their source may have been in the mantle, not within the crust. Therefore, differing source areas over time may characterize parts of the Elkhorn Mountains Volcanics. A complete analysis of this possibility awaits further study.

CONCLUSIONS

The gold-mineralized breccia pipe at the Golden Sunlight mine, southwestern Montana, cuts strata of the Belt Supergroup and sills of Late Cretaceous rhyolite. Within the pipe, rhyolite forms the matrix for downdropped fragments and is mineralized by disseminated, auriferous pyrite, molybdenite, and hematite. The pipe is inferred to grade downward into an alkalic, porphyry molybdenum deposit. Dikes and sills of alkalic and sub-alkalic lamprophyre cut the pipe, and they possibly locally remobilized minor amounts of gold along their margins. Late shear zones and veins that contain high-grade gold also contain mineralized lamprophyre bodies. Determining the petrogenesis and age of the rhyolite, gold mineralization, and lamprophyres was the focus of this investigation.

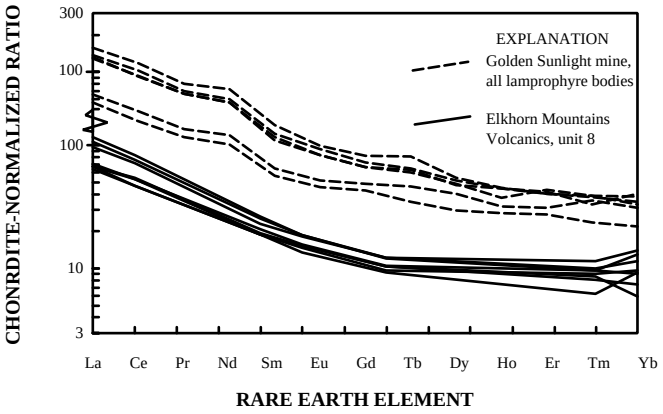

Figure 42. Chondrite-normalized rare-earth-element plot for mafic volcanic rocks in unit 8 of the Elkhorn Mountains Volcanics. Data from Rutland (1985). Lamprophyre of group 1 (CO_2 less than 2 percent) from Golden Sunlight mine plotted for comparison. Top four dashed curves are for alkalic lamprophyre; bottom two dashed curves are for sub-alkalic lamprophyre.

The rhyolite was difficult to characterize chemically because of its altered nature. Least altered samples are alkali-calcic, mildly peraluminous, very sodic, and Mg rich. Alteration near the breccia pipe creates hydrothermal sericite and orthoclase and turns the rhyolite into an alkalic quartz syenite that is strongly peraluminous, potassic to very potassic, and Fe rich to very Fe rich. No REE mobility was verified during alteration.

Figure 43 (following page). Major-element plots of Cretaceous-Tertiary felsic rocks in the Elkhorn Mountains Volcanics, western Montana. Field of "unaltered" rhyolite at the Golden Sunlight mine shown by stippled area. Elkhorn air-fall tuff, air-fall tuff from the Elkhorn Mountains Volcanics; data from Rutland (1985). Elkhorn 01 through 13, welded tuff from the Elkhorn Mountains Volcanics [numbers increase up-section]; data from Rutland (1985). Elkhorn, lower, welded tuff from lower part of the Elkhorn Mountains Volcanics; data from Ruppel (1963). Elkhorn, middle, middle part of the Elkhorn Mountains Volcanics; data from Smedes (1966) and Klepper and others (1971). Elkhorn, upper, upper part of the Elkhorn Mountains Volcanics; data from Knopf (1913), Ruppel (1963), and Robertson (1953). *A*, R_1 versus R_2 plot (De LaRoche and others, 1980); T Bas, trachybasalt; Lat Bas, latibasalt; And-Bas, andesitic basalt (gabbro-diorite is plutonic equivalent); T And, trachyandesite; Lat, latite (monzonite is plutonic equivalent); Lat-And, lati-andesite; And, andesite (diorite is plutonic equivalent); Tr, trachyte; Q Tr, quartz trachyte; Q Lat, quartz latite; Dac, dacite; R Dac, rhyodacite; Rhy, rhyolite; Alk Rhy; alkali rhyolite. Fields of alkalinity modified slightly from DeWitt (1989). *B*, SiO_2 versus A/CNK plot; A/CNK, molar alumina/sum of molar calcium, sodium, and potassium; field of unaltered igneous rocks from DeWitt (unpub. data, 1994). *C*, $K_2O/(K_2O+Na_2O)$ versus SiO_2 plot; *x*-axis is "K number" listed in table 1; field boundaries from DeWitt (unpub. data, 1995). *D*, $(FeO+0.89Fe_2O_3)/(FeO+0.89\ Fe_2O_3+MgO)$ versus SiO_2 plot; *x*-axis is "Fe number" listed in table 1; field boundaries modified from DeWitt (1989).

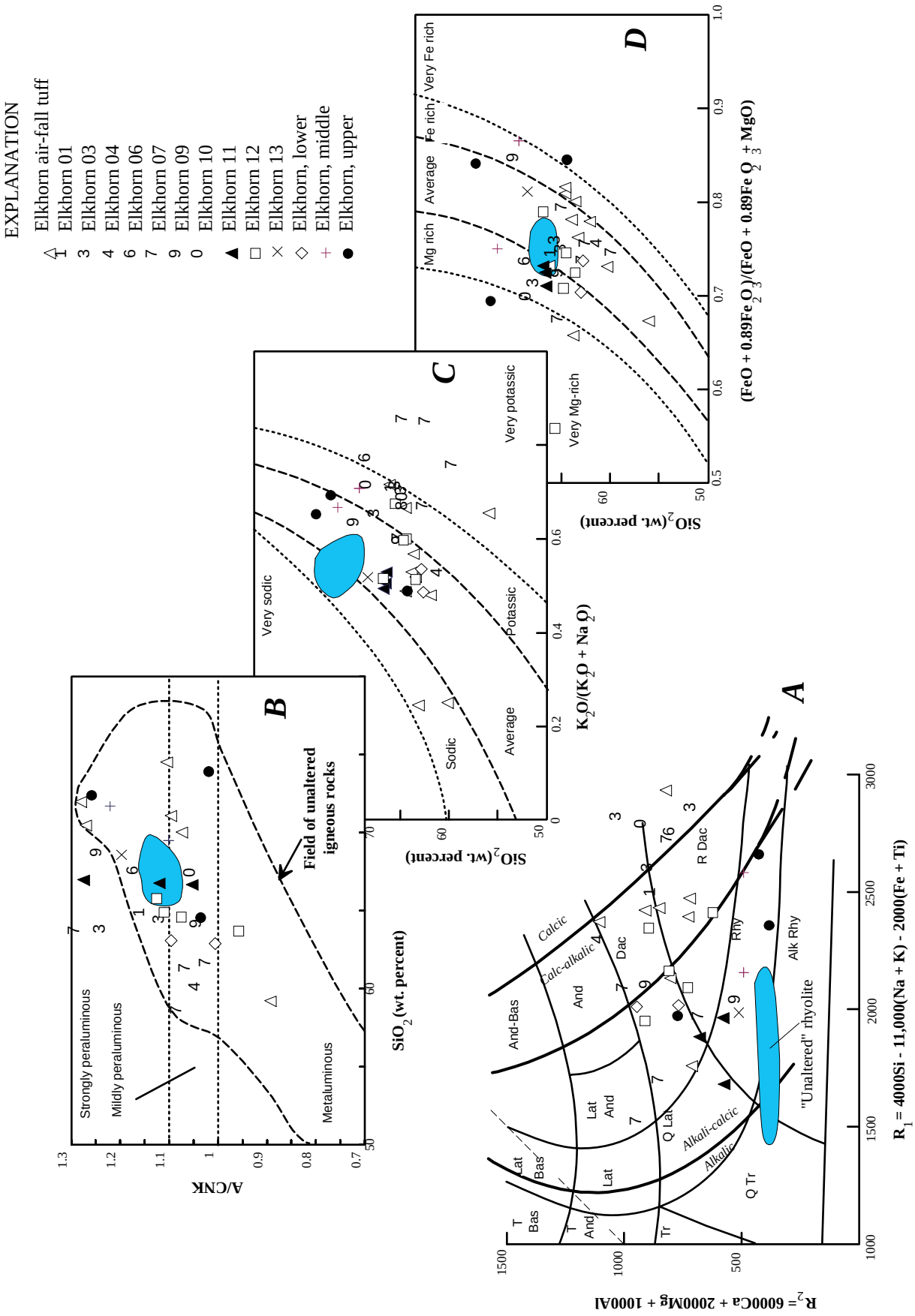
EXPLANATION
Elkhorn air-fall tuff
Elkhorn 01
Elkhorn 03
Elkhorn 04
Elkhorn 06
Elkhorn 07
Elkhorn 09
Elkhorn 10
Elkhorn 11
Elkhorn 12
Elkhorn 13
Elkhorn, lower
Elkhorn, middle
Elkhorn, upper
A
B
C
D
Strongly peraluminous
Mildly peraluminous
Metaluminous
Field of unaltered igneous rocks
A/CNK
SiO2 (wt. percent)
Very sodic
Sodic
Average
Potassic
Very potassic
K2O/(K2O + Na2O)
SiO2 (wt. percent)
Mg rich
Average Fe rich
Very Fe rich
Very Mg-rich
(FeO + 0.89Fe2O3)/(FeO + 0.89Fe2O3 + MgO)
SiO2 (wt. percent)
Calcic
Calc-alkalic
Alkali-calcic
Alkalic
And-Bas
And
Dac
R Dac
Lat And
Lat
Q Lat
Rhy
Alk Rhy
"Unaltered" rhyolite
T Bas
T And
Lat Bas
Tr
Q Tr
R2 = 6000Ca + 2000Mg + 1000Al
R1 = 4000Si - 11,000(Na + K) - 2000(Fe + Ti)

Determination of a precise crystallization age of the rhyolite from analysis of zircon by the U-Th-Pb method was made difficult by the presence of inherited lead or inherited zircon of Late Archean age. If an emplacement age of about 80 Ma is assumed for the rhyolite, an age of inheritance of 2,600 Ma can be calculated. That age agrees with basement ages determined for much of southwestern Montana. Determination of a crystallization age of the rhyolite by fission-track methods was not possible, but the zircon fission-track data are permissive of indicating slow uplift during Laramide time. Additional data would be necessary to corroborate this possibility.

Common lead dating of altered Belt Supergroup strata and rhyolite in and near the breccia pipe resulted in a ^{206}Pb-^{238}U date of 84±18 Ma. We interpret the alteration to be related to gold deposition in the breccia pipe. Other Pb-Pb dating techniques corroborate this date, but are less precise. Attempts to date hydrothermal sericite from the rhyolite were unsuccessful, possibly in part because of chemical treatments that had to be employed during the mineral-separation process.

Lamprophyre dikes and sills that cut the breccia pipe are of two distinct groups, one alkalic and the other sub-alkalic. The alkalic group is predominately alkali gabbro that is metaluminous, very potassic, and has little iron enrichment. The sub-alkalic group is gabbro-diorite that is metaluminous very potassic, and very Mg rich. The lamprophyre bodies are heterogeneous, show wide variation in phenocryst mineral percentages, and range from CO_2 poor to CO_2 rich (0.2–20 weight percent CO_2). Primary igneous textures are generally well preserved. The alkalic lamprophyre averages 3.8 percent K_2O, 0.9 percent TiO_2, 87 ppm Ni, and 337 ppm Cr. The sub-lamprophyre averages 3.1 percent K_2O, 0.64 percent TiO_2, 250 ppm Ni, and 640 ppm Cr. Phenocrysts (in decreasing order of abundance) in both groups are clinopyroxene (diopsidic augite), olivine (about $Fo_{85–90}$), and much lesser amounts of biotite that has elevated concentrations of Cr, Ni, V, and Ba. Magnesium numbers indicate that the CO_2-poor, sub-alkalic lamprophyres represent primitive magmas that are somewhat enriched in incompatible elements. The two groups are interpreted to be cogenetic, but they possibly were derived from different degrees of partial melting or different source regions in the mantle.

Extensive CO_2 metasomatism of both groups resulted in destruction of olivine phenocrysts and creation of an alteration assemblage dominated by magnesite. CO_2-rich lamprophyre has olivine relicts that are replaced by: (1) limonite(?) and magnesite, (2) magnesite, sericite, and minor biotite, and (3) magnesite. Skeletal diopsidic augite is altered to dolomite and minor amounts of magnesite. Quartz is present in one sample as a breakdown product of augite but is absent in all other rocks. Biotite phenocrysts are mostly unaltered but are strongly embayed by groundmass minerals. Much biotite in the groundmass is unaffected, but some is replaced by sericite. Where carbonate metasomatism is extreme (10–20 percent CO_2), clinopyroxene is completely replaced by dolomite, magnesite, and minor siderite. Sanidine in the groundmass may or may not be replaced by sericite. Metasomatic alteration of the lamprophyres involved introduction of CO_2, and depletion of CaO, Fe_2O_3, Na_2O, Al_2O_3, SiO_2, and FeO, in decreasing percentages.

The two groups of CO_2-poor lamprophyres have similarly shaped chondrite-normalized rare-earth-element (REE) patterns, but the alkalic group plots above and distinctly separate from the sub-alkalic group. With increasing concentration of CO_2, lamprophyres retain their La/Yb_{CN} values, but possess overall lower concentration of all REE. This apparent decrease may be simply a function of the most olivine-rich lamprophyres having originally had the lowest concentrations of REE. True mobility of rare earth elements during CO_2 metasomatism cannot be documented.

The lamprophyres possibly began to crystallize at depths between 24 and 41 km and temperatures of about 1,210°–1,270°C (Swanson, 1989). Initial crystallization involved precipitation of olivine and clinopyroxene followed by phlogopite-biotite. Strong zoning of clinopyroxene suggests highly variable physico-chemical conditions during crystallization, which may have been caused by rapid ascent of the magma during clinopyroxene crystallization. Crystallization of the fine-grained groundmass took place during or after dike emplacement because no subsolidus deformation or flow foliation is noted. Textural evidence indicates that CO_2 metasomatism during and after(?) dike emplacement was caused by an alkali-rich, CO_2-rich fluid that was out of equilibrium with early-formed phenocrysts, but in equilibrium with sanidine, biotite, and apatite in the groundmass. The extent to which lamprophyre bodies were CO_2 metasomatized was controlled by the percentage of olivine and clinopyroxene phenocrysts that were available to be altered. The CO_2-rich fluid is presumed to be of magmatic origin and related to generation of the lamprophyres from mantle materials.

Two biotite separates from different lamprophyre bodies have a conventional K-Ar date of 79.8±2.8 Ma and a ^{40}Ar-^{39}Ar plateau date of 76.9±0.5 Ma. We interpret the 76.9-Ma date to indicate lamprophyre emplacement in Late Cretaceous time. Whether or not the generation of CO_2-rich lamprophyre magma from mantle depths had any impact on the generation of the Golden Sunlight breccia pipe cannot be proven without additional isotopic data.

Some volcanic rocks in southwestern Montana bear close chemical similarity to both rhyolite and lamprophyre at the Golden Sunlight mine. Rhyolitic ash flow tuffs in the Elkhorn Mountains Volcanics, especially informally named units 7, 9, and 11 (Rutland, 1985), are very similar chemically to the least altered rhyolite at the mine. The estimated age of The Elkhorn Mountains Volcanics of about 75 to 80 Ma is in agreement with the estimated age of the rhyolite at the mine. The Adel Mountains Volcanics are slightly more

felsic than lamprophyre bodies at the mine, but are chemically very similar. Estimated ages of the Adel Mountains Volcanics of 75 to 76 Ma are in excellent agreement with the 77-Ma age of biotite from the lamprophyre. Informally named mafic unit 8 of the Elkhorn Mountains Volcanics is also very similar to both alkalic and sub-alkalic lamprophyre at the mine. If the correlation of unit 8 and the lamprophyre at the mine is valid, unit 8 may prove to be a time line for the Elkhorn Mountains Volcanics.

REFERENCES CITED

Alexander, R.G., Jr., 1955, Geology of the Whitehall area, Montana: Yellowstone-Bighorn Research Association Contribution 195, 111 p.

Ballard, D.W., Burton, B.R., Lageson, D.R., and Warne, J.R., 1993, Drilling experience at Devils Fence anticline, Jefferson County, Montana; baseline data for future activity in a promising overthrust province, *in* Hunter, L.D.V., ed., Energy and Mineral Resources of Central Montana: Montana Geological Society 1993 Field Conference Guidebook, p. 159–168.

Burton, B.R., Perkins, M.J., Ballard, D.W., Warne, J.R., and Lageson, D.R., 1991, Regional structural implications of drilling results at Devils Fence anticline, Jefferson County, Southwest Montana [abs.]: Rocky Mountain Section Meeting, American Association of Petroleum Geologists–Society of Economic Paleontologists and Mineralogists, p. 30.

Clabaugh, S.E., 1952, Corundum deposits of Montana: U.S. Geological Survey Bulletin 983, 100 p.

Dahy, J.P., 1991, Geology and igneous rocks of the Yogo sapphire deposit, Little Belt Mountains, Montana, *in* Baker, D.W., and Berg, R.B., eds., Guidebook of the Central Montana Alkalic Province; Geology, Ore Deposits, and Origin: Montana Bureau of Mines and Geology Special Publication 100, p. 45–54.

Deer, W.A., Howie, R.A., and Zussman, J., 1977, An Introduction to the Rock-Forming Minerals: Longman, London, 528 p.

De LaRoche, H., Leterrier, J., Grandclaude, P., and Marchal, M., 1980, A classification of volcanic and plutonic rocks using R_1-R_2 diagram and major-element analyses—Its relationship with current nomenclature: Chemical Geology, v. 29, p. 183–210.

DeWitt, Ed, 1989, Geochemistry and tectonic polarity of Early Proterozoic (1,700–1,750 Ma) plutonic rocks, north-central Arizona, *in* Jenney, J.P., and Reynolds, S.J., eds., Geologic Evolution of Arizona: Arizona Geological Society Digest 17, p. 149–164.

Edgar, A.D., 1987, The genesis of alkaline magmas with emphasis on their source regions; inferences from experimental studies, *in* Fitton, J.G., and Upton, B.G.J., eds., Alkaline Igneous Rocks: Geological Society of London Special Publications, v. 30, p. 29–52.

Embry, P.A., 1987, Petrogenesis of the Yogo Peak stock, Little Belt Mountains: Missoula, University of Montana, M.S. thesis, 94 p.

Foster, Fess, 1991a, Geology and general overview of the Golden Sunlight mine, Jefferson County, Montana, *in* Schafer, R.W., ed., Ore Deposits of Western Montana: Association of Exploration Geochemists 15th International Geochemical Exploration Symposium Field Trip Guidebook 11, p. 26–36.

———1991b, Geology and genetic model based on field studies of the Golden Sunlight mine area, Montana: Geological Society of Nevada Newsletter, February, 1991.

Foster, Fess, and Chadwick, Tom, 1990, Relationship of the Golden Sunlight mine to the Great Falls tectonic zone, *in* Moye, F.S., ed., Geology and Ore Deposits of the Trans-Challis Fault System/Great Falls Tectonic Zone: Guidebook of the Fifteenth Annual Tobacco Root Geological Society Field Conference, p. 77–81.

Frey, F.A., Green, D.H., and Roy, S.D., 1978, Integrated models of basalt petrogenesis; a study of quartz tholeiites to olivine melilitites from southeastern Australia utilizing geochemical and experimental petrological data: Journal of Petrology, v. 19, p. 463–513.

Gunderson, J.A., and Sheriff, S. D., 1991, A new Late Cretaceous paleomagnetic pole from the Adel Mountains, west-central Montana: Journal of Geophysical Research, v. 96, p. 317–326.

Harlan, S.S., Mehnert, H.H., Snee, L.W., Sheriff, S., and Schmidt, R.G., 1991, New ^{40}Ar–^{39}Ar isotopic dates from the Adel Mountain Volcanics; implications for the relationship between deformation and magmatism in the Montana disturbed belt, western Montana [abs.]: Geological Society of America Abstracts with Programs, v. 23, p. A136.

Hurford, A.J., and Green, P.F., 1983, The zeta age calibration of fission-track dating: Isotope Geoscience, v. 1, p. 285–317.

Ivy, S.D., 1988, Source, evolution, and eruptive history of the Cold Spring Creek volcanics, Beaverhead County, Montana: Corvallis, Oregon State University, M.S. thesis, 132 p.

Klepper, M.R., Ruppel, E.T., Freeman, V.L., and Weeks, R.A., 1971, Geology and mineral deposits, east flank of the Elkhorn Mountains, Broadwater County, Montana: U.S. Geological Survey Professional Paper 665, 66 p.

Knopf, Adolph, 1913, Ore deposits of the Helena mining region, Montana: U.S. Geological Survey Bulletin 527, 143 p.

Lambe, R.H., 1981, Crystallization and petrogenesis of the southern portion of the Boulder batholith, Montana: Berkeley, University of California, Ph.D. dissertation, 171 p.

LeBas, M.J., LeMaitre, R.W., Streckeisen, A., and Zanettin, B.A., 1986, Chemical classification of volcanic rocks based on the total alkali-silica diagram: Journal of Petrology, v. 27, p. 745–750.

LeMaitre, R.W., 1976, The chemical variability of some common igneous rocks: Journal of Petrology, v. 17, p. 589–637.

———1984, A proposal by the IUGS Subcommission on the systematics of igneous rocks for a chemical classification of volcanic rocks based on the total alkali silica (TAS) diagram: Australian Journal of Earth Sciences, v. 31, p. 243–255.

———1989, A classification of igneous rocks and glossary of terms; recommendations of the International Union of Geological Sciences Subcommission on the Systematics of Igneous Rocks: Oxford, Blackwell Scientific Publications, 193 p.

Lindquist, A.E., 1966, Structure and mineralization of the Whitehall mining district, Jefferson County, Montana: Butte, Montana College of Mineral Science and Technology, M.S. thesis, 104 p.

Ludwig, K.R., 1991a, PBDAT, a computer program for processing Pb-U-Th isotopic data [revision]: U.S. Geological Survey Open-File Report 88-542, 40 p. and floppy disk.

———1991b, ISOPLOT, a plotting and regression program for radiogenic isotope data: U.S. Geological Survey Open-File Report 91-445, 41 p. and floppy disk.

Marvin, R.F., Witkind, I.J., Keefer, W.R., and Mehnert, H.H., 1973, Radiometric ages of intrusive rocks in the Little Belt Mountains, Montana: Geological Society of America Bulletin, v. 84, p. 1977–1986.

Naeser, C.W., 1978, Fission track dating: U.S. Geological Survey Open-File Report 76-190.

Perry, W.J., Jr., Nichols, D.J., Dyman, T.S., and Haley, C.J., 1992, Sequential Laramide deformation of the Rocky Mountain foreland of southwestern Montana, Wyoming, and north-central Colorado, *in* Thorman, C.H., ed., Application of Structural Geology to Mineral and Energy Resources of the Central and Western United States: U.S. Geological Survey Bulletin 2012, p. C1–C14.

Porter, E.W., and Ripley, Edward, 1985, Petrologic and stable isotope study of the gold-bearing breccia pipe at the Golden Sunlight deposit, Montana: Economic Geology, v 80, p. 1689–1706.

Prostka, H.J., 1966, Igneous geology of the Dry Mountain quadrangle, Jefferson County, Montana: U.S. Geological Survey Bulletin 1221–F, 21 p.

Rhodes, J.M., 1981, Characteristics of primary basaltic magmas, *in* Basaltic Volcanism on the Terrestrial Planets: New York, Pergamon, p. 409–432.

Robertson, F.S., 1953, Geology and mineral deposits of the Zosell (Emery) mining district, Powell County, Montana: Montana Bureau of Mines and Geology Memoir 34, 29 p.

Robinson, G.D., 1963, Geology of the Three Forks quadrangle, Montana: U.S. Geological Survey Professional Paper 370, 140 p.

Rock, N.M.S., 1984, Nature and origin of calc-alkaline lamprophyres: minettes, vogesites, kersantites and spessartites: Transactions of the Royal Society of Edinburgh, v. 74, p. 193–227.

———1987, The nature and origin of lamprophyres: an overview, *in* Fitton, J.G., and Upton, B.G.J., eds., Alkalic Igneous Rocks: Geological Society of London Special Publication 30, p. 191–226.

———1991, Lamprophyres: Glasgow and London, Blackie and Son Limited, 285 p.

Rock, N.M.S., and Groves, D.I., 1988, Can lamprophyres resolve the genetic controversy over mesothermal gold deposits?: Geology, v. 16, p. 538–541.

Ruppel, E.T., 1963, Geology of the Basin quadrangle, Jefferson, Lewis and Clark, and Powell Counties, Montana: U.S. Geological Survey Bulletin 1151, 121 p.

Russell, J.K., and Nicholls, J., 1988, Analysis of petrologic hypotheses with Pearce element ratios: Contributions to Mineralogy and Petrology, v. 99, p. 25–35.

Rutland, Carolyn, 1985, Geochemistry of the Elkhorn Mountains Volcanics, southwestern Montana; implications for the early evolution of a volcanic-plutonic complex: East Lansing, Michigan State University, Ph.D. dissertation, 96 p.

Schmidt, C.J., Genovese, P., and Foster, Fess, 1989, Trip 6 road log; structure and economic geology along the transverse thrust zone of southwestern Montana, *in* French, D.E., and Grabb, R.F., eds., Geologic Resources of Montana, Volume II—Road Logs: Montana Geological Society Field Conference Guidebook, p. 482–501.

Schmidt, C.J., O'Neill, J.M., and Brandon, W.C., 1988, Influence of Rocky Mountain foreland uplifts on the development of the frontal fold and thrust belt, southwestern Montana, *in* Schmidt, C.J. and Perry, W.J., Jr., eds., Interaction of the Rocky Mountain Foreland and the Cordilleran Thrust Belt: Geological Society of America Memoir 171, p. 171–201.

Schmidt, R.G., 1978, Rocks and mineral resources of the Wolf Creek area, Lewis and Clark and Cascade Counties, Montana: U.S. Geological Survey Bulletin 1441, 91 p.

Smedes, H.W., 1966, Geology and igneous petrology of the northern Elkhorn Mountains, Jefferson and Broadwater Counties, Montana: U.S. Geological Survey Professional Paper 510, 116 p.

Streckeisen, Albert, 1979, Classification and nomenclature of volcanic rocks, lamprophyres, carbonatites, and melilitic rocks; recommendations and suggestions of the IUGS Subcommission on the Systematics of Igneous Rocks: Geology, v. 7, p. 331–335.

Swanson, Matt [compiled by Coppinger, Walter], 1989, Petrology and geochemistry of late Cretaceous(?) mafic intrusives, southwestern Montana: National Conference for Undergraduate Research, Trinity University, and senior research project, 26 p.

Tilling, R.I., Klepper, M.R., and Obradovich, J.D., 1968, K-Ar ages and time span of emplacement of the Boulder batholith, Montana: American Journal of Science, v. 266, p. 671–689.

Velde, D., 1968, Les transformations de l'olivine das les lamprophyres et lamproites: Bull. Soc. Geol. Fr., v. 10, p. 601–612.

———1971, Les kersantites: etude des lamprophyres a plagioclase et biotite: Bull. Soc. Fr. Mineral. Crystallogr., v. 94, p. 411–426.

Wertz, J.B., 1971, Analysis of major-, minor- and trace-element data for latite porphyry and Greyson Shale: Unpublished company report for Placer Management, Ltd., 7 p. and appendix.

Zartman, R.E., 1992, Archean crustal lead in the Helena embayment of the Belt Basin, Montana, *in* Bartholomew, M.J., Hyndman, D.W., Mogk, D.W., and Mason, R., eds., Basement Tectonics 8: Characterization and Comparison of Ancient and Mesozoic Continental Margins—Proceedings of the 8th International Conference of Basement Tectonics, Butte, Montana, 1988: Dordrecht, The Netherlands, Kluwer Academic Publishers, p. 699–709.

Zartman, R.E., and Stacey, J.S., 1971, Lead isotopes and mineralization ages in the Belt Supergroup rocks, northwestern Montana and northern Idaho: Economic Geology, v. 66, p. 849–860.

Published in the Central Region, Denver, Colorado
Manuscript approved for publication June 17, 1996
Edited by Richard W. Scott, Jr.
Photocomposition by Carol A. Quesenberry
Graphics by Ed DeWitt
Online composition by Joan Nadeau, Carol Quesenberry, Jim Hoffman, and Rob Wells